Tutorial No. 4

EV Charging Technologies: Power Electronics and Quality

Zian Qin
Associate Professor, PhD
Delft University of Technology
Netherlands

Lu Wang
Scientist, PhD
Hitachi Energy Research Center
Sweden

TU Delft

Hitachi Energy

INSTRUCTORS

Zian Qin is an associate professor with the Department of Electrical Sustainable Energy at Delft University of Technology, the Netherlands. He received the B.Sc. degree from Beihang University, Beijing, China, in 2009; M.Sc. degree from Beijing Institute of Technology, Beijing, China, in 2012; and Ph.D. degree from Aalborg University, Aalborg, Denmark, in 2015; all in electrical engineering. In 2014, he was a Visiting Scientist at RWTH Aachen University, Aachen, Germany. His research interests include power quality and stability of power electronics-based grids, solid-state transformers, and battery energy storage. He has more than 100 journals/conference papers, 4 book chapters, and 2 international patents, and he has worked on several European, Dutch national and industrial projects in these areas.

He is an associate editor of IEEE TPEL, TIE and JESTPE. He is the Founding Chair of the IEEE Transportation Electrification Council Benelux Chapter and the Dutch National Member in the Cigre WG 4.101 Grid-Forming Energy Storage Application. He served as the technical program chair of IEEE-PEDG 2024, IEEE-PEDG 2023, IEEE-ISIE 2020, IEEE-COMPEL 2020, etc. He is a winner of IEEE Open Journal in Power Electronics Prize Paper Award for the year 2020~2023 and IEEE International Challenge in Design Methods for Power Electronics Excellent Innovation Award 2023.

INSTRUCTORS

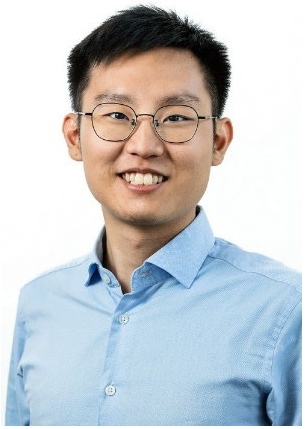

Lu Wang is a research scientist with Hitachi Energy Research Center in Västerås, Sweden. He received the B.Sc. degree from Beijing Institute of Technology, Beijing, China, in 2015; M.Sc. degree and Ph.D. degree from Delft University of Technology, Delft, the Netherlands, in 2018 and 2024, respectively; all in electrical engineering. From 2018 to 2019, he was a power electronics engineer with United Automotive Electronic Systems Co., Ltd, Shanghai, China. From 2019 to 2020, he was an electronics designer with Prodrive Technologies B.V., Eindhoven, the Netherlands. His research interests include EV charging, power quality, and stability of power electronics-based grids.

Acknowledgement goes to:

My (former) PhD students:
Dr. Dingishao Lyu
Dr. Yang Wu
Mr. Adnan Ahmad
Mr. Zhengzhao Li
Mr. Reza Mirzadarani

ECS4DRES is supported by the Chips Joint Undertaking under grant agreement number 101139790 and its members, including the top-up funding by Germany, Italy, Slovakia, Spain and The Netherlands.

OUTLINES

9:30 ~ 11:00

I. Introduction

- Standards
- Power conversion
- Grid impact
- Technical trends

11:00 ~ 11:15

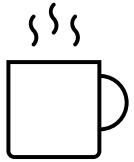

11:15 ~ 12:45

II. Dynamic modelling

- Impedance modelling
- Gray-box modelling
- Solutions and implementations

III. Analytic control design

- Motivations
- Small-signal stability criteria for charger's PFC
- Analytical derivation of design boundaries
- Analytic design procedure

12:45 ~ 13:30

IV. Q&A

OUTLINES

I. Introduction
- Standards
- Power conversion
- Grid impact
- Technical trends

II. Dynamic modelling
- Impedance modelling
- Gray-box modelling
- Solutions and implementations

III. Analytic control design
- Motivations
- Small-signal stability criteria for charger's PFC
- Analytical derivation of design boundaries
- Analytic design procedure

IV. Q&A

E-MOBILITY ECO-SYSTEM

Source: evRoaming4EU
Realising cross-border charging in Europe

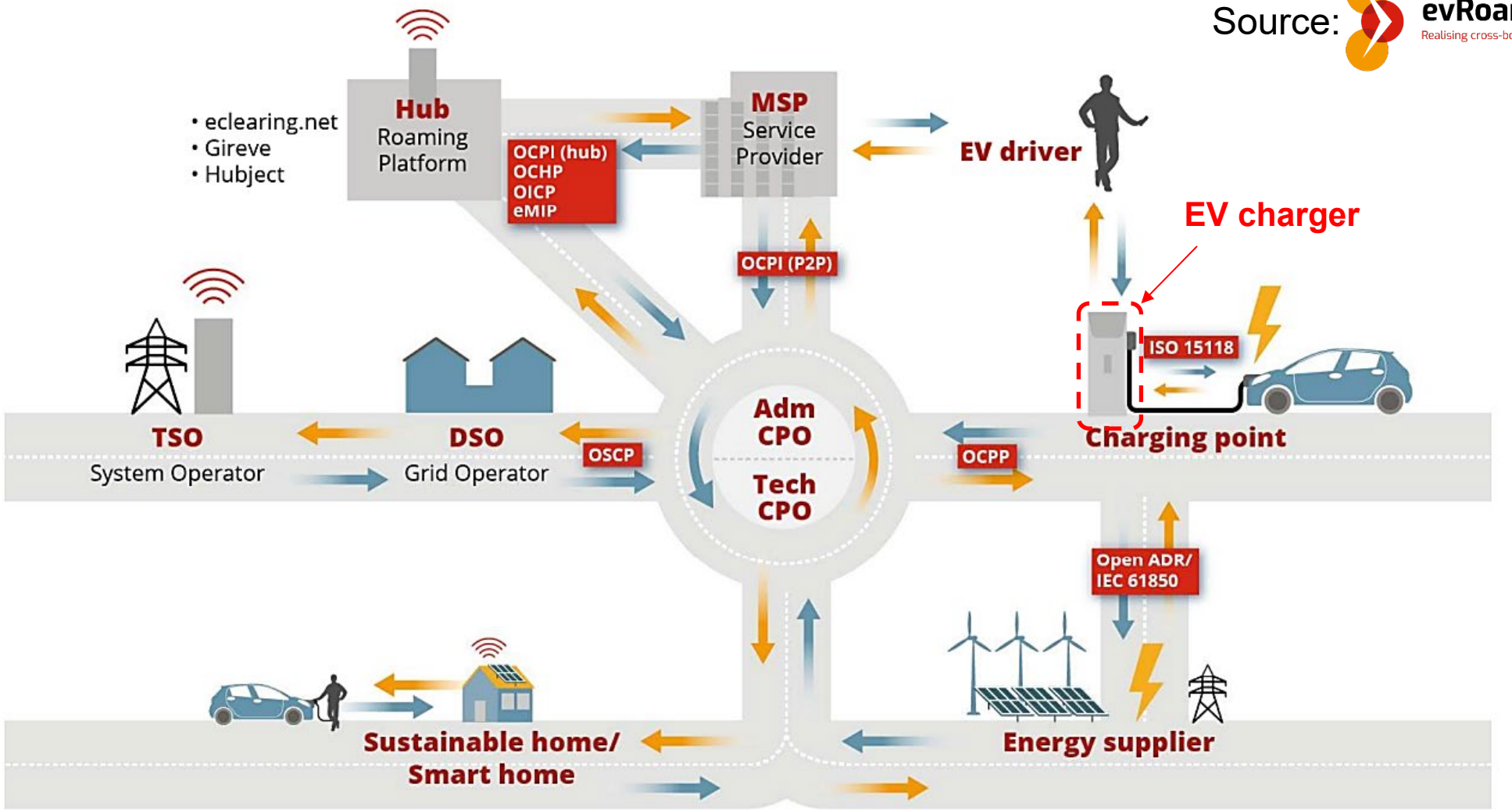

POWER CONVERSION

Duties of AC/DC

- To ensure low harmonics
- To ensure high power factor
- Grid support (advanced)

Duties of DC/DC

- To control charging current
- To ensure high efficiency even the battery voltage varies a lot

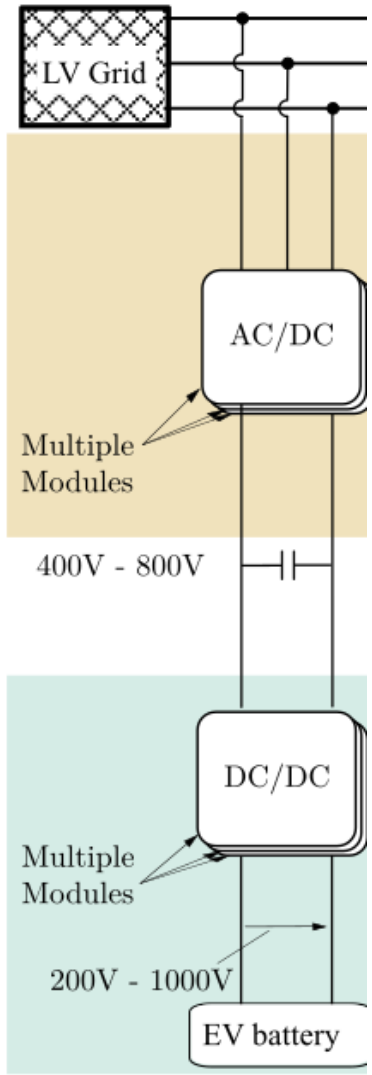

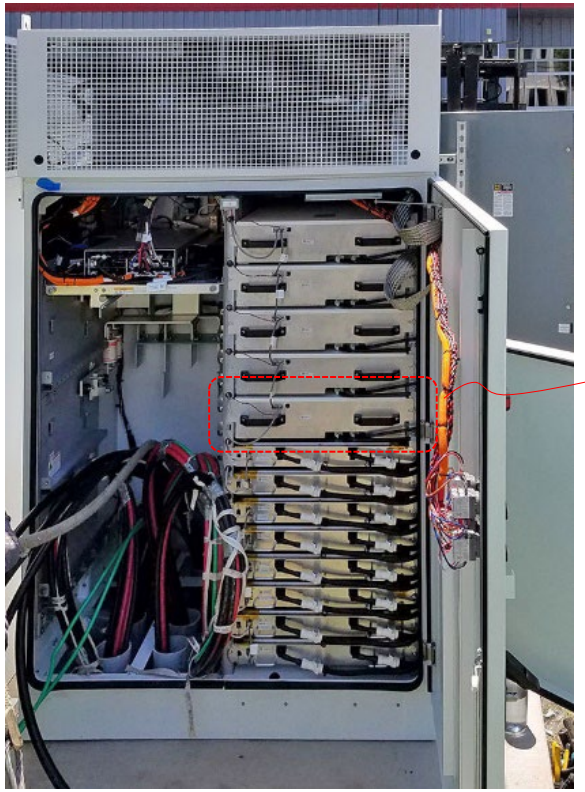

Modular design

@Tesla

POWER ELECTRONICS TOPOLOGIES

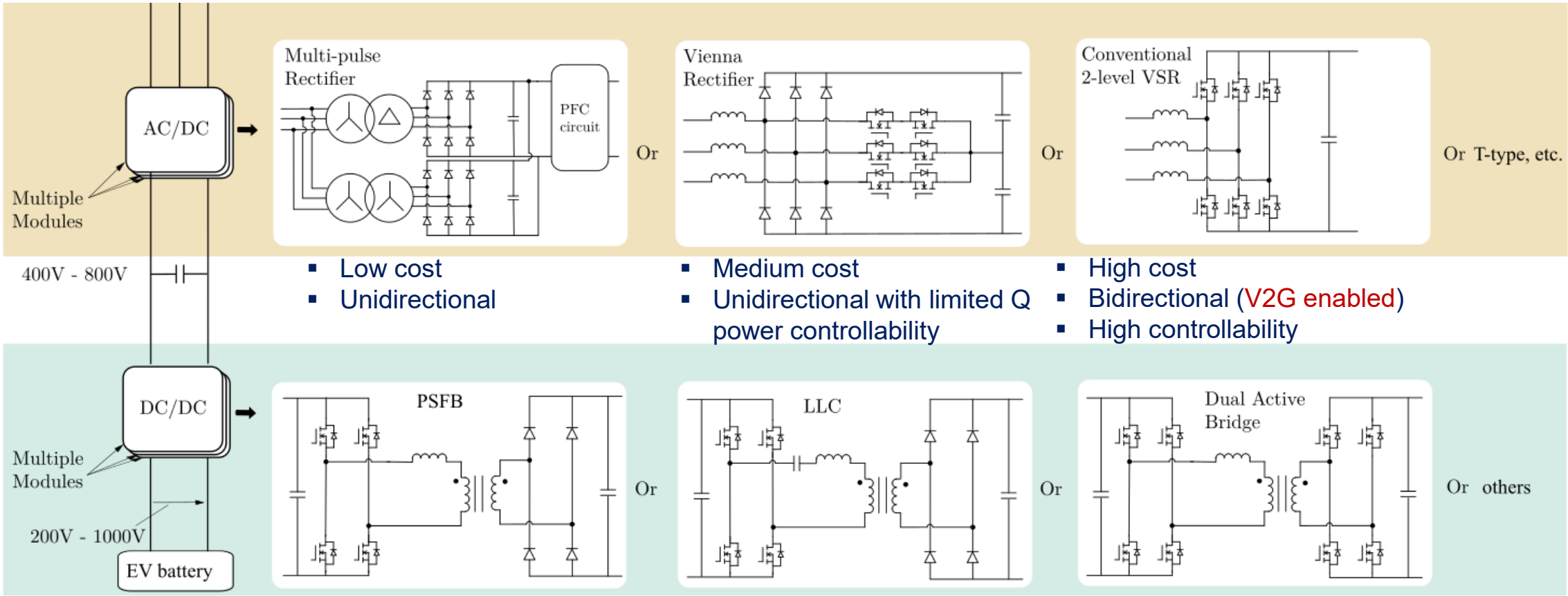

- Low cost
- Unidirectional

- Medium cost
- Unidirectional with limited Q power controllability

- High cost
- Bidirectional (V2G enabled)
- High controllability

- ZVS, difficult in lagging leg
- high conduction loss
- Unidirectional

- ZVS
- low conduction loss
- Unidirectional
- Narrow voltage range

- ZVS
- high conduction loss
- Bidirectional (V2G enabled)
- Simple bidirectional power control

Source: L Wang, et al., "Grid Impact of Electric Vehicle Fast Charging Stations: Trends, Standards, Issues and Mitigation Measures-An Overview", *IEEE-OJPE*, 2021

AC vs DC CHARGERS

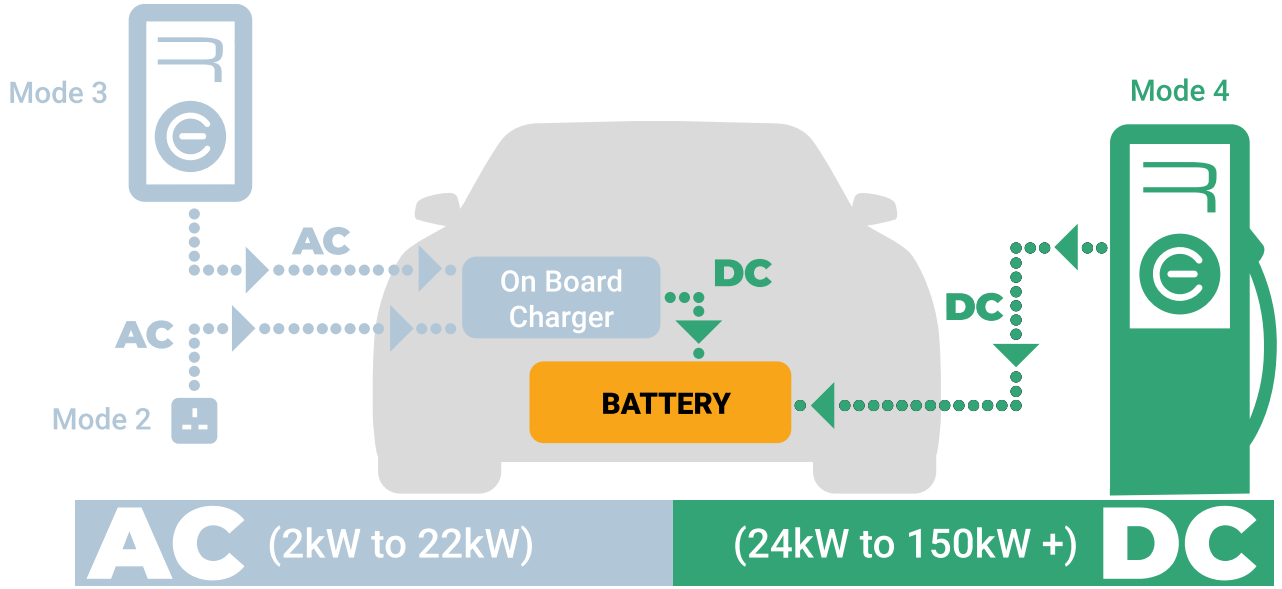

Residential AC charger
(2 kW)

Commercial AC charger
(11 kW)

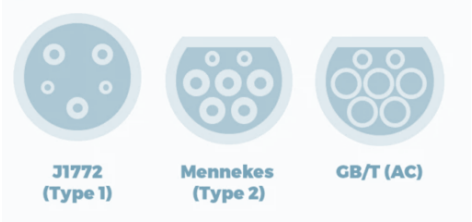

NA
JP

EU
&
rest MKT

CN

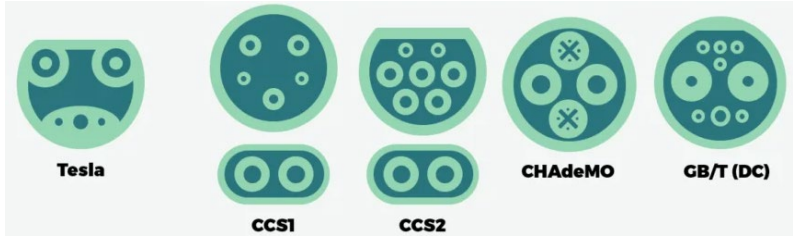

NA

EU
&
rest MKT

JP

CN

@Replenishh

DC fast charger
(350 kW)

Source: Z Qin, et al., “Electric vehicle charging technology and its control”, *Control of Power Electronic Converters and Systems V4*, Academic Press, 241-307, 2024

CHARGER PLUGS

Standard	CHAdeMO	GB/T	CCS Type 1	CCS Type 2	Tesla	ChaoJi
Compliant Standards	IEEE 2030.1.1 IEC 62916-3	IEC 62916-3	SAE J1772 IEC 62916-3	IEC 62916-3	No related items	CHAdeMO and GB/T (IEC and CCS not yet but is ongoing)
Connector Inlet						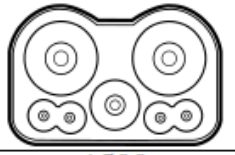
Maximum Voltage (V)	1000	750	600	900	410	1500
Maximum Current (A)	400	250	400	400	330	600
Maximum Power (kW)	400	185	200	350	135	900
Maximum Market Power (kW)	150	125	150	350	120	N.A.
Communication Protocol	CAN		PLC		CAN	CAN
V2X Function	Yes	No			Unknown	Yes
Start year	2009	2013	2014	2013	2012	2020

Source: Netherlands Enterprise Agency, *The Electric vehicle charging – Definitions and explanations*, version January 2019

CHARGING POWER IS INCREASING

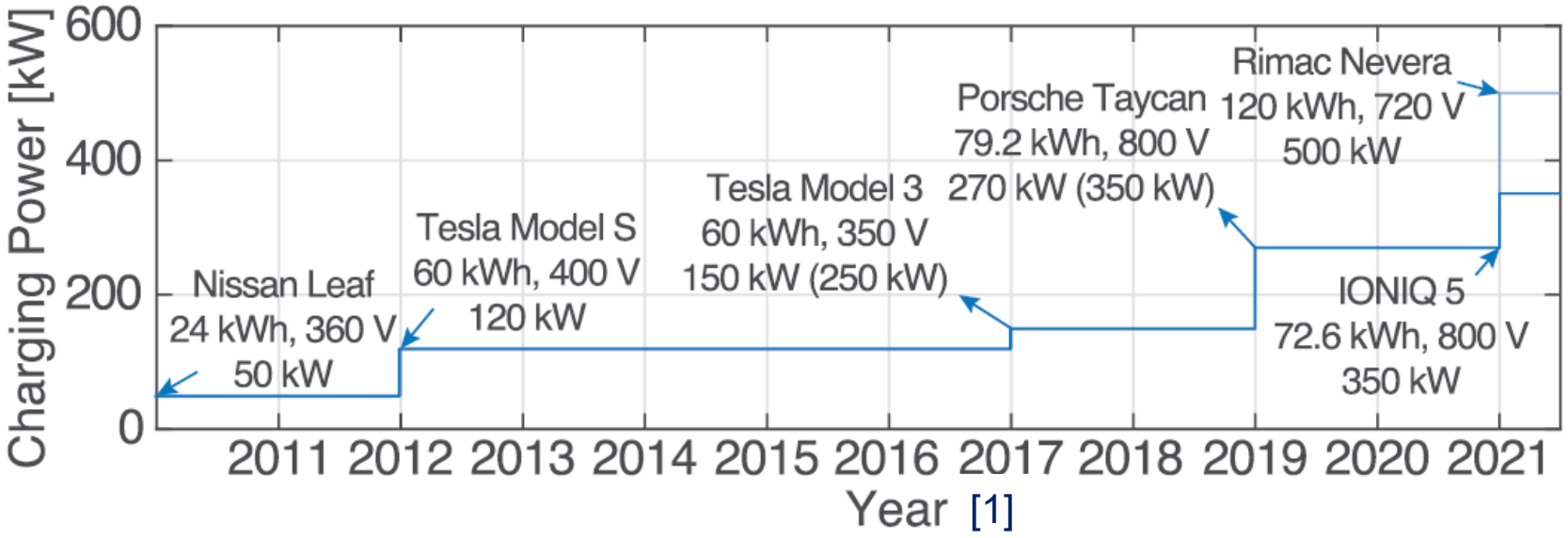

ABB Terra HP
Max. 350kW

EVBox Ultroniq
Max. 350kW

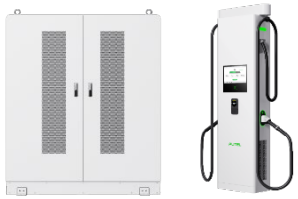

Autel DC fast charger
Max. 350 kW

Source: [1] Rivera et al., Charging Infrastructure and Grid Integration for Electromobility, *Proceedings of IEEE*, 2023

LAB FACILITIES

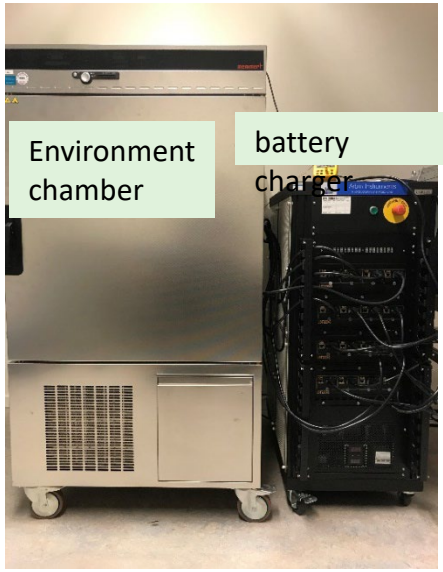

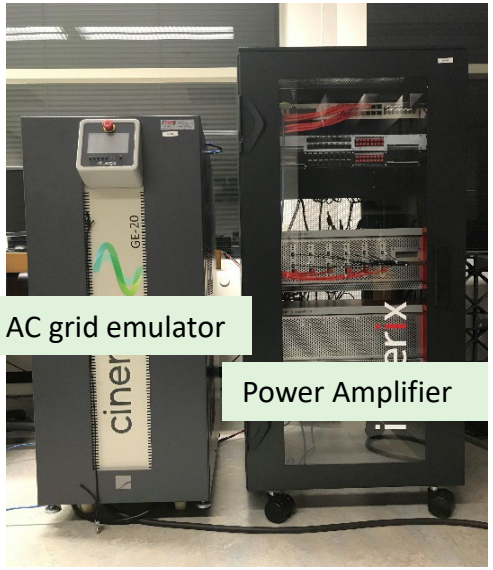

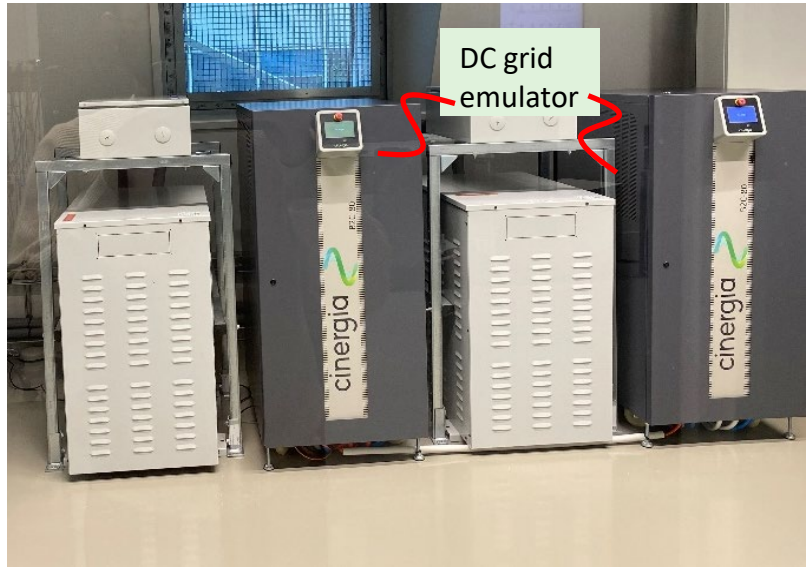

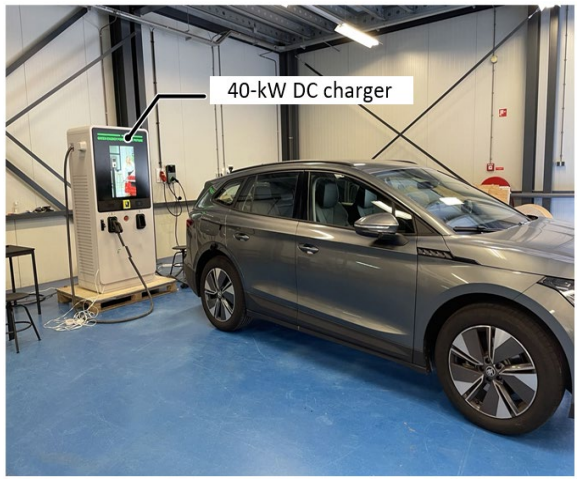

BATTERY VOLTAGE IS INCREASING

- EVs with 800V batteries are increasing in numbers. Chargers that can cover 300V~900V will have a good market

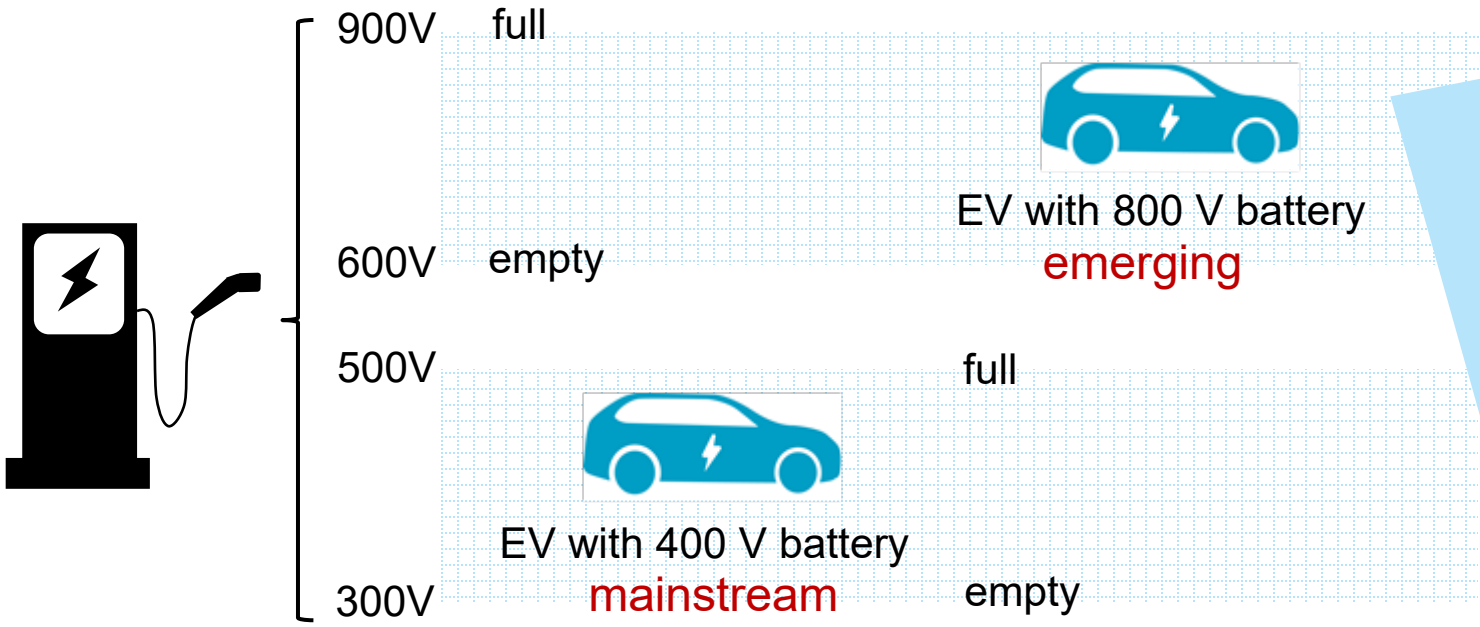

- Porsche: Taycan
- Tesla: Cyber truck
- Kia: EV6, EV9
- Hyundai: IONIQ 5/6
- BYD: ATTO 3, Dolphin, etc.
- XPeng: G9
- etc.

RECONFIGURABLE TOPOLOGY

- Switching between parallel and series to maintain a steady operation condition of each port

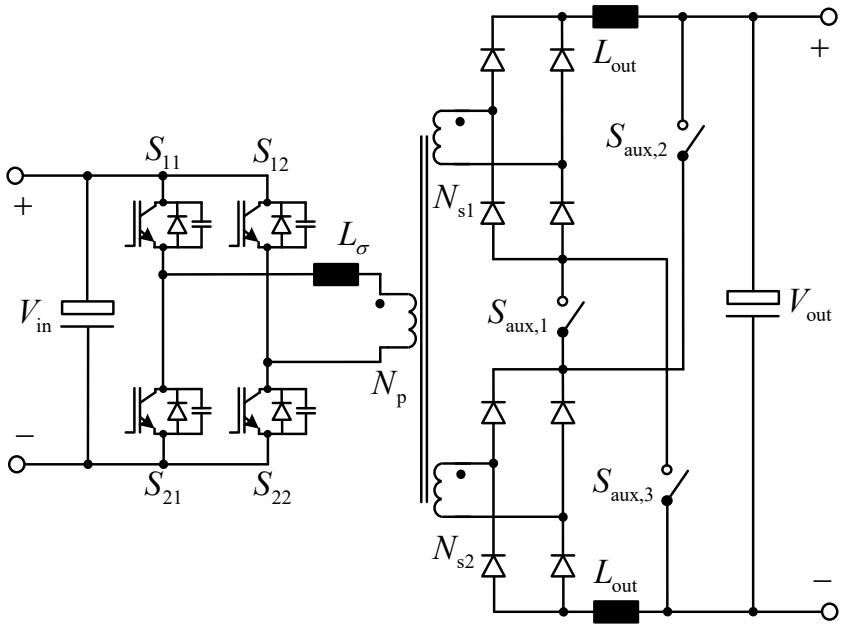

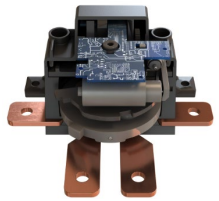

@Eaton BCS

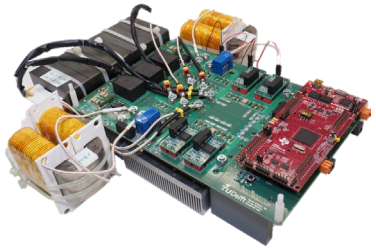

10 kW FSFB module

- 640-840V V_{in}
- 200-1000 V_{out}
- 30A $I_{out(max)}$

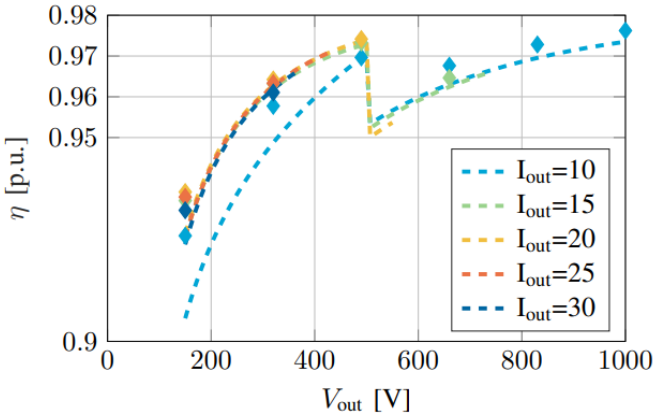

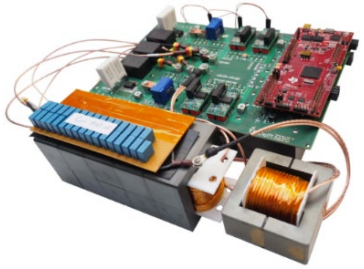

10 kW LLC module

- 640-840V V_{in}
- 200-1000 V_{out}
- 30A $I_{out(max)}$

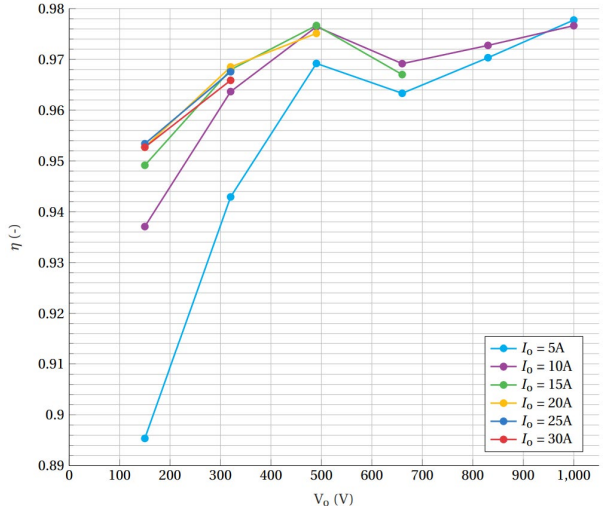

Source: D Lyv, et al., "Design and Implementation of a Re-configurable Phase-Shift Full-Bridge Converter for Wide Voltage Range EV Charging Application," *TTE*, 2022

HYBRID OPERATION MODE

- Hybrid modulation strategies and variable switching frequency
- Maximize the ZVS region and minimize switching loss

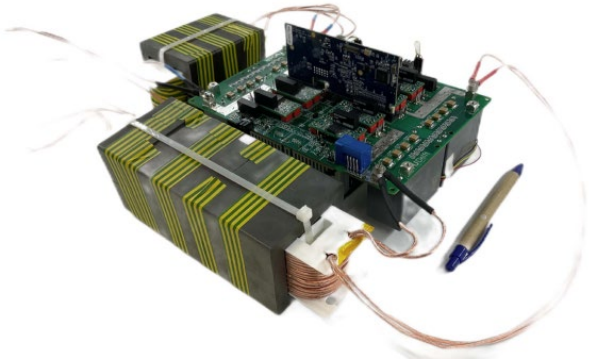

11 kW DAB module

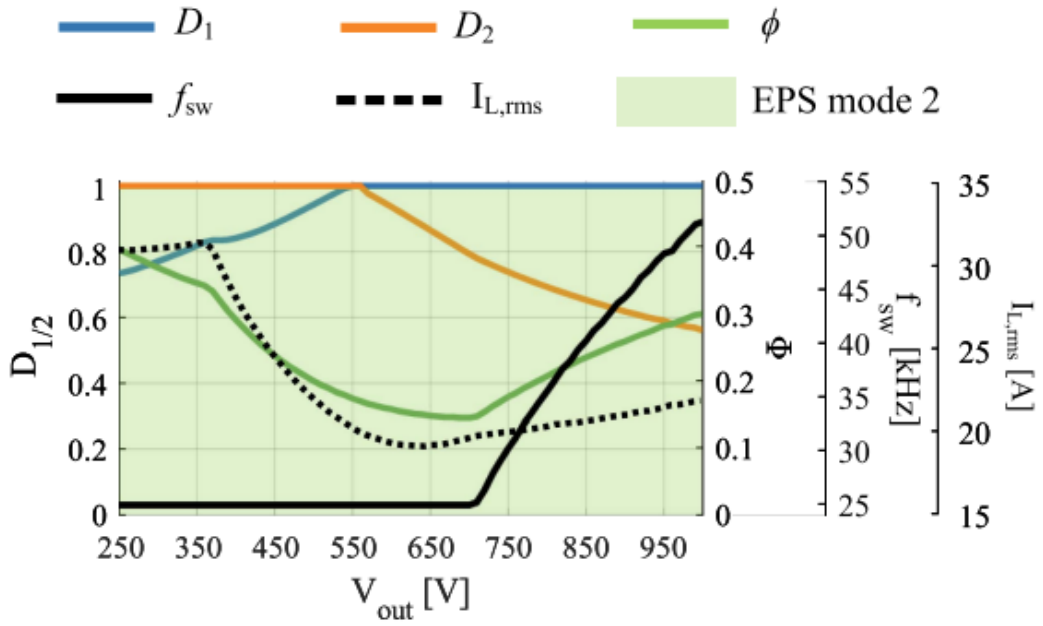

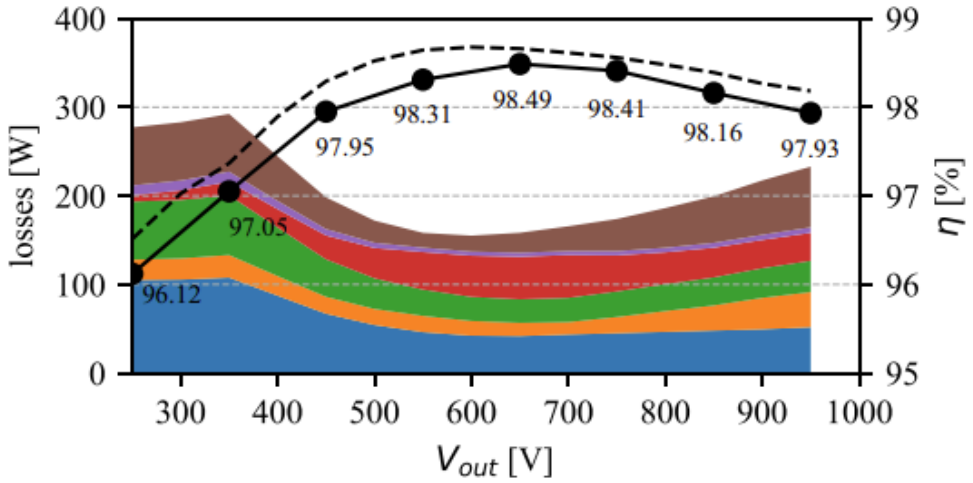

Source: D Lyv, et al., "ZVS-Optimized Constant and Variable Switching Frequency Modulation Schemes for Dual Active Bridge Converters," *IEEE OJPEL*, 2023

HYBRID OPERATION MODE

- DC blocking capacitor voltage control
- Operation switching between the full and half-bridge mode
- Change hard-switching to soft-switching
- Reduce core loss

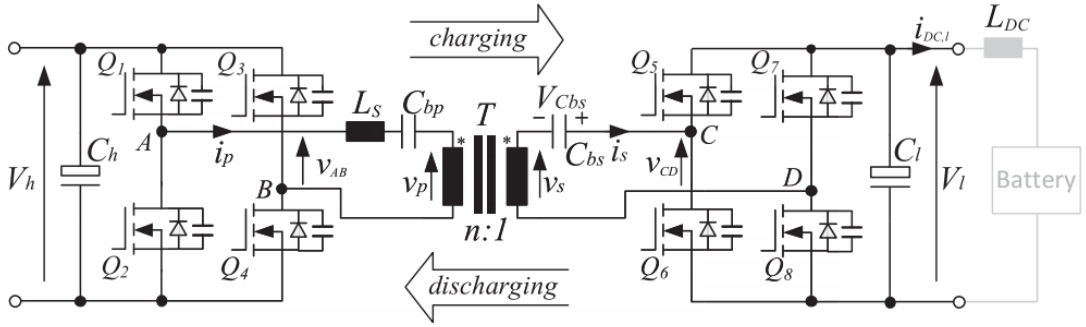

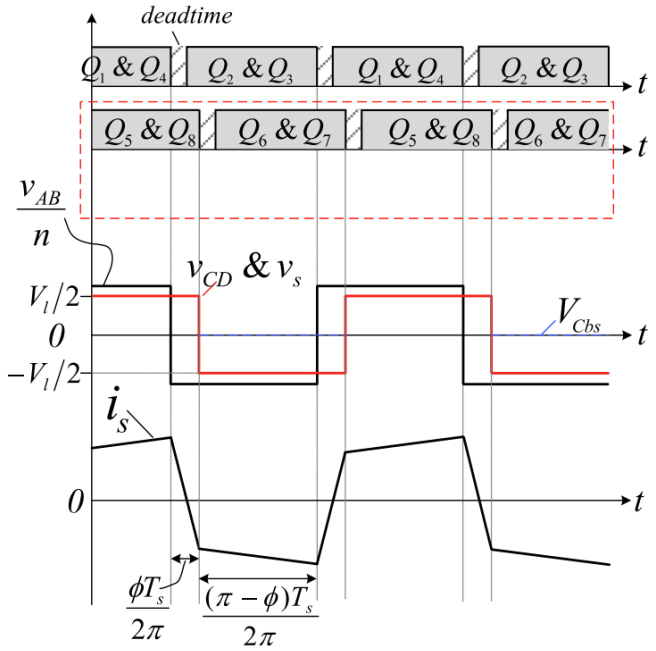

@ low V_{batt}, *full bridge mode*, $V_{cbs} = 0$

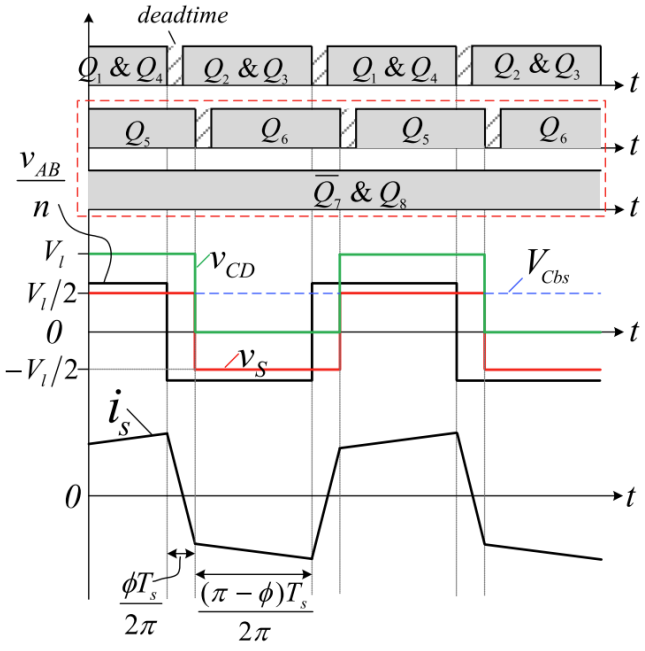

@ high V_{batt}, *half bridge mode*, $V_{cbs} = V_{batt}/2$

Source: Z Qin, et al., "A Dual Active Bridge Converter With an Extended High-Efficiency Range by DC Blocking Capacitor Voltage Control," *IEEE TPEL*, 2018

HYBRID OPERATION MODE

- DC blocking capacitor voltage control
- Change hard-switching to soft-switching

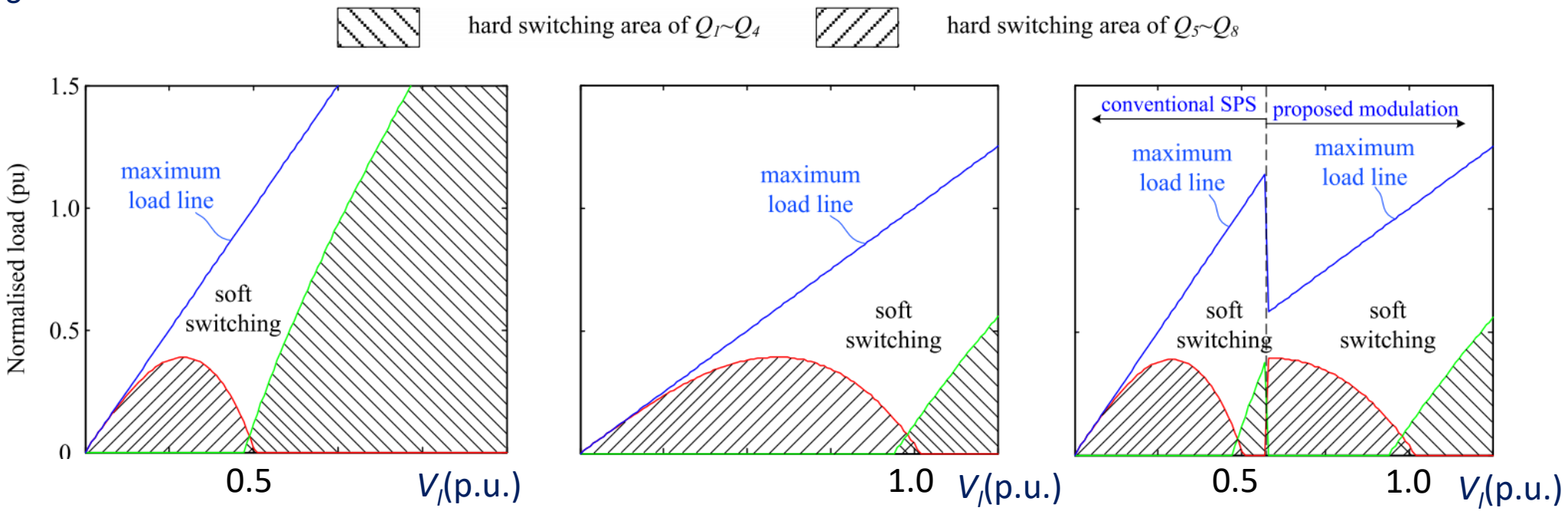

Full bridge mode, $V_{cbs} = 0$ | Half bridge mode, $V_{cbs} = V_{batt}/2$ | Hybrid mode

Source: Z Qin, et al., "A Dual Active Bridge Converter With an Extended High-Efficiency Range by DC Blocking Capacitor Voltage Control," *IEEE TPEL*, 2018

HYBRID OPERATION MODE

- DC blocking capacitor voltage control
- Operation switching between the full and half-bridge mode
- Change hard-switching to soft-switching
- Reduce core loss

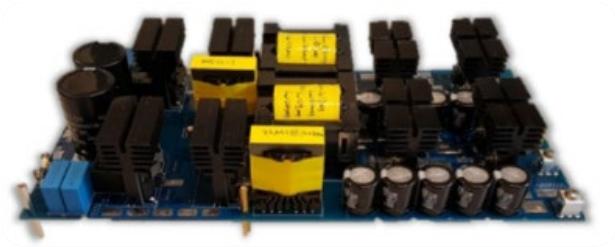

5 kW DAB module

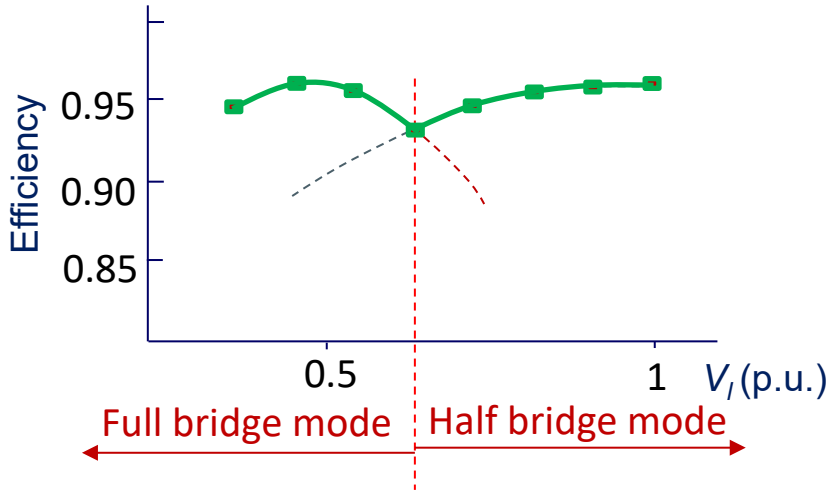

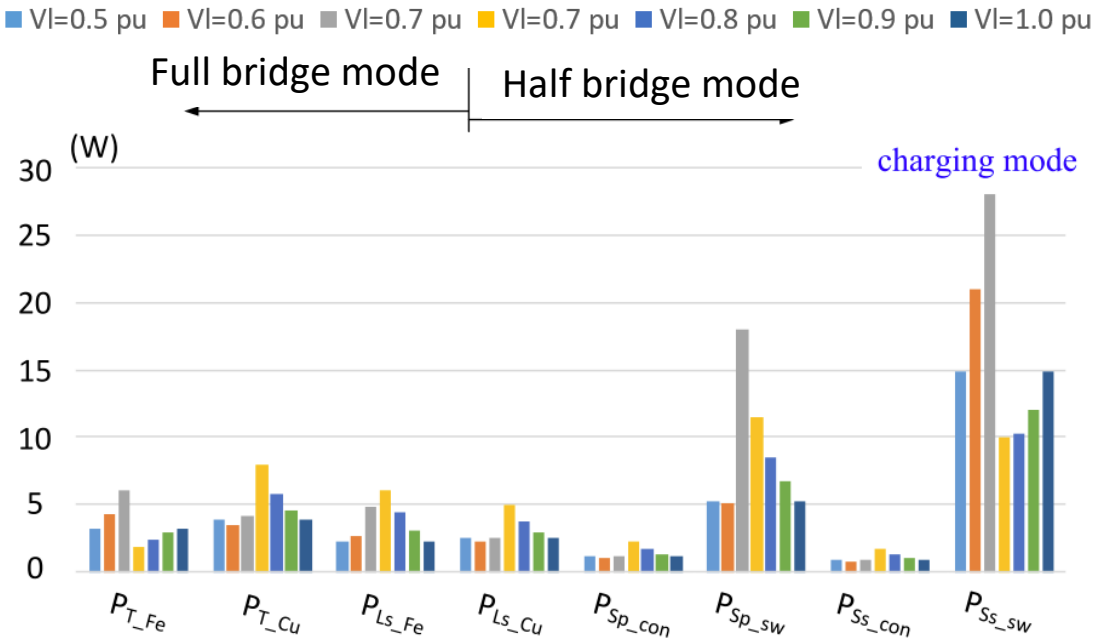

Loss breakdown

Source: Z Qin, et al., "A Dual Active Bridge Converter With an Extended High-Efficiency Range by DC Blocking Capacitor Voltage Control," *IEEE TPEL*, 2018

HYBRID OPERATION MODE

- DC blocking capacitor voltage control
- Change hard-switching to soft-switching

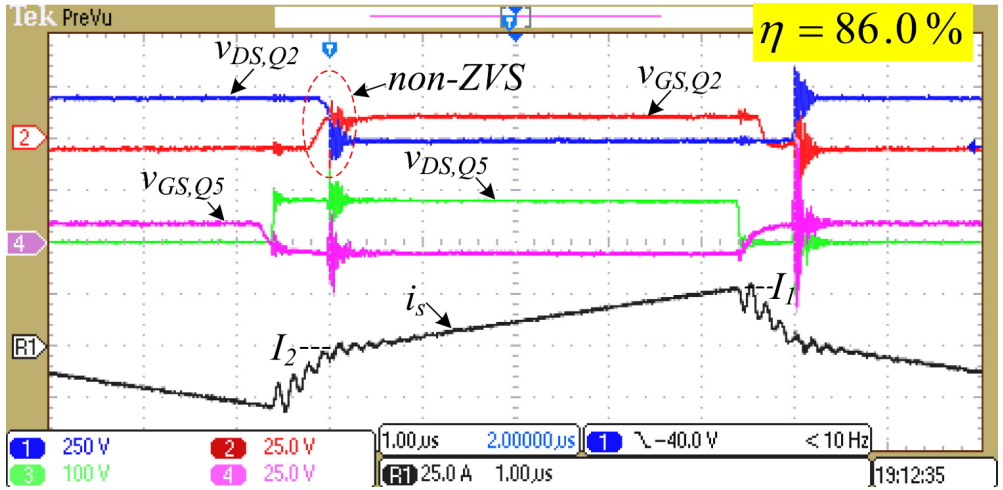

Full bridge mode, $V_{cbs} = 0$
Hard-switching

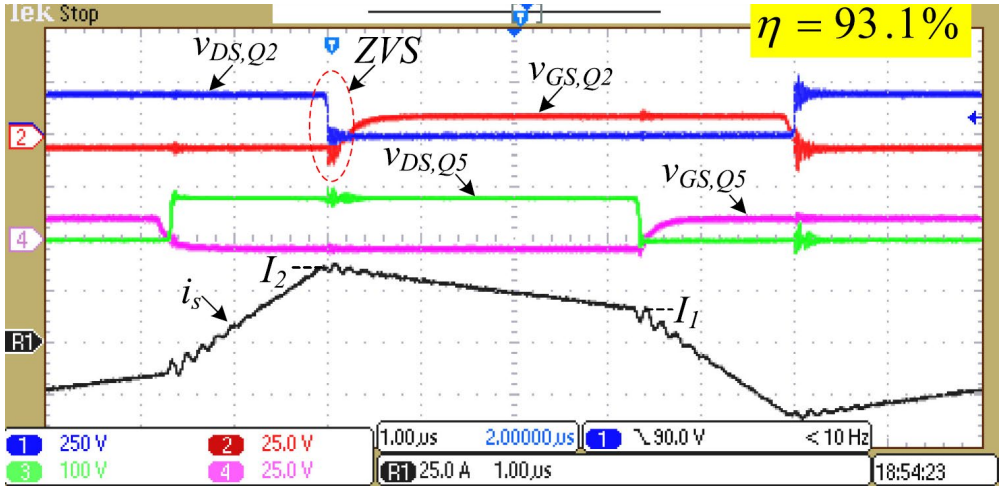

Half bridge mode, $V_{cbs} = V_{batt}/2$
Soft-switching

@Vl = 0.7 pu

Source: Z Qin, et al., "A Dual Active Bridge Converter With an Extended High-Efficiency Range by DC Blocking Capacitor Voltage Control," *IEEE TPEL*, 2018

MULTI-PORT CONVERTER

- Share the power electronics for a lower cost and more compact system
- Power coupling between ports
- Decoupling by control is complicated [1]

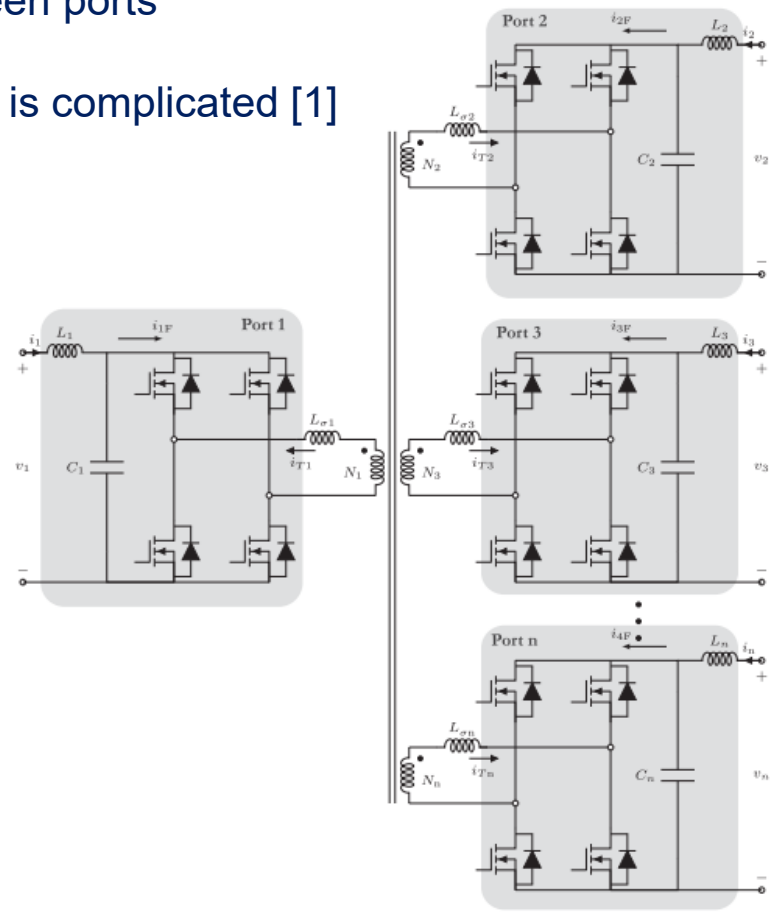

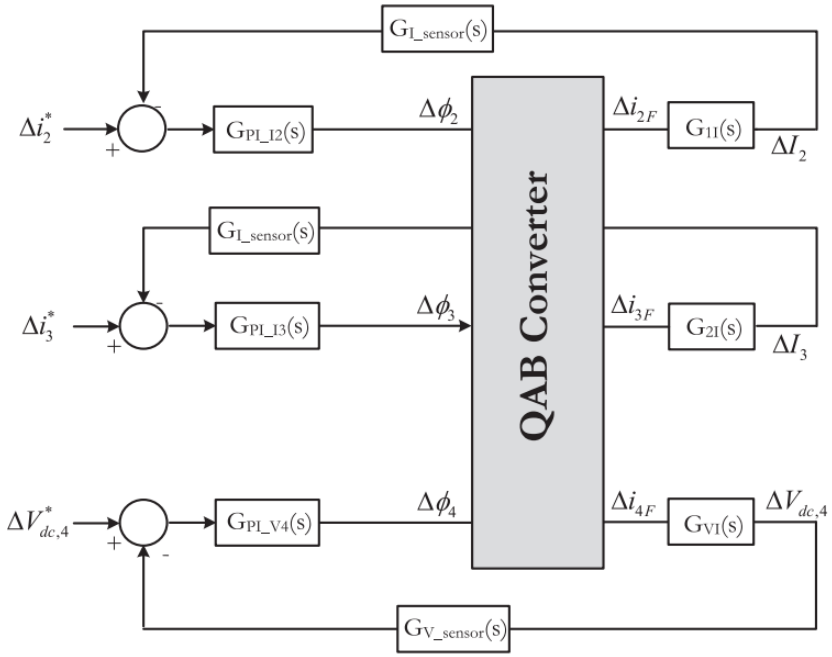

$$\begin{bmatrix}\Delta i_{2F}\\ \Delta i_{3F}\\ \Delta i_{4F}\end{bmatrix} = \begin{bmatrix}G_{22} & G_{23} & G_{23}\\ G_{32} & G_{33} & G_{34}\\ G_{42} & G_{43} & G_{44}\end{bmatrix}\begin{bmatrix}\Delta\phi_2\\ \Delta\phi_3\\ \Delta\phi_4\end{bmatrix}$$

Model of MAB [2]

Source:
[1] S Bandyopadhyay, et. al. “Decoupling Control of Multi-Active Bridge Converters using Active Disturbance Rejection,” *TIE*, 2021
[2] S Bandyopadhyay, et. al., “A Multiactive Bridge Converter With Inherently Decoupled Power Flows,” *TPEL*, 2021

MULTI-PORT CONVERTER

- Share the power electronics for lower cost and compact system
- Power coupling between ports

$$\begin{bmatrix} \Delta i_{2F} \\ \Delta i_{3F} \\ \Delta i_{4F} \end{bmatrix} = \begin{bmatrix} G_{22} & G_{23} & G_{23} \\ G_{32} & G_{33} & G_{34} \\ G_{42} & G_{43} & G_{44} \end{bmatrix} \begin{bmatrix} \Delta\phi_2 \\ \Delta\phi_3 \\ \Delta\phi_4 \end{bmatrix}$$

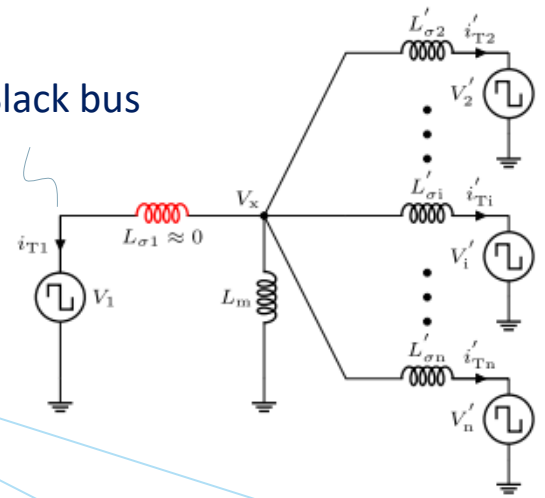

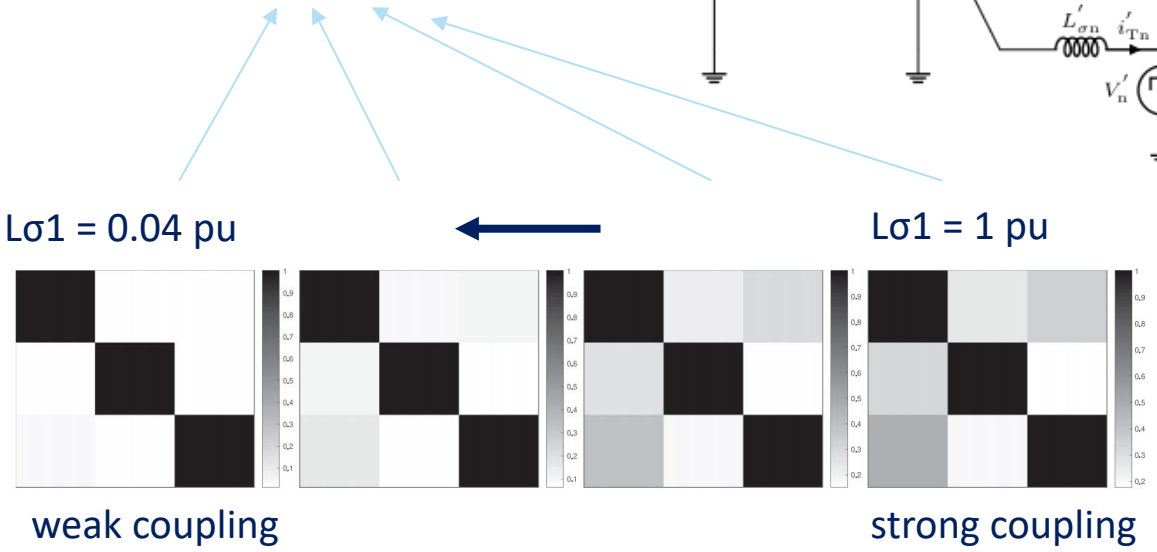

- Power flow between the ports are decoupled by minimizing the leakage inductance of the slack bus

Source:
[1] S Bandyopadhyay, et. al., "A Multiactive Bridge Converter With Inherently Decoupled Power Flows," *TPEL*, 2021
[2] S Bandyopadhyay, et. al. "Power module, multi-port power converter and energy system comprising the same," *NL Patent NL2029574B1*, 2023

MULTI-PORT CONVERTER

- Share the power electronics for lower cost and compact system
- Power coupling between ports

Port 4 is disturbed by other ports

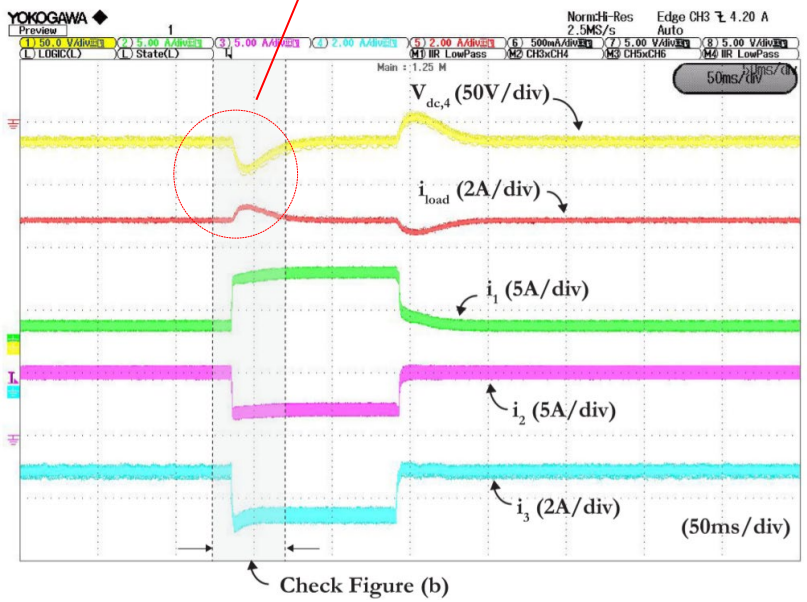

Lσ1 = 0.6 pu

Port 4 is not disturbed by other ports

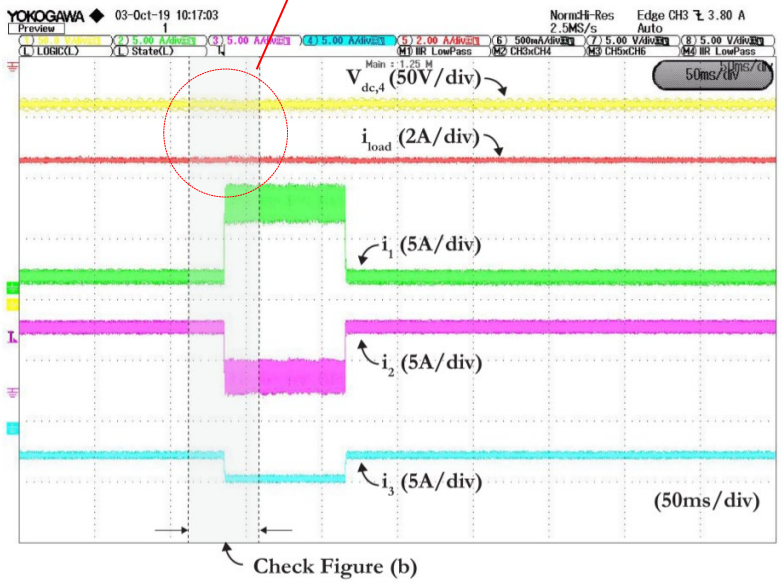

Lσ1 = 0

Source: S Bandyopadhyay, et al., "A Multiactive Bridge Converter With Inherently Decoupled Power Flows," *TPEL*, 2021

Power Quality Issues

- EV charging is associated with power quality issues, especially flickers and supraharmonics

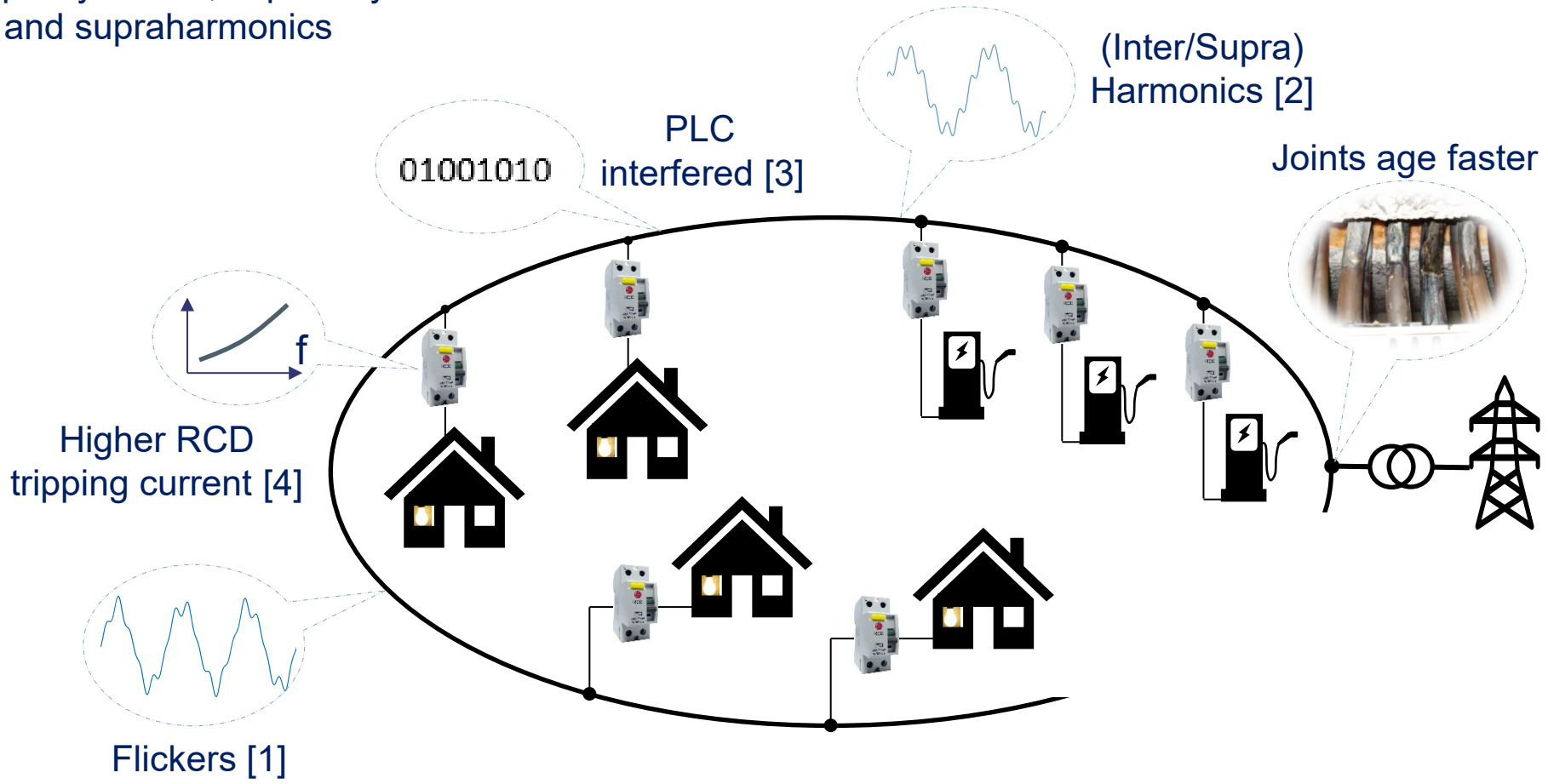

Source:
[1] https://teslamotorsclub.com/tmc/threads/lights-in-house-flicker-while-charging-new-model-3.149841/
[2] T Slangen, V Ćuk, S Cobben, “Summation of supraharmonic currents (2–150 kHz) from EV fast charging stations,” Electric Power Systems Research 220, 2023
[3] L Hasselgren, G Mademlis, Å Lindbeck, et. al. “Inverter Interference on Charging Communication System during 400 V DC Charging of Vehicle,” EMC Europe, 2022
[4] T Slangen, B Lustenhouwer, JFG S Cobben, et. al. “The Effects of High-Frequency Residual Currents on the Operation of Residual Current Devices,” in the Proc. Of ICREPQ 2021

Power Quality Issues

- Harmonics are reducing in high voltage grids, and increasing in low and medium voltage grids

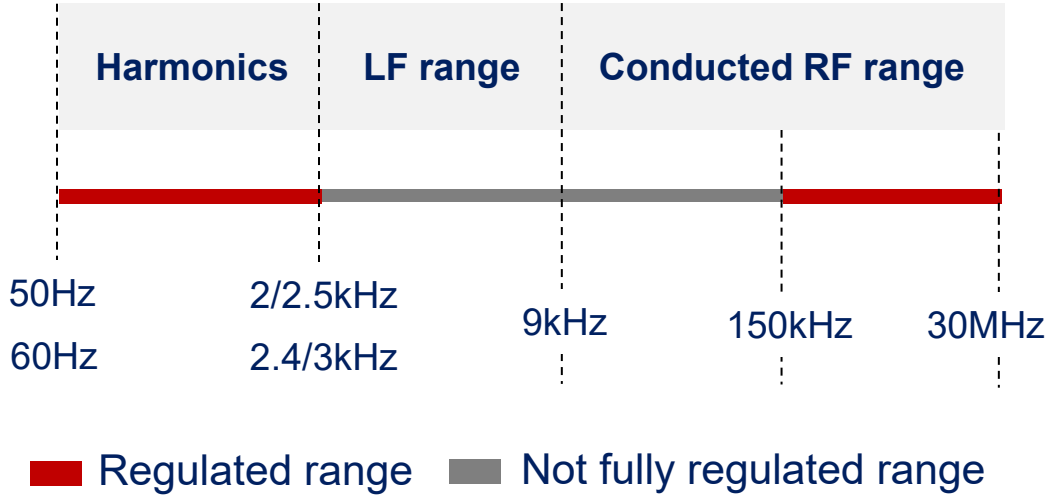

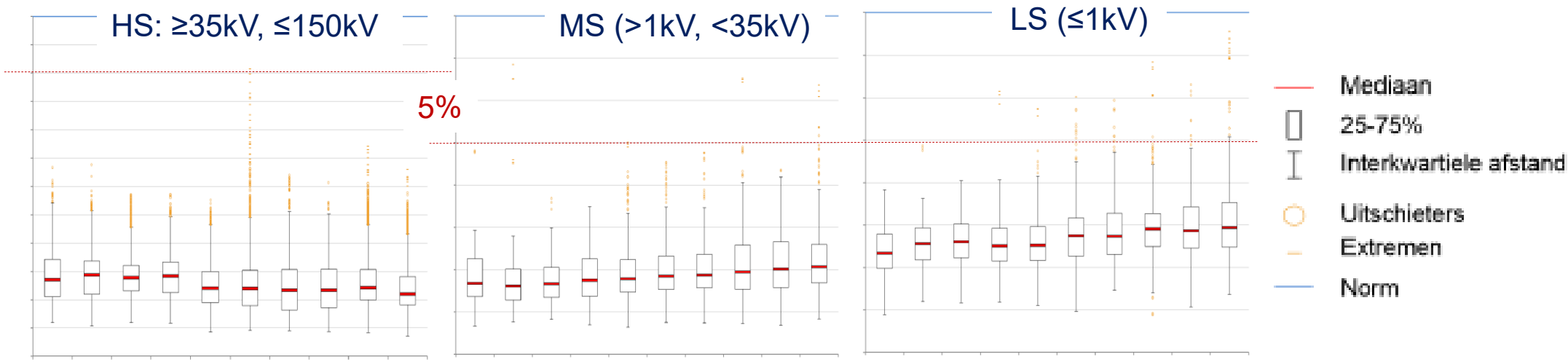

Jaartal THD 95% (2011~2020) [1]

Source: [1] Spanningskwaliteit in Nederland - Resultaten 2020

HARMONIC LIMITS VS IMPEDANCE

- Voltage distortion is an essential concern.
- Current harmonics and network impedance are reasons
- Network and converter impedance are necessary for harmonic calculation

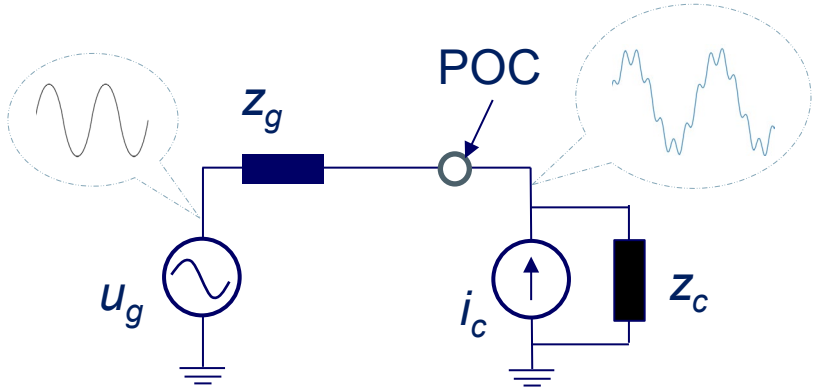

Harmonic Current Limits in IEEE-519

	Maximum harmonic distortion of the individual harmonic order in percent of I_L					
I_{SC}/I_L	$3 \leq h < 11$	$11 \leq h < 17$	$17 \leq h < 23$	$23 \leq h < 35$	$35 \leq h < 50$	TDD
< 20	4.0	2.0	1.5	0.6	0.3	5.0
$20 < 50$	7.0	3.5	2.5	1.0	0.5	8.0
$50 < 100$	10.0	4.5	4.0	1.5	0.7	12.0
$100 < 1000$	12.0	5.5	5.0	2.0	1.0	15.0
> 1000	15.0	7.0	6.0	2.5	1.4	20.0

Note:

- Limits for even harmonics are 25% of the odd harmonic limits
- DC offset in current is not allowed
- I_L: maximum demand load current
- I_{SC}: maximum short circuit current at PCC

Source: L Wang, et al., "Grid Impact of Electric Vehicle Fast Charging Stations: Trends, Standards, Issues and Mitigation Measures-An Overview", *IEEE-OJPE*, 2021

GRAY BOX IMPEDANCE MODELLING

- White box modelling needs the hardware and control parameters as input, but usually unavailable
- Black box modelling doesn't need the parameters, but cannot cover the whole operation range
- Gray box modelling has advantages of both of them

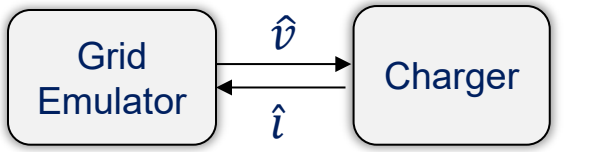

Black box modelling $z = \frac{\hat{v}}{\hat{\imath}}$

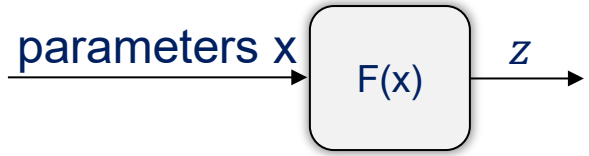

White box modelling

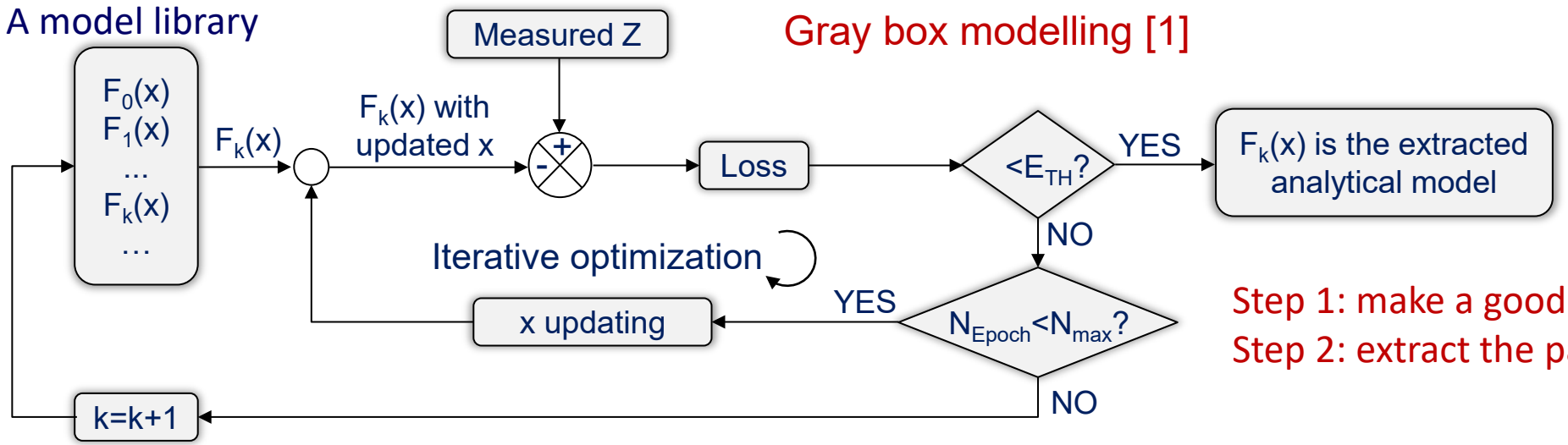

Gray box modelling [1]

Step 1: make a good guess of the model
Step 2: extract the parameter values

Source: [1] L Wang, et. al. "A gradient-descent optimization assisted gray-box impedance modeling of ev chargers," *TPEL*, 2023

SUPRAHARMONICS MITIGATION

- Fixed switching frequency creates harmonics with high peak
- Variable switching frequency will spread out the harmonics.
- THD is still the same

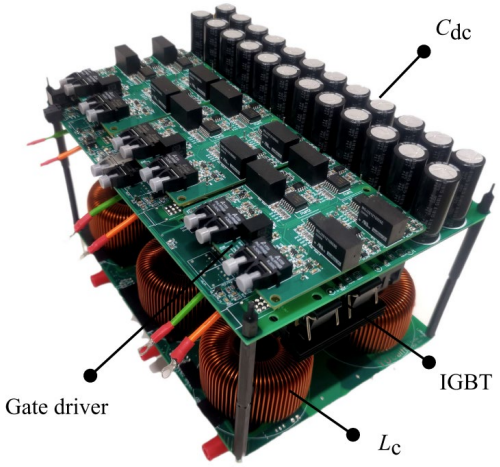

- 10 kW rectifier module
- Peak efficiency 98.6%

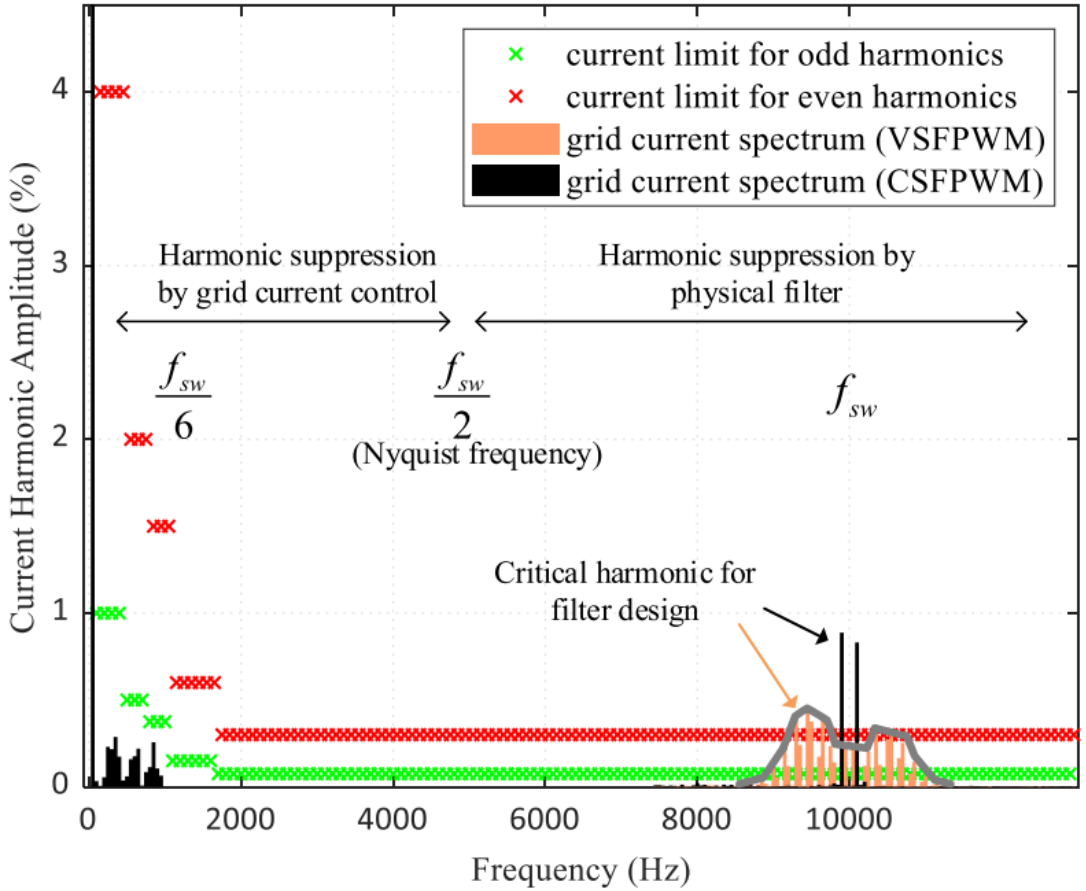

IEEE-519 harmonic current standard and typical grid current harmonic spectrum with CSFPWM and VSFPWM.

Source: Y Wu, et. al. “Frequency Design of Three-phase Active Front-End Converter with Reduced Filter in EV Chargers,” *TTE*, 2024

SUPRAHARMONICS MITIGATION

- Fixed switching frequency creates harmonics with high peak
- Variable switching frequency will spread out the harmonics.
- THD is still the same

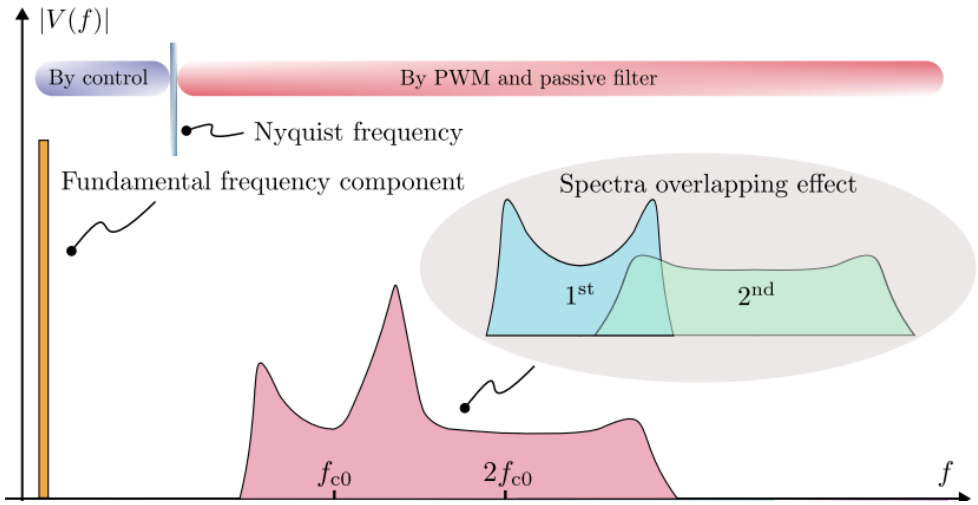

- The spead out of the harmonics may have overlap with each other and create peak again

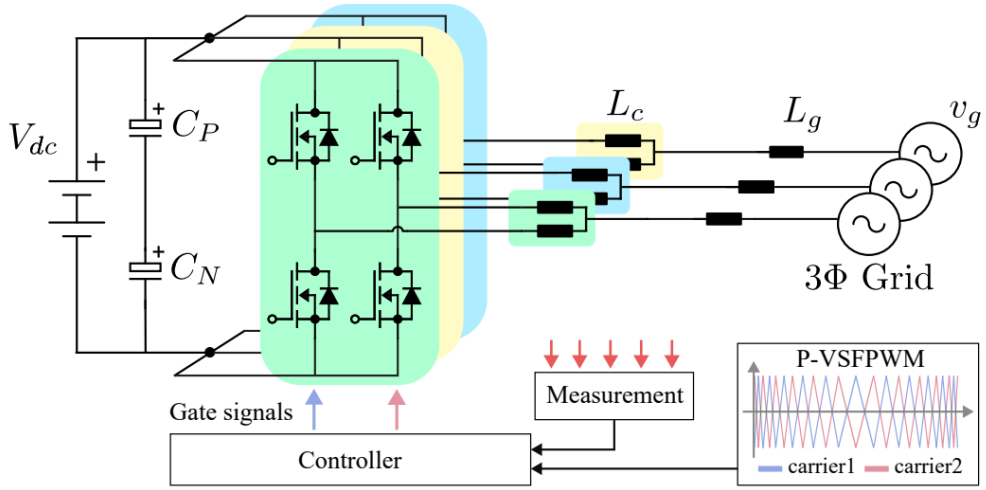

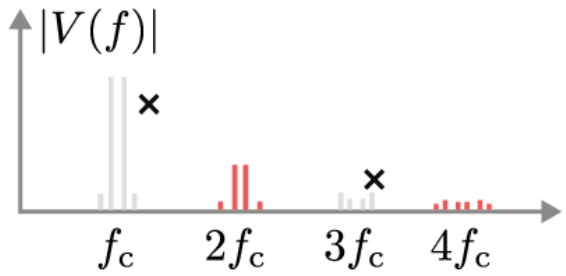

- Interleaving will solve the problem

Source: Y Wu, et. al. "Frequency Design of Three-phase Active Front-End Converter with Reduced Filter in EV Chargers," *TTE*, 2024

SUPRAHARMONICS MITIGATION

- Fixed switching frequency creates harmonics with high peak
- Variable switching frequency will spread out the harmonics.
- THD is still the same

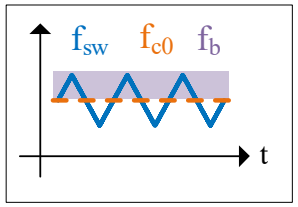

Triangle profile

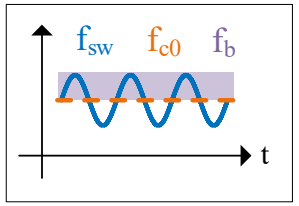

Sinusoidal profile

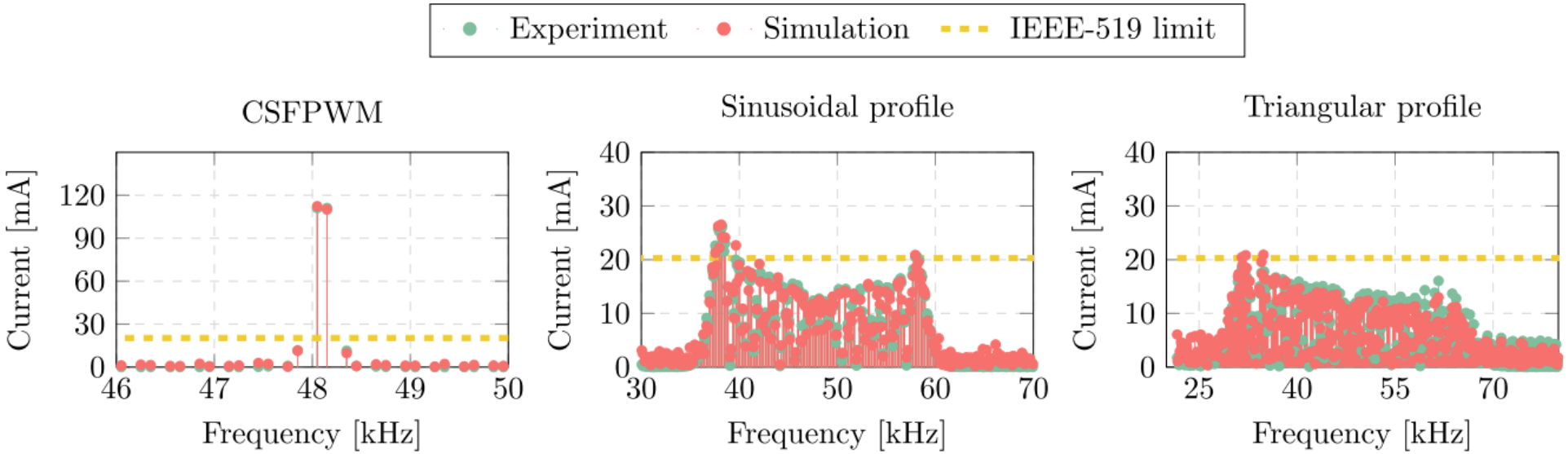

Source: Y Wu, et. al. "Frequency Design of Three-phase Active Front-End Converter with Reduced Filter in EV Chargers," *TTE*, 2024

MEGA WATT CHARGING

- Medium voltage grid connection
- Energy storage integration

@Cavotec

@Zinus

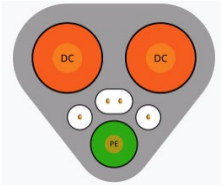

MW Charging System (MCS)
DC, Vmax: 1.25kV, Imax: 3 kA,
Pmax: 3.75 MW

@Cavotec

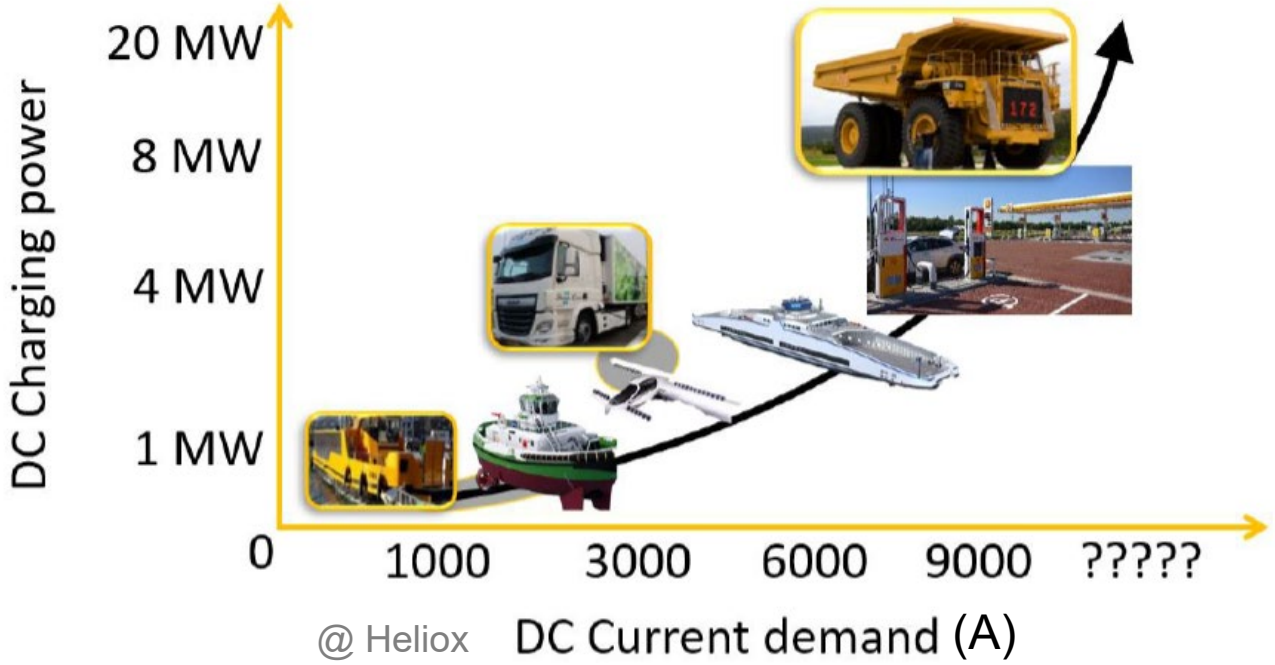

@ Heliox

GRID FEE

Connection capacity	One-off connection fee (€)	Annual fee to maintain the connection (€)
> 175 kVA to 630 kVA via LS measurement	34002	1455
> 630 kVA to 1000 kVA via LS measurement	36000	
> 1000 kVA to 1750 kVA via MS measurement	58000	
> 1750 kVA to 5000 kVA	330000	3642

Contracted transport capacity	Transportation service			
	Fixed charge	Variable tarief		
	Transport per month (€)	kW contract per month per kW (€)	Double tarief per kWh (€)	Reactive power consumption per kVARh (€)
151 to 1500 kW	36.75	2.0250	0.0198	0.017
> 1500kW	230	1.8958	0.0198	0.017

LS: ≤1kV;
MS: > 1kV, ≤20kV;
TS: 50kV;
HS: > 50 kV

- When connected to grid, **you pay** not only per kWh, but also **per kW**
- You pay more with higher peak grid power, even with fixed average grid power

Source: published data from Stedin – A DSO in Netherlands. The data is for year 2025

GRID CONGESTION

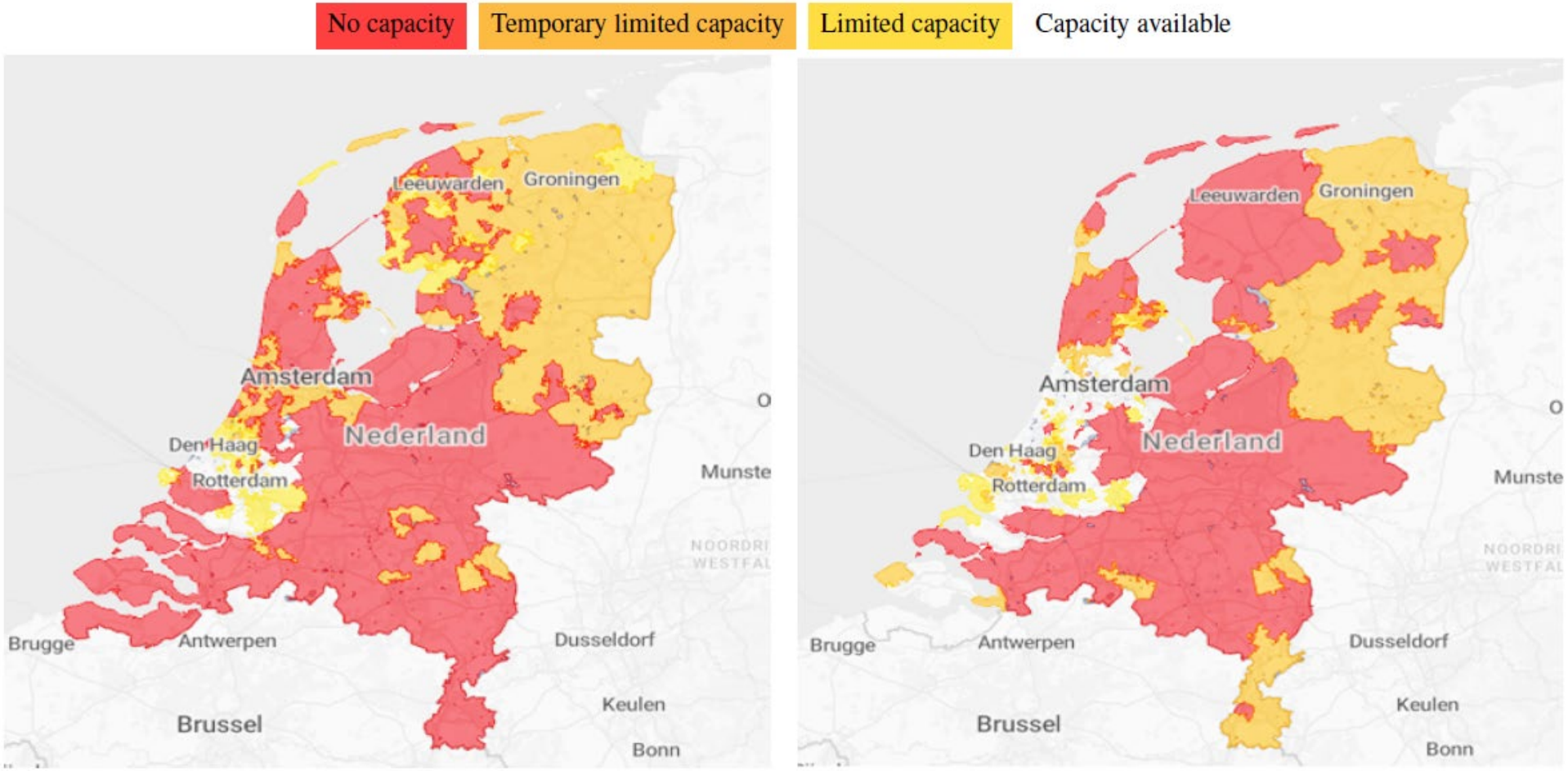

(a) Consumption contingency

(b) Generation contingency

- Grid congestion leads to higher grid fee, especially the per kW tarief

Source: CFP Green Buildings, Grid congestion: what is it and how can you avoid it?

ENERGY STORAGE INTEGRATION

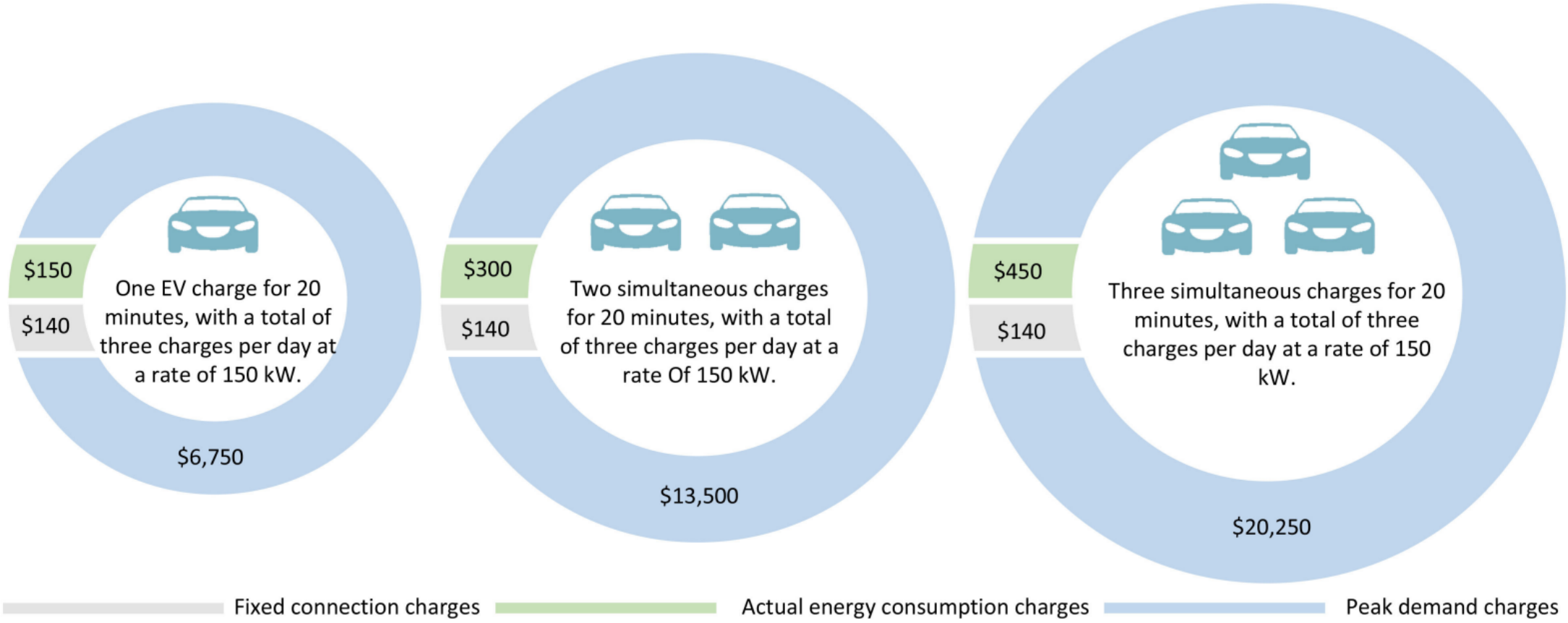

- The peak demand charge can be significant especially for the load with high peak and low average

Source: A Ahmad, et. al. "An Overview on Medium Voltage Grid Integration of Ultra-Fast Charging Stations: Current Status and Future Trends," *IEEE OJIES*, 2022

ENERGY STORAGE INTEGRATION

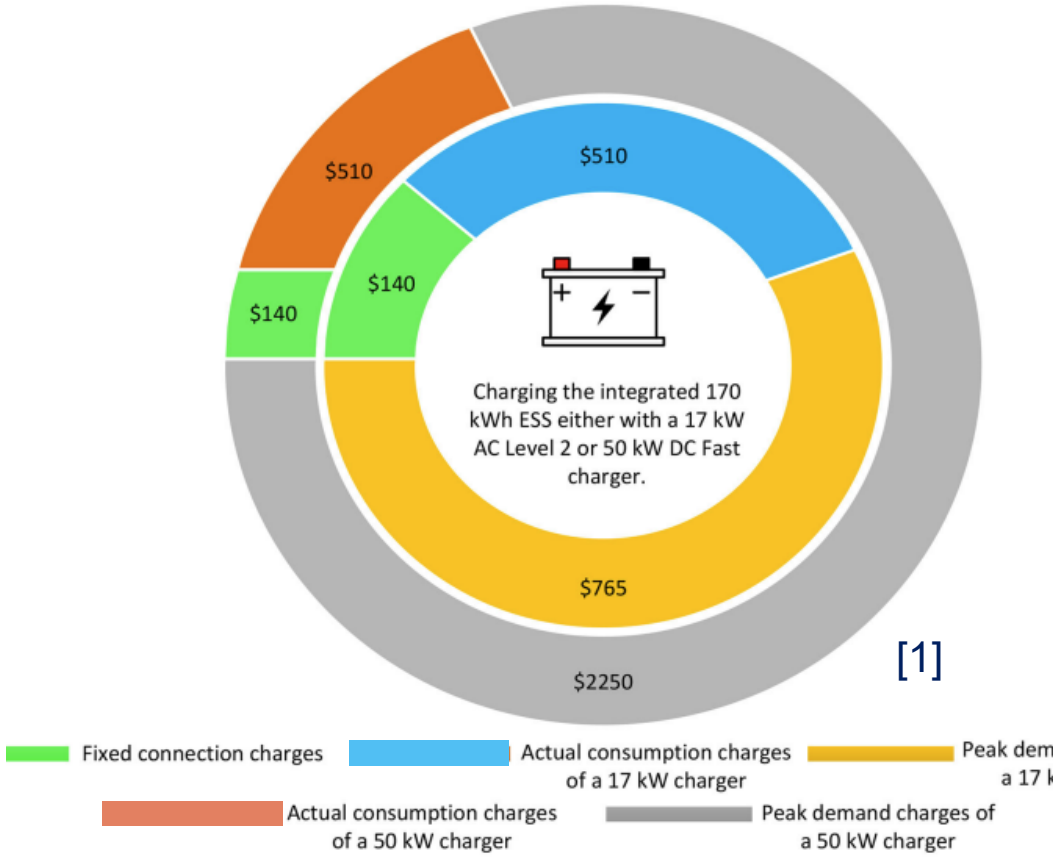

[1]

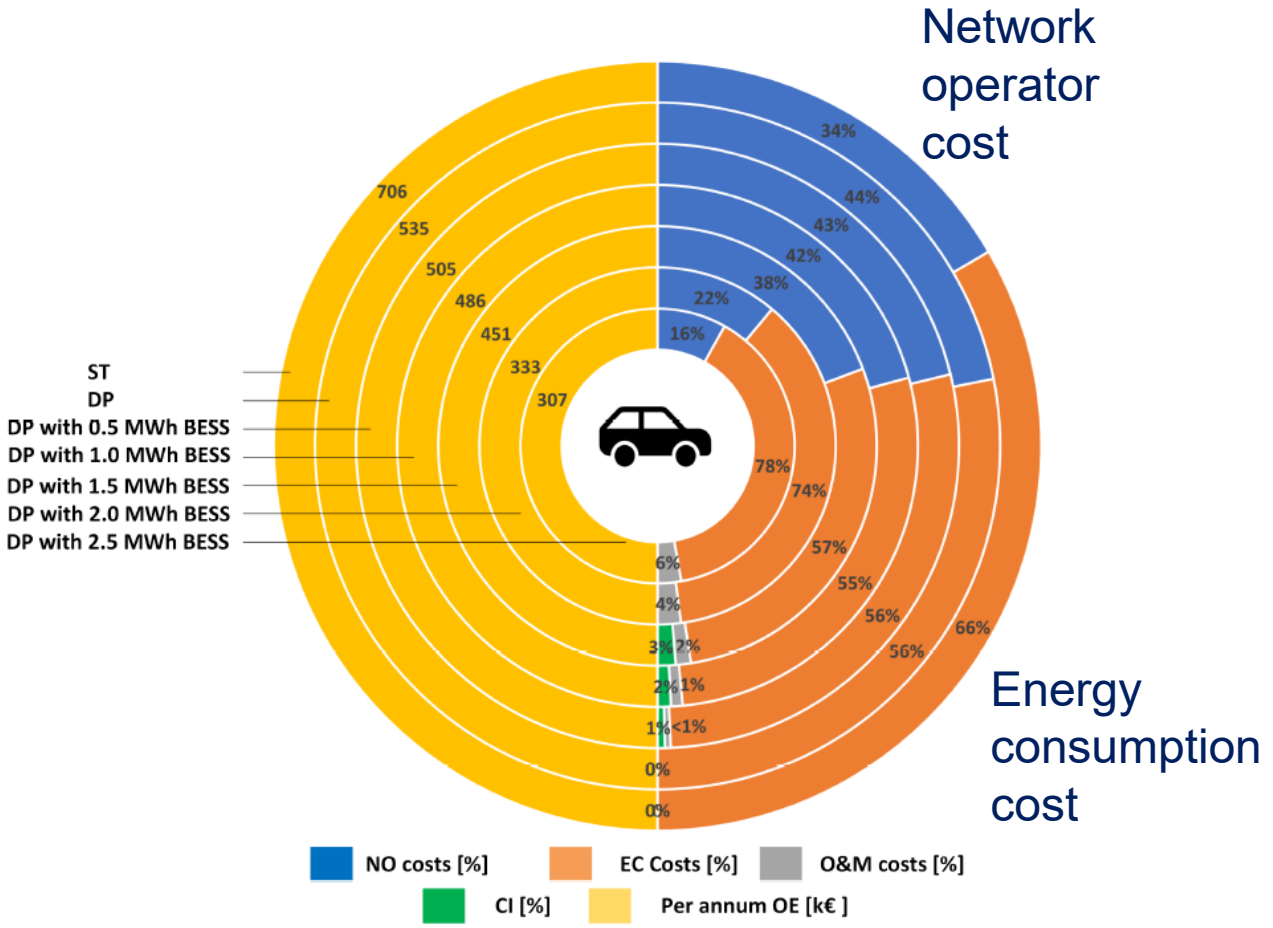

- Energy storage can help to reduce the grid fee

Source:
[1] A Ahmad, et. al. “An Overview on Medium Voltage Grid Integration of Ultra-Fast Charging Stations: Current Status and Future Trends,” *IEEE OJIES*, 2022
[2] A. Ahmad, et al, “Techno-Economic Analysis of Energy Storage Systems Integrated with Ultra-Fast Charging Stations: A Dutch Case Study,” eTransportation, in press, 2025

ENERGY STORAGE INTEGRATION

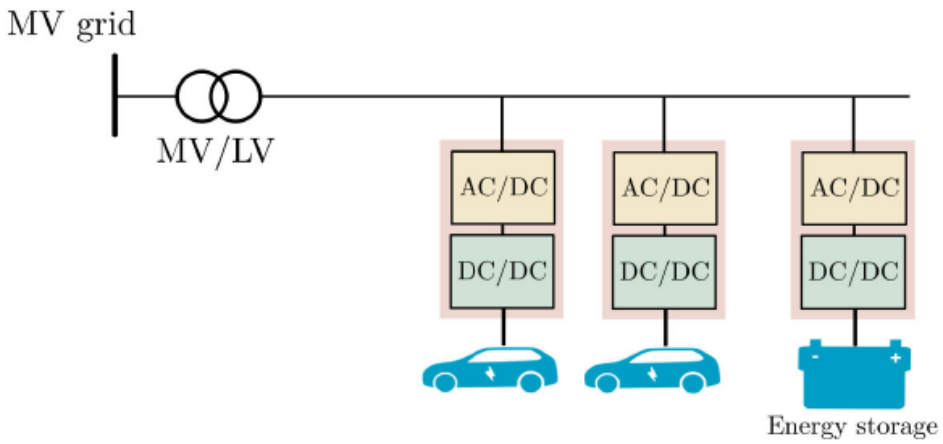

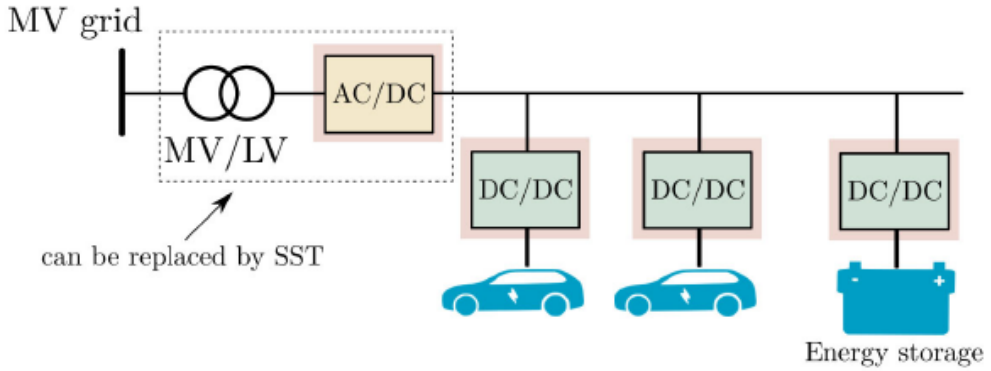

- Integration of BESS reduces the grid connection capacity and thereby CAPEX
- Less power conversion stages between ESS and vehicles, higher efficiency

Note: if the BESS is integrated, the bidirectional front-end AC/DC is preferred to enable grid ancillary service to maximize the benefit

Source: L Wang, et al., “Grid Impact of Electric Vehicle Fast Charging Stations: Trends, Standards, Issues and Mitigation Measures-An Overview”, *IEEE-OJPE*, 2021

SST BASED MV MW CHARGER

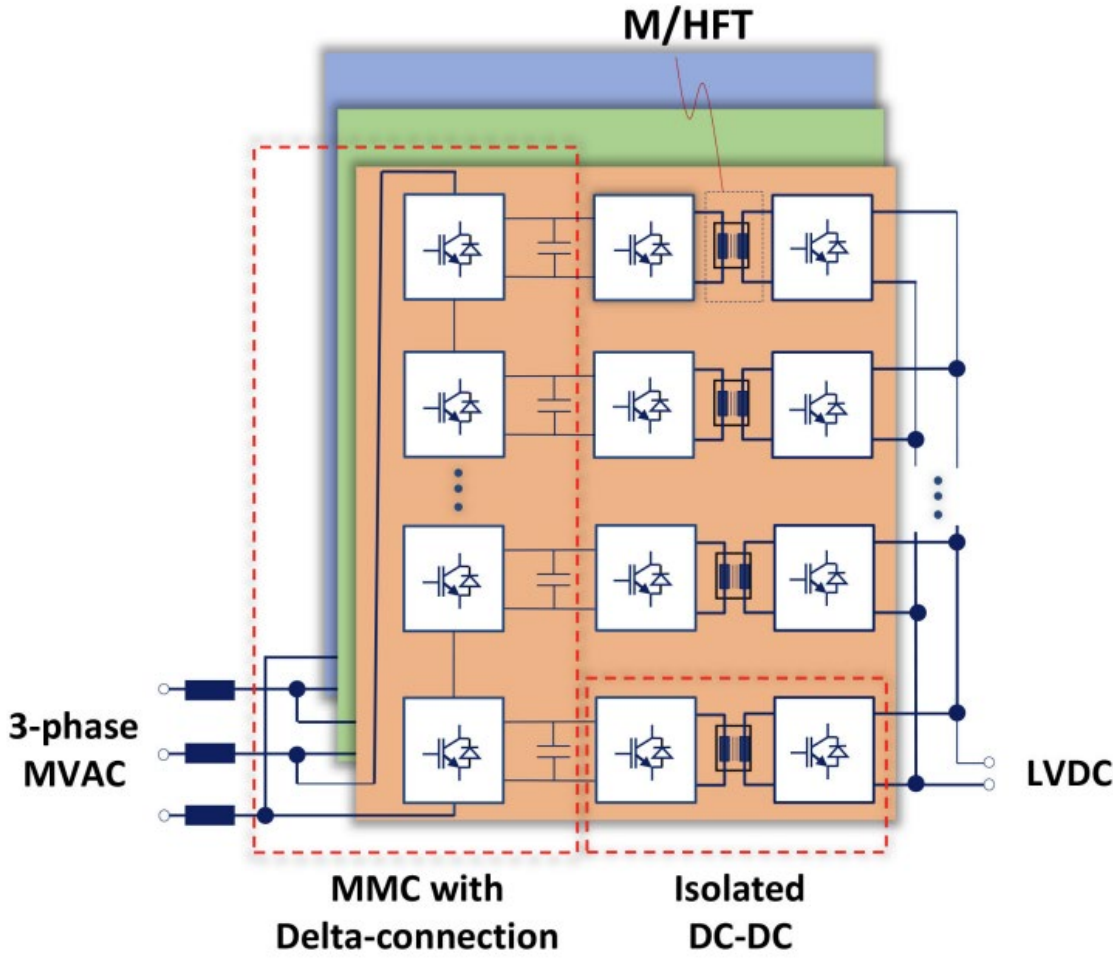

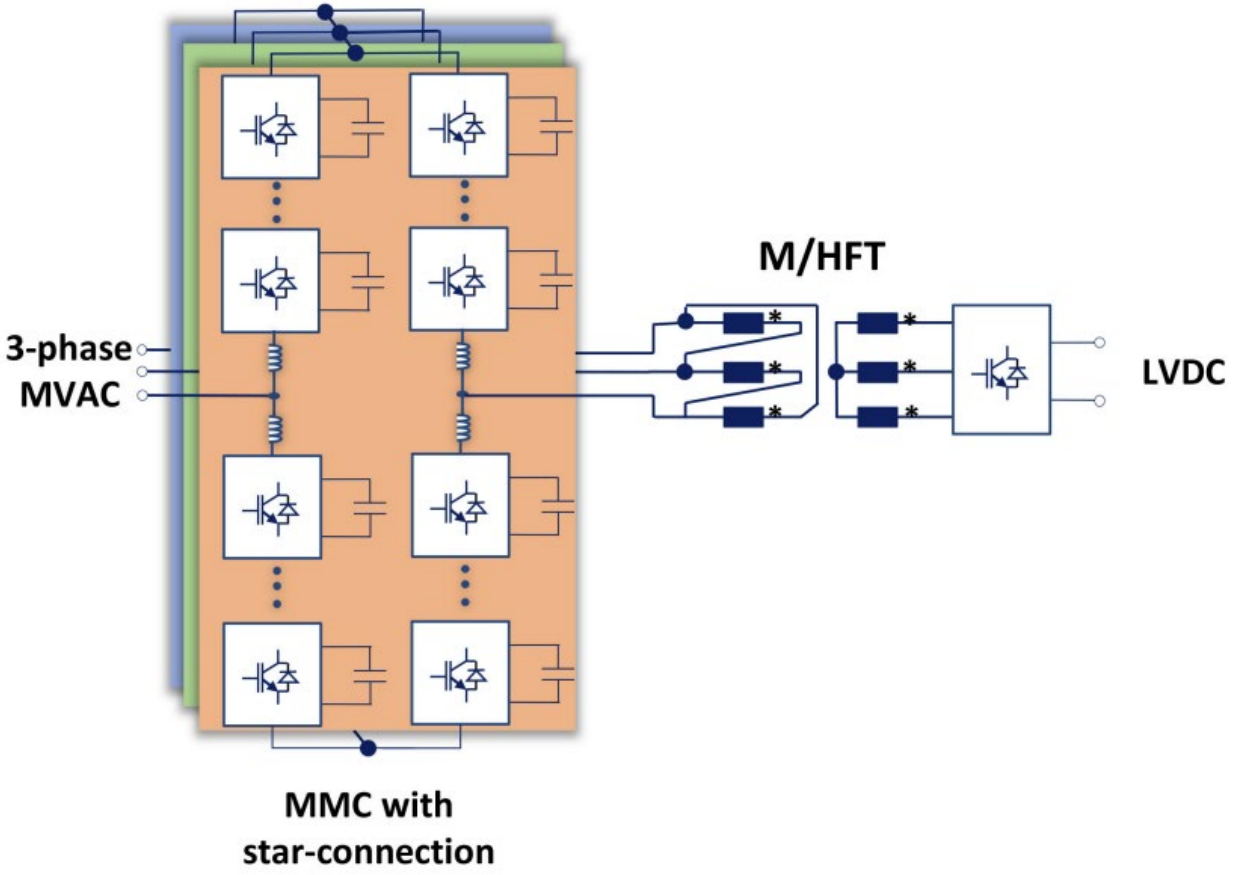

- Modular transformer -> LV on windings
- Each trafo needs MV isolation

- Single transformer -> MV on windings
- More compact

Source: A Ahmad, et. al. “An Overview on Medium Voltage Grid Integration of Ultra-Fast Charging Stations: Current Status and Future Trends,” *IEEE OJIES*, 2022

SST BASED MV MW CHARGER

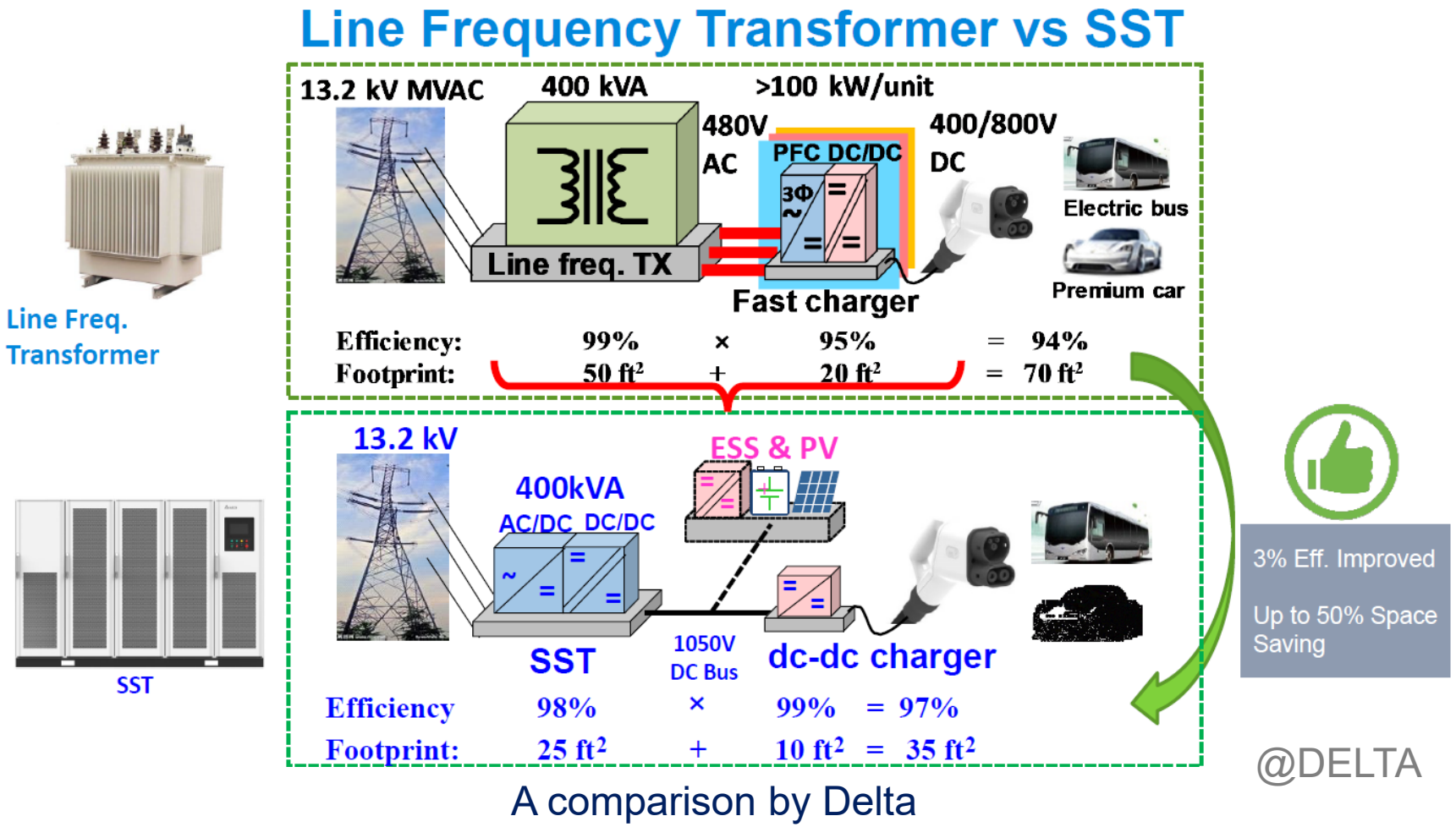

A comparison by Delta

- SST becomes appealing, especially if there is DC in the power conversion

Source: Delta

WRAP UP

- **The DC chargers' power rating is increasing** to reduce the charging time. The battery voltage is increasing to 800 V to adapt to higher charging power. DC Chargers have to **cover from 200~1000 V** for a better market share

- In heavy-duty e-transportation, the charger is typically connected to a medium voltage grid and rated at MWs. For **MV MW chargers, SST becomes appealing and even viable** for the MVAC/LVDC power conversion

- **Charging is triggering more power quality issues** in the distribution network, especially the high-frequency harmonics, i.e. supraharmonics. It is not fully regulated yet and needs more attention.

- **Grid congestion** is becoming more significant. **Integration of batteries** is promising and necessary to reduce the overall cost of energy, by reducing the grid fee

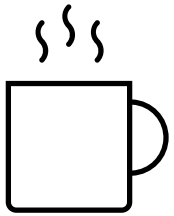

Coffee break 15 mins

OUTLINES

I. Introduction
- Standards
- Power conversion
- Grid impact
- Technical trends

II. Dynamic modelling
- Impedance modelling
- Gray-box modelling
- Solutions and implementations

III. Analytic control design
- Motivations
- Small-signal stability criteria for charger's PFC
- Analytical derivation of design boundaries
- Analytic design procedure

IV. Q&A

IMPEDANCE-BASED APPROACH

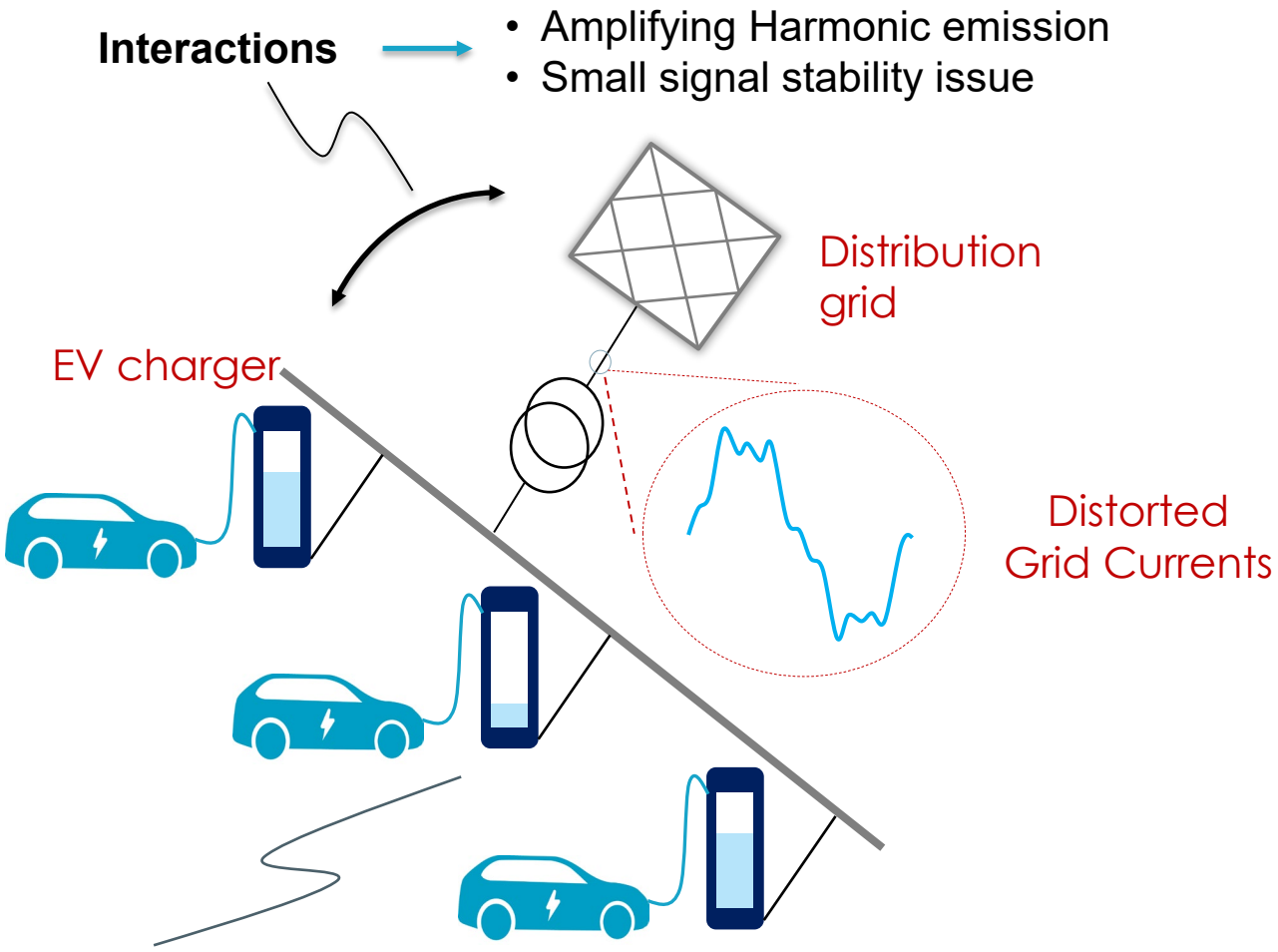

slow change of charging power
(compare to converter dynamics)

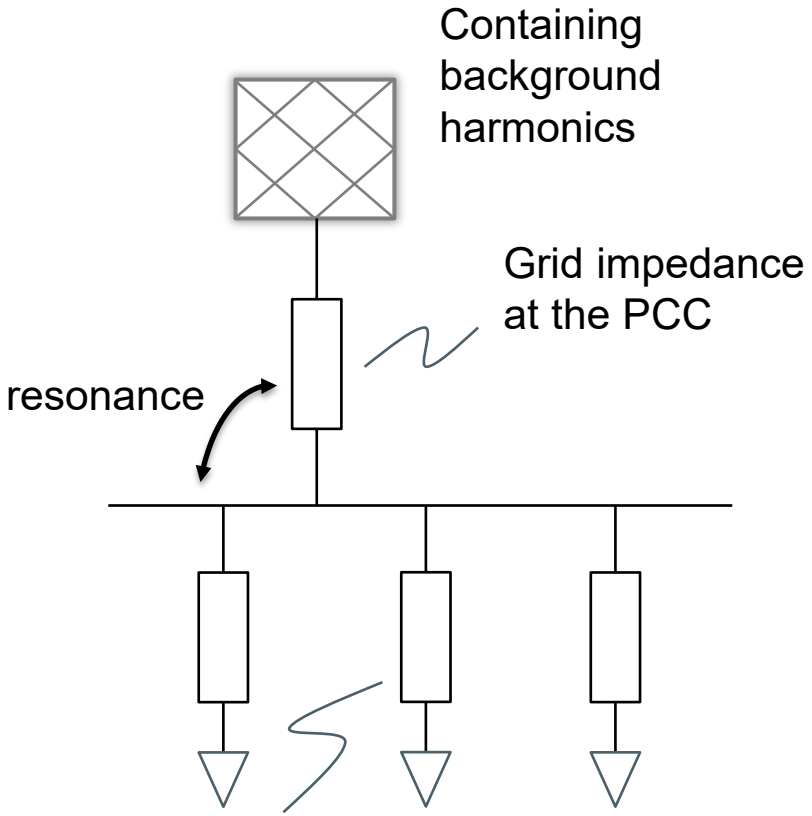

Charger's input impedance
at an operating point

EV CHARGER DESIGN

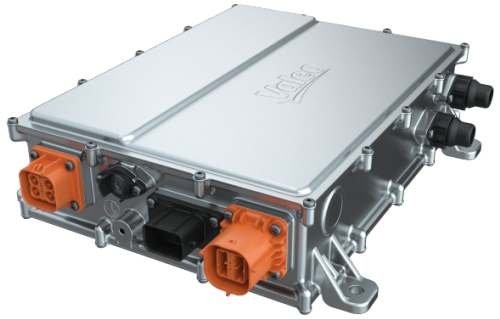

On-Board Charger (@Valeo)
6.6 kW, 11 kW, 22 kW

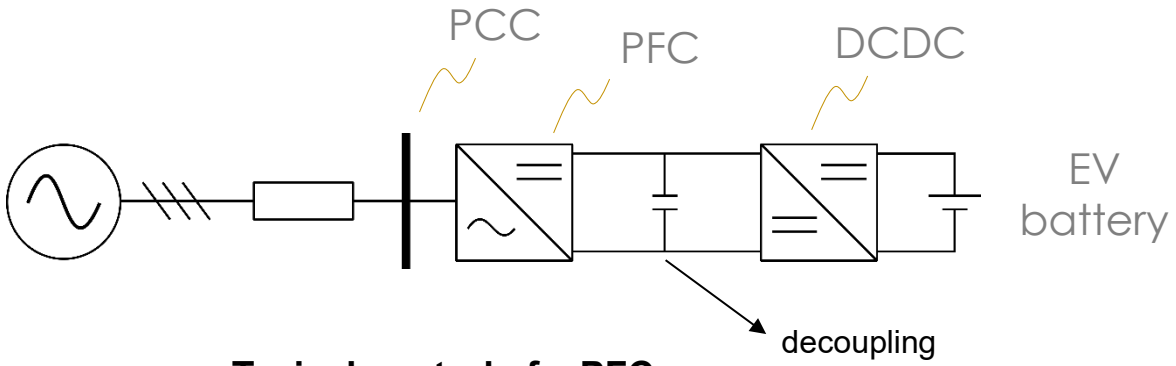

Typical control of a PFC

Off-Board Charger (@Autel)
> 50 kW

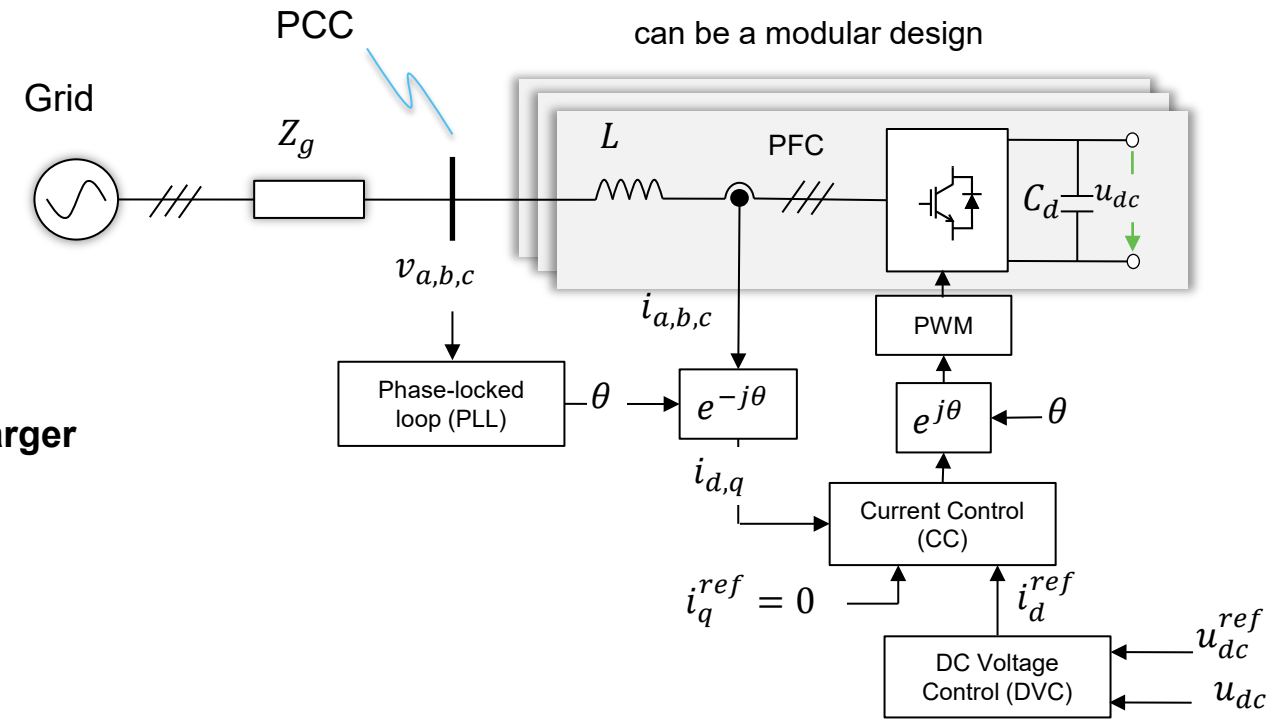

IMPEDANCE MODELLING

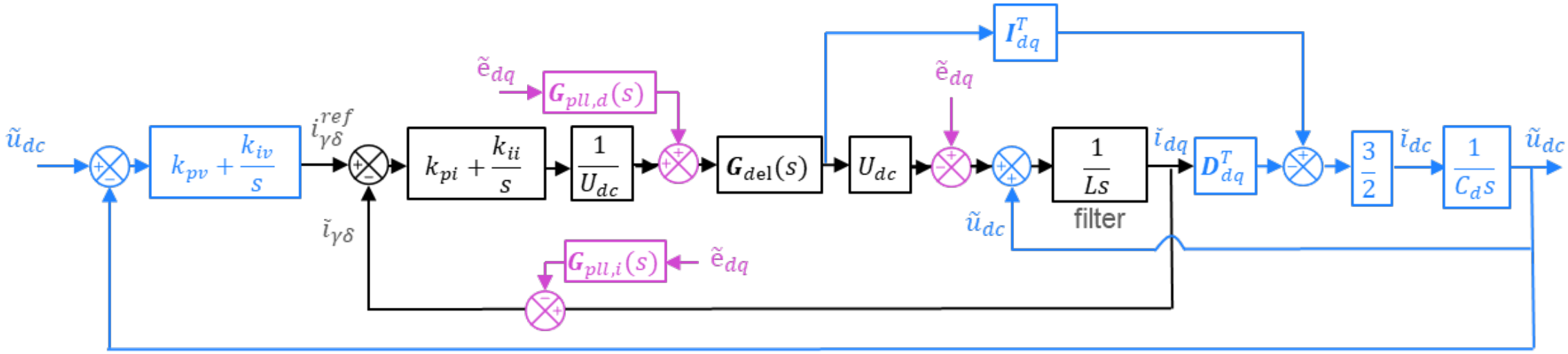

Current dynamics (CL) Grid voltage dynamics (PLL)
DC voltage dynamics (VL)

Model in the dq-domain

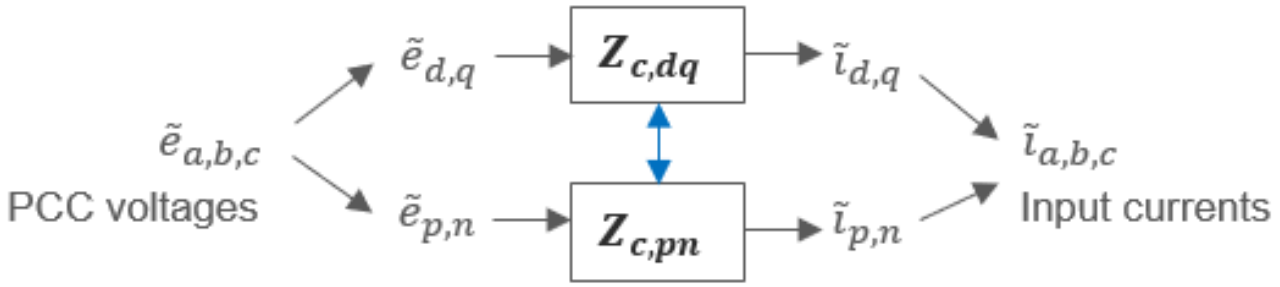

Model in the sequence-domain

$$Z_{c,\mathrm{dq}}(s) = \begin{bmatrix} Z_{dd}(s) & Z_{dq}(s) \\ Z_{qd}(s) & Z_{qq}(s) \end{bmatrix}$$

CHALLENGE OF WHITE BOX APPROACH

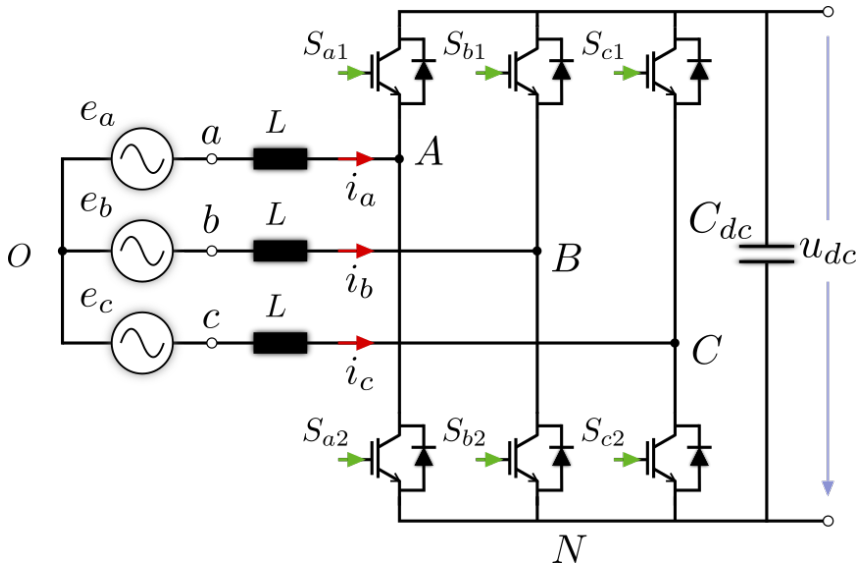

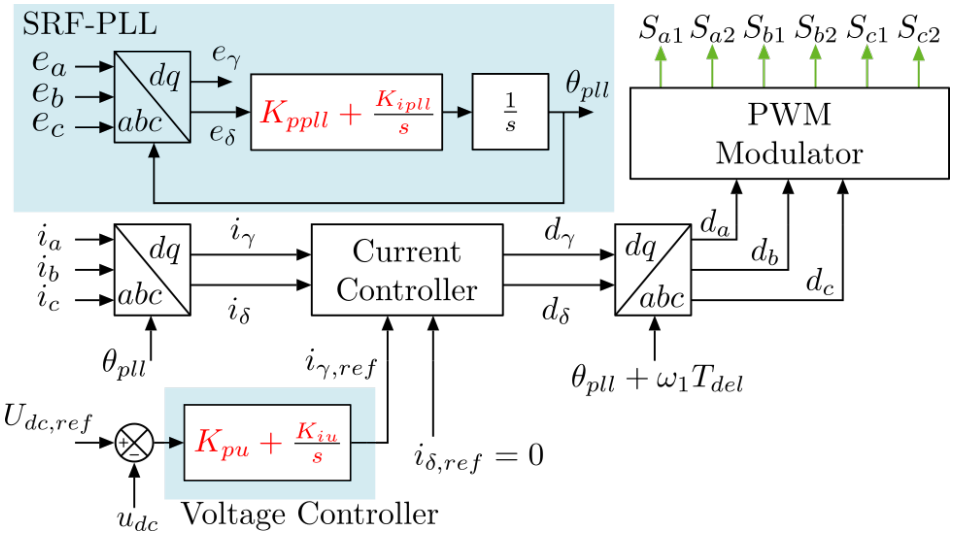

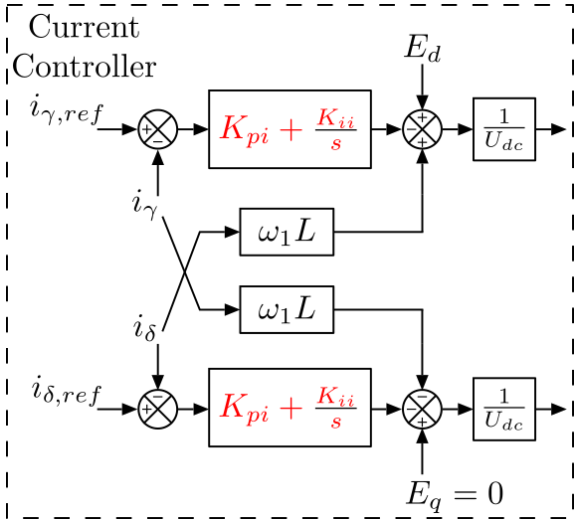

Industry Encryption

White box modelling

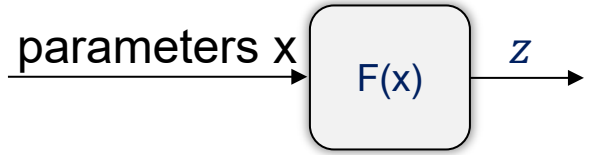

Lack design information especially the values of the **controller parameters** and the **circuit parameters**

CHALLENGE OF BLACK BOX APPROACH

Frequency sweep to scan the input impedance of the charger

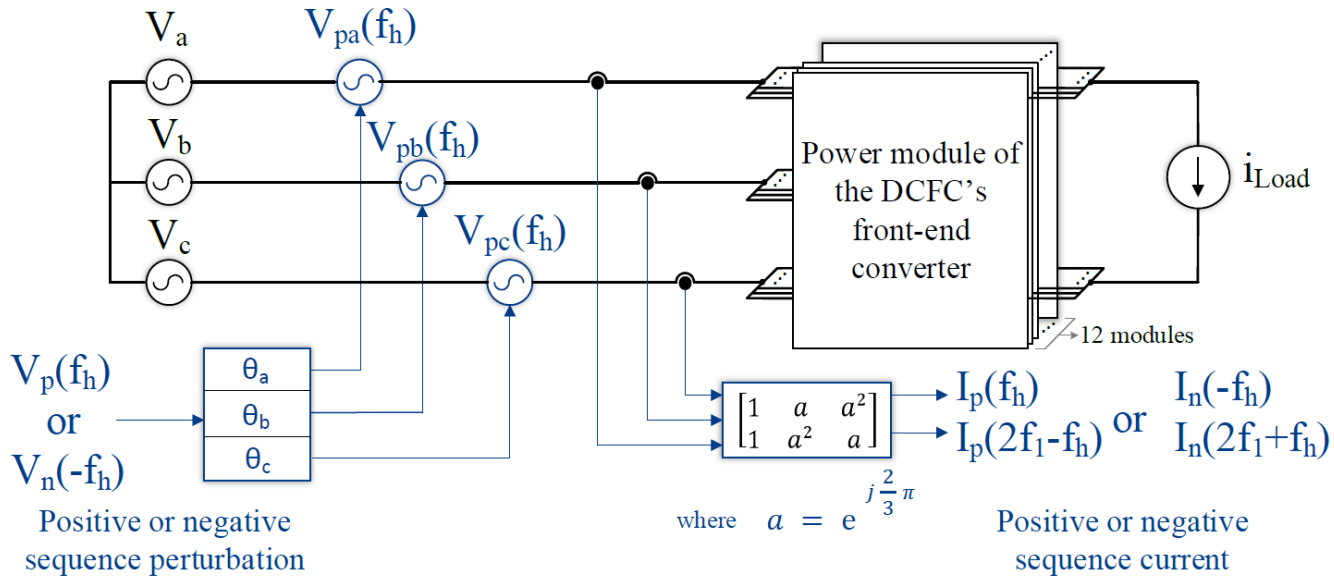

$$Z_p(f_h) = \frac{V_p(f_h)}{I_p(f_h)} \quad \text{and} \quad Z_n(f_h) = \frac{V_n(f_h)}{I_n(f_h)}$$

Black box modelling

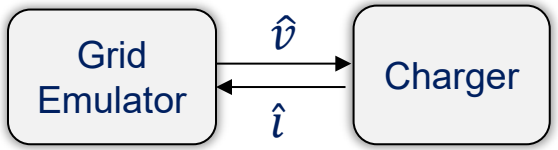

$$z = \frac{\hat{v}}{\hat{\imath}}$$

- Time consuming (impedance is different at different charging power)
- Sensitive to noises
- Difficult to get a complete impedance profile for a comprehensive analysis

CONCEPT OF GRAY BOX MODELLING

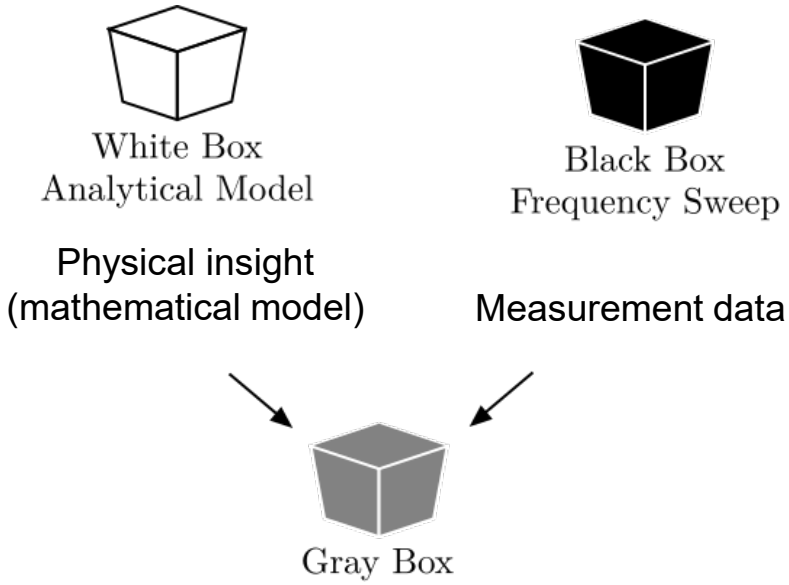

Gray box modelling [1]

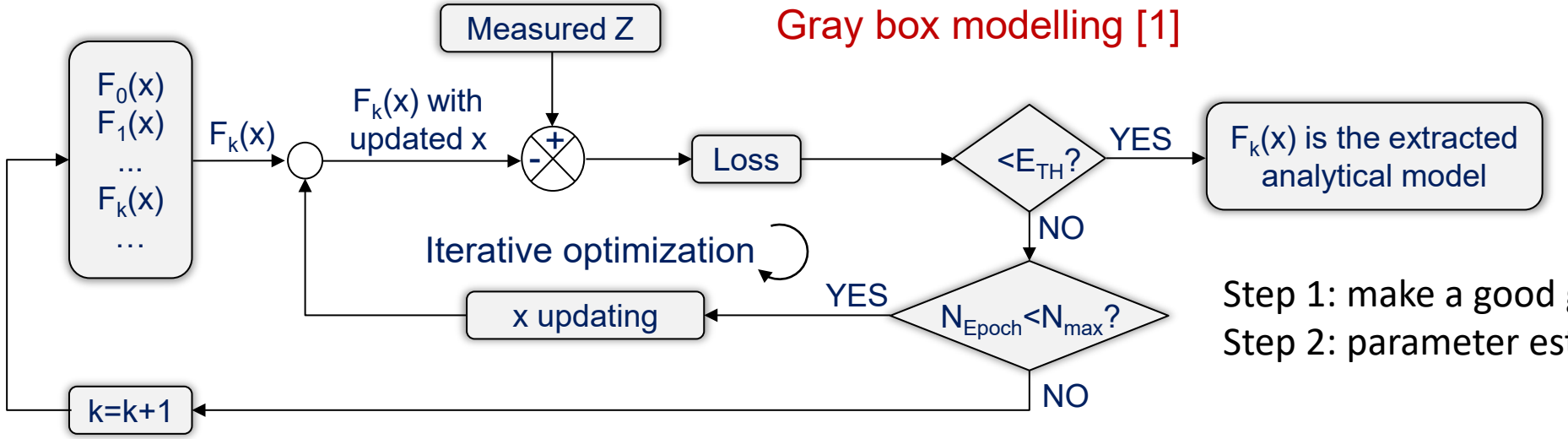

Step 1: make a good guess of the model
Step 2: parameter estimation

Source: [1] L Wang, et. al. "A gradient-descent optimization assisted gray-box impedance modeling of ev chargers," *TPEL*, 2023

CONCEPT OF GRAY BOX MODELLING

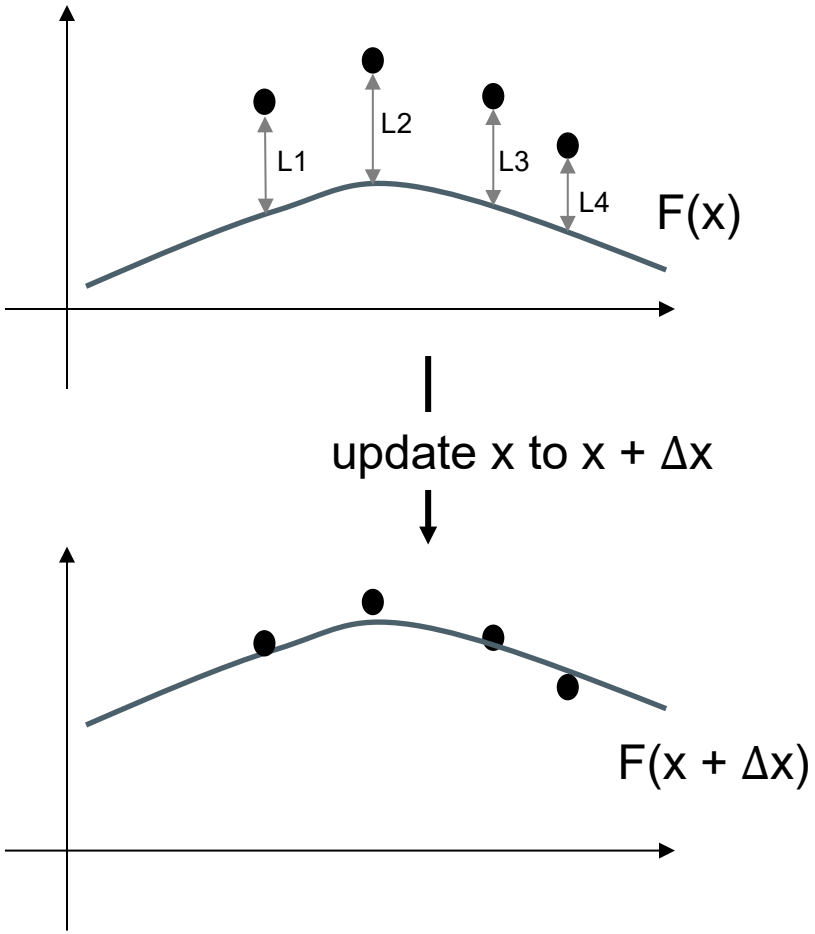

Parameter identification: An optimization problem

Parameters to be identified:

L	K_{pi}	K_{ii}	K_{ppll}	K_{ipll}	K_{pu}	C_{out}	K_{iu}

Analytical impedance model:

$$\boldsymbol{Z}(L, K_{pi}, K_{ii}, K_{ppll}, K_{ipll}, K_{pu}, K_{iu}, C_{out}, f)$$

$$= \begin{bmatrix} Z_{dd}(j2\pi f) & Z_{dq}(j2\pi f) \\ Z_{qd}(j2\pi f) & Z_{qq}(j2\pi f) \end{bmatrix} \rightarrow \begin{cases} |Z_{dd}|, \angle Z_{dd} \\ |Z_{dq}|, \angle Z_{dq} \\ |Z_{qd}|, \angle Z_{qd} \\ |Z_{qq}|, \angle Z_{qq} \end{cases}$$

CHALLENGES OF GRAY BOX MODELLING

TU Delft

Comparison of different optimization methods

Method	Type	Key idea	Pros	Cons	Application
Gradient Descent	Deterministic	Iteratively updates parameters in the direction of the negative gradient.	Fast; efficient for differentiable problems; Scalable for high-dimensional problems	Stuck in local minima and saddle points; Local search	Machine learning training
Genetic Algorithm	Stochastic	maintaining a population of candidate solutions and evolving them over generations.	No mathematical model required; Global search; Avoids local minima; Suitable for non-convex	Slow; Computationally expensive;	feature selection; Hyperparameters tuning of NN.
Particle Swarm	Stochastic	find the best solution in a search space by adjusting the positions of multiple candidate solutions (particles)	No mathematical model required; Global search; Less sensitive to the initial starting positions	Slow; Can be stuck in local minima	Hyperparameters tuning of NN; NN structure selection
Newton-Raphson	Deterministic	iteratively approaches the solution using second-order derivatives	Converges very quickly for convex problems	Requires second-order derivatives; Expensive for large problems	Solving non-linear equations, convex problems.

CHALLENGES OF GRAY BOX MODELLING

The magnitude difference among different parameters to be estimated is big and we cannot normalize them.

Loss function:

$$e\left(L, C_{dc}, k_{pi}, k_{ii}, k_{ppll}, k_{ipll}, k_{pv}, k_{iv}\right)$$
$$= \frac{1}{8}\sum_m\left[\frac{1}{N}\sum_{i=1}^{N}\left[\left(\left|\hat{Z}_m(f_i)\right| - \left|Z_m(f_i)\right|\right)^2 + \left(\angle\hat{Z}_m(f_i) - \angle Z_m(f_i)\right)^2\right]\right]$$

$\downarrow$

dd, dq, qd, qq

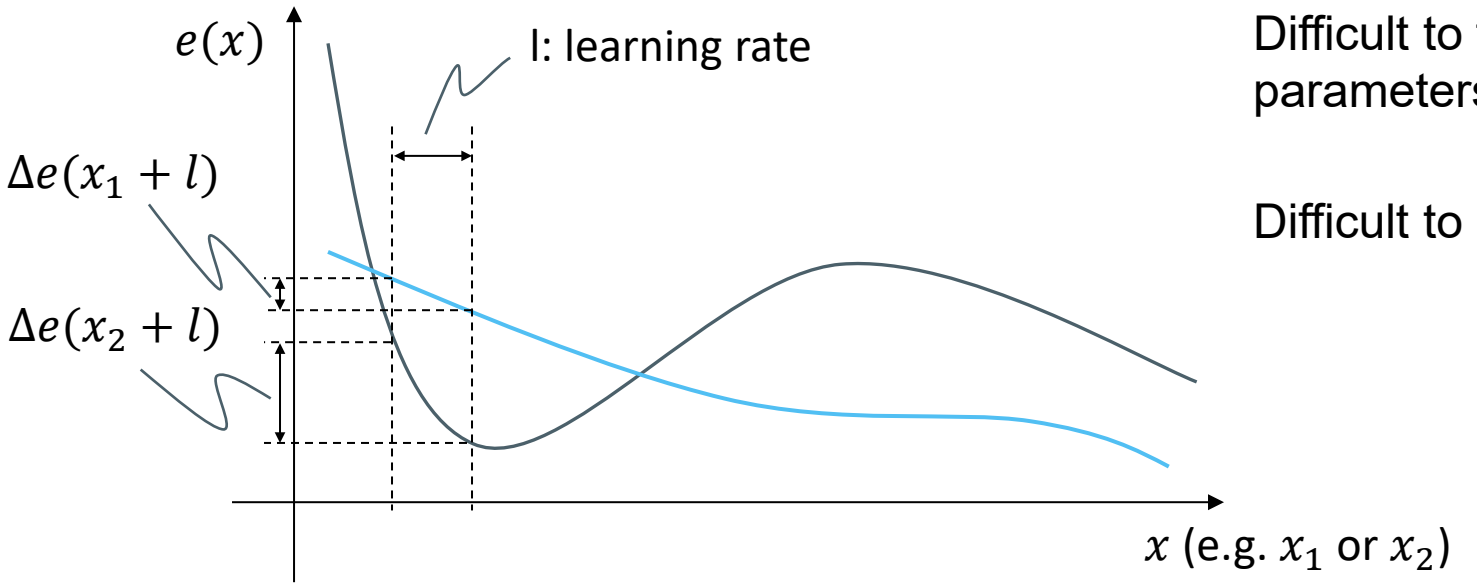

Difficult to find a learning rate suitable for all the parameters

$\downarrow$

Difficult to estimate all the parameters together

CHALLENGES OF GRAY BOX MODELLING

The loss is non-convex in such a high-dimension problem

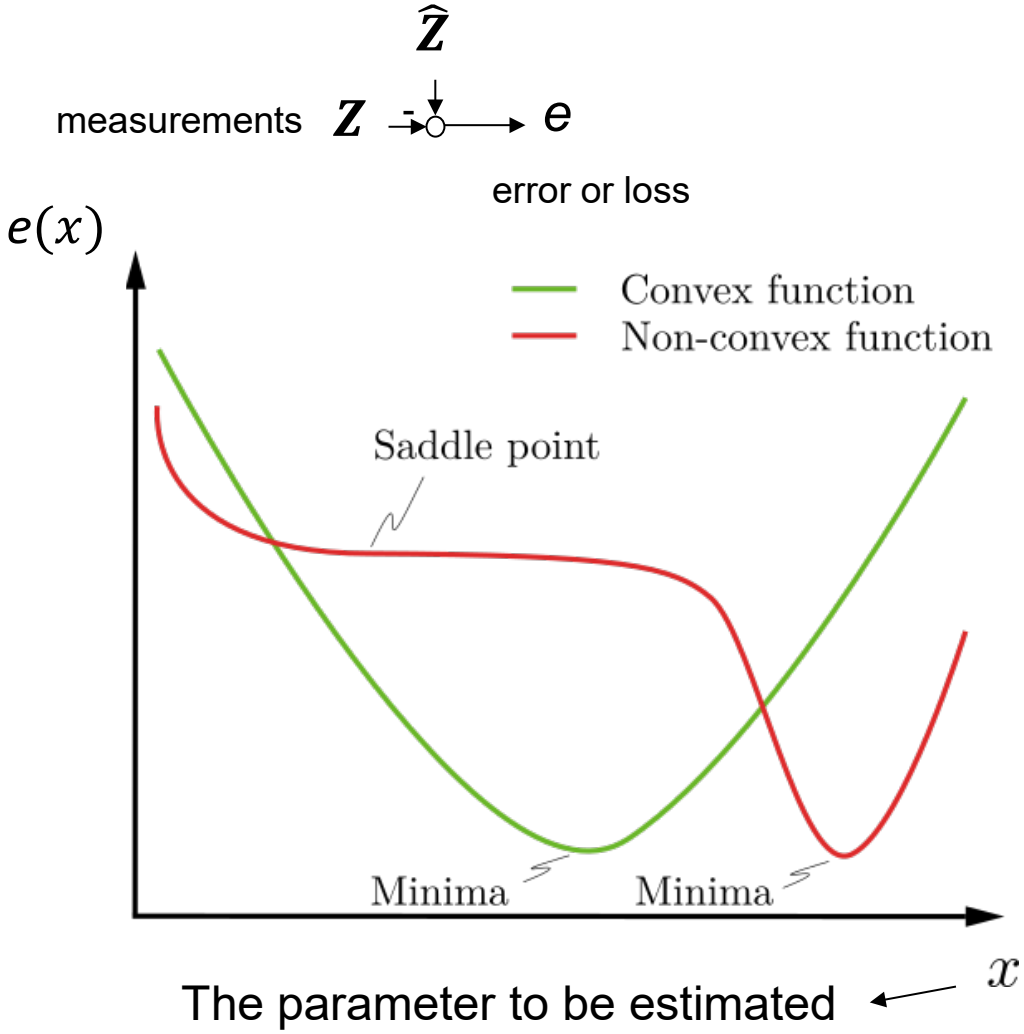

$$e\left(L, C_{dc}, k_{pi}, k_{ii}, k_{ppll}, k_{ipll}, k_{pv}, k_{iv}\right)$$
$$= \frac{1}{8}\sum_{m}\left[\frac{1}{N}\sum_{i=1}^{N}\left[\left(\left|\hat{Z}_m(f_i)\right| - \left|Z_m(f_i)\right|\right)^2 + \left(\angle\hat{Z}_m(f_i) - \angle Z_m(f_i)\right)^2\right]\right]$$

$\downarrow$

dd, dq, qd, qq

Saddle points occur when the estimated impedance is insensitive to the change of the parameter. Very common in high-dimension problems.

Solution:
It is noted that different parameters

- Influence different impedance components, namely $Z_{dd}, Z_{dq}, Z_{qd}, Z_{qq}$.
- have different influential frequency ranges

REVISITING IMPEDANCE MODEL

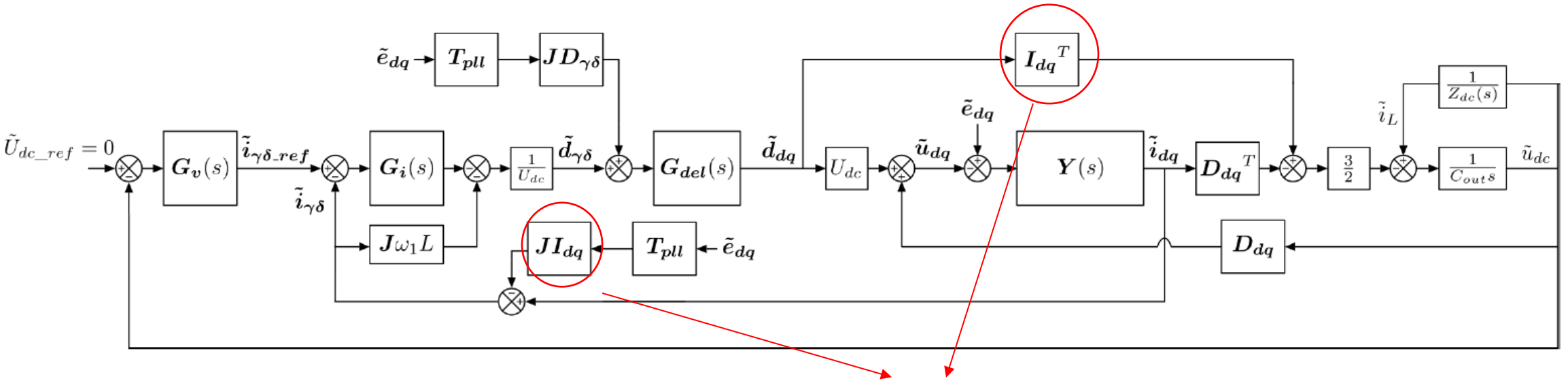

= 0 when P=Q=0, simpler expressions

Expressions of the impedance matrix elements when P=Q=0

$$Z_{dd\_0}(s) = \left(Ls + R + \frac{3E_g^2}{2C_d U_{dc}^2 s}\right)\left(1 + G_{oi,dd}(s)\right)\left(1 + G_{ov}(s)\right)$$

$$Z_{dq\_0}(s) = -\omega_1 L(1 - e^{-sT_{del}})$$

$$Z_{qd\_0}(s) = (Ls + R)\frac{\omega_1 L(1-e^{-sT_{del}})}{1-G_{cpll}(s)e^{-sT_{del}}}$$

$$Z_{qq\_0}(s) = (Ls + R)\frac{1+G_{oi,qq}(s)}{1-G_{cpll}(s)e^{-sT_{del}}}$$

T_{del}: digital control delay 1.5 switching period.
G_{ov}: open-loop transfer function of the voltage loop.
G_{oi}: open-loop transfer function of the current loop
G_{cpll}: close-loop transfer function of the PLL

REVISITING IMPEDANCE MODEL

$$Z_{dd\_0}(s) = \left(Ls + R + \frac{3E_g^2}{2C_d U_{dc}^2 s}\right)\left(1 + G_{oi,dd}(s)\right)\left(1 + G_{ov}(s)\right)$$

≈ 0 when $\omega \gg \omega_{ci}$

$$Z_{dq\_0}(s) = -\omega_1 L(1 - e^{-sT_{del}})$$

$$Z_{qd\_0}(s) = (Ls + R)\frac{\omega_1 L(1 - e^{-sT_{del}})}{1 - G_{cpll}(s)e^{-sT_{del}}}$$

$$Z_{qq\_0}(s) = (Ls + R)\frac{1 + G_{oi,qq}(s)}{1 - G_{cpll}(s)e^{-sT_{del}}}$$

Observations:

- Z_{dq_0} is only influenced by L
- Z_{dd_0} is not influenced by the PLL parameters
- Z_{qq_0} is not influenced by the VL parameters
- Controller parameters do not influence the impedance shape beyond the cut-off frequency of the control loop
- Beyond the cut-off frequency of all control loops, the input impedance is basically the filter impedance

REVISITING IMPEDANCE MODEL

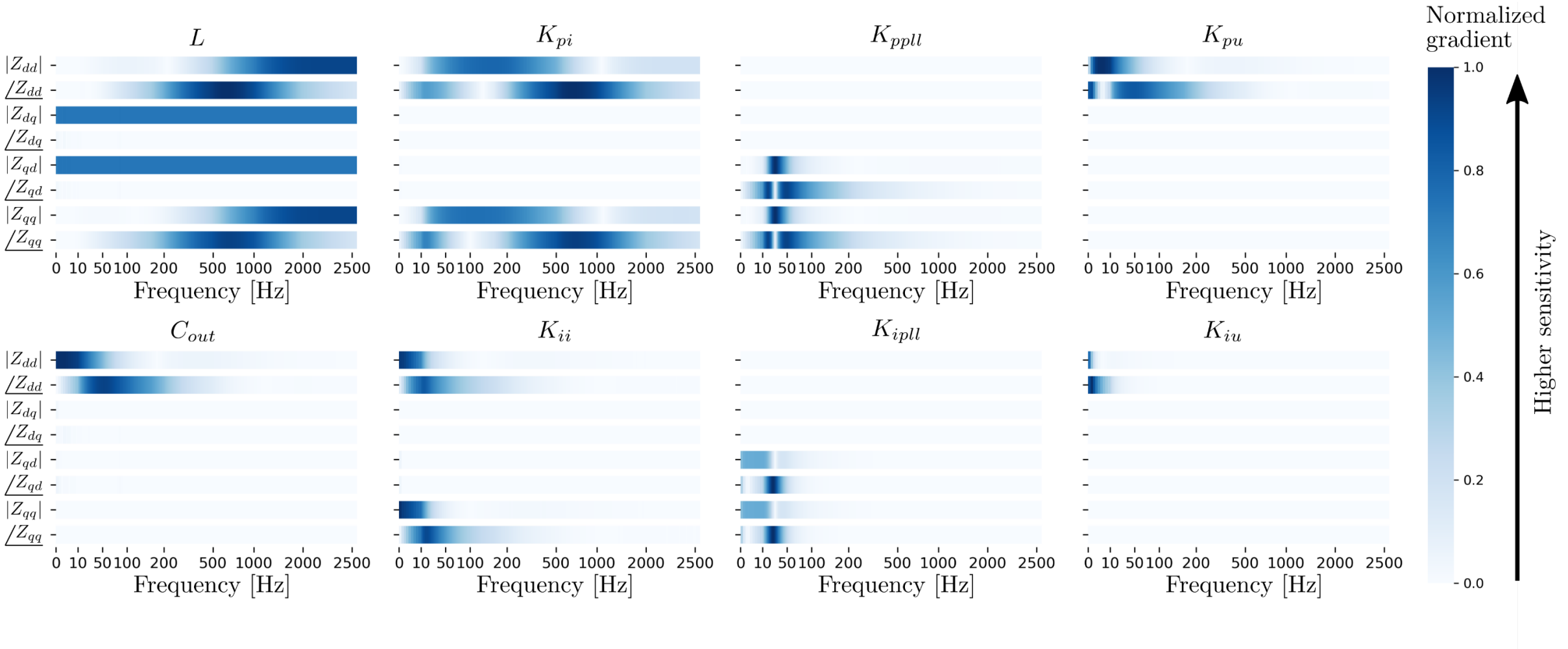

PARAMETER ESTIMATION METHOD

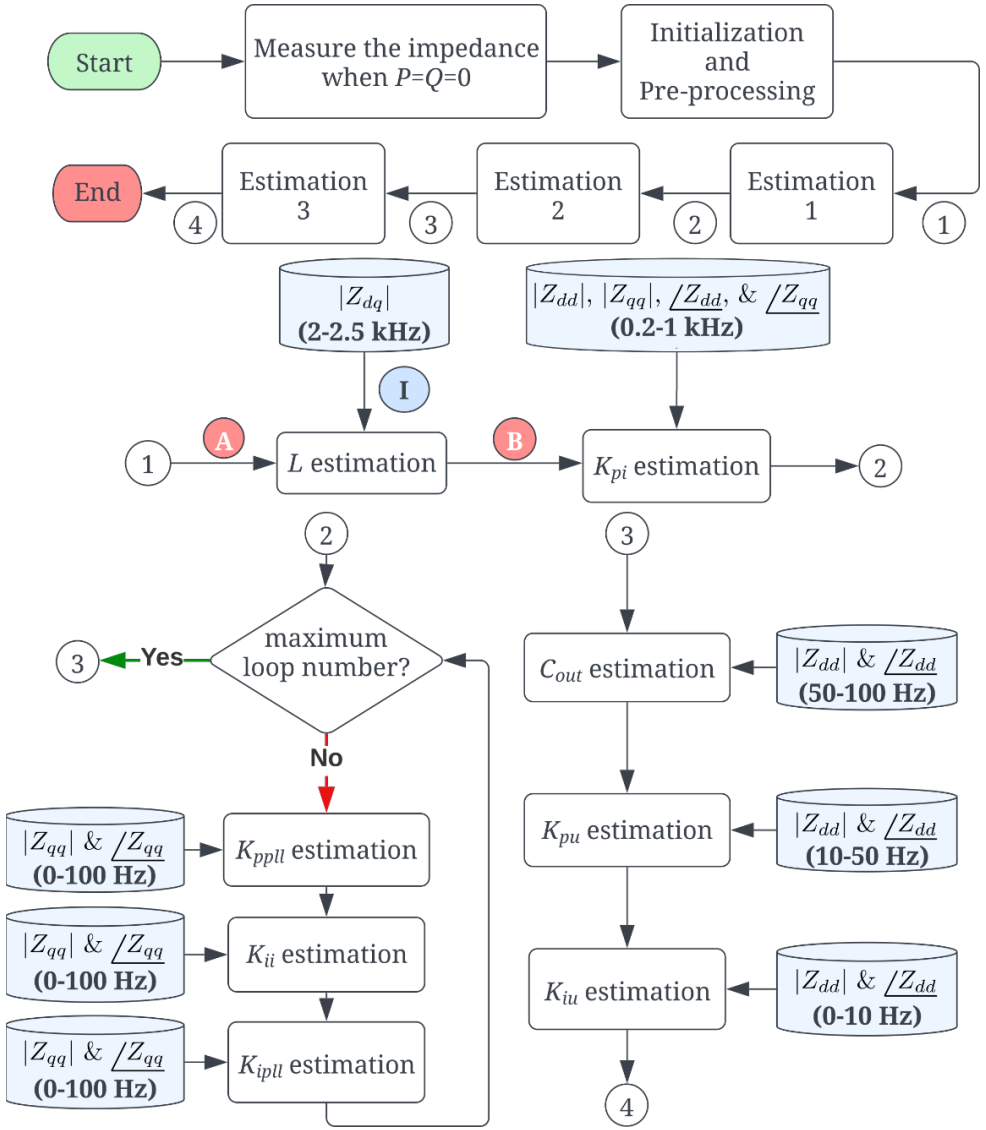

- Identify the parameters in sequence
- Use the impedance segment sensitive to the parameter to construct the loss function to prevent creating saddle points in the loss function

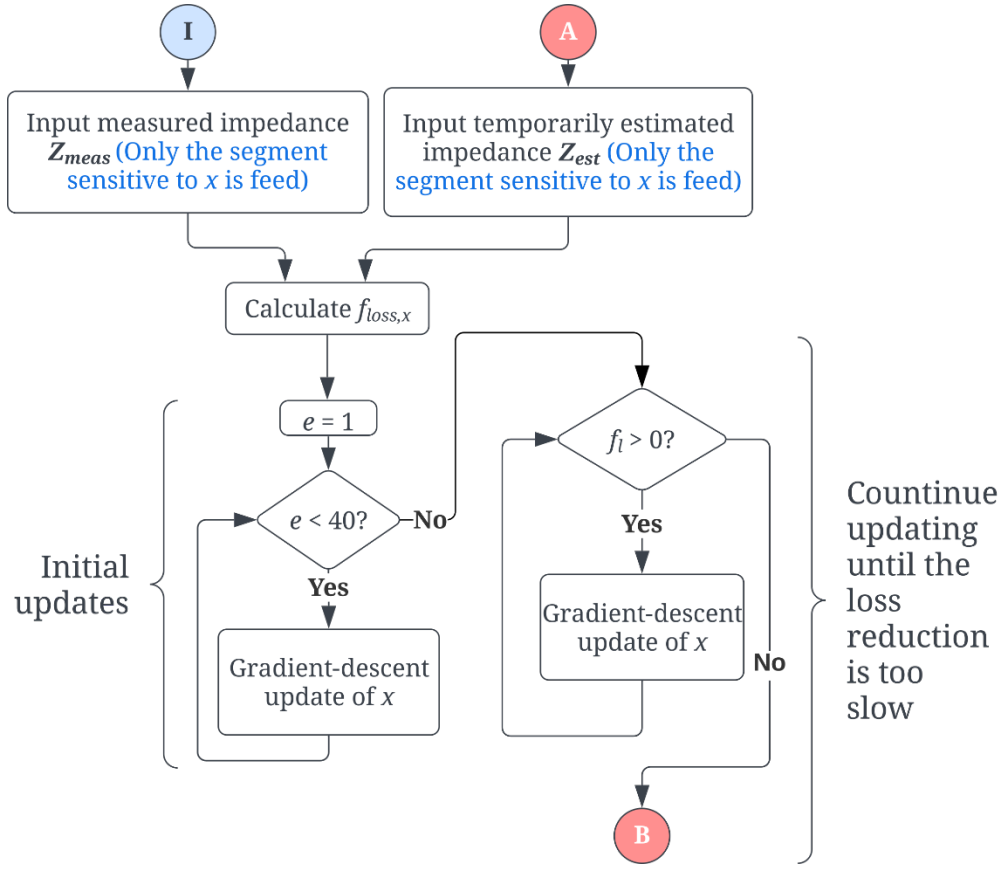

IMPLEMENTATION OF THE METHOD

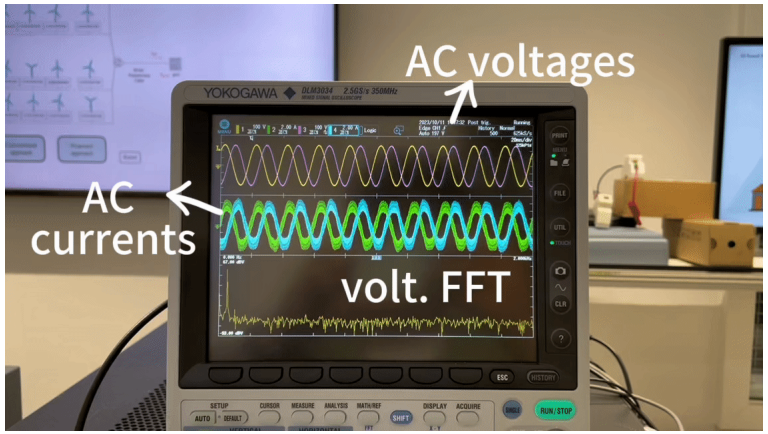

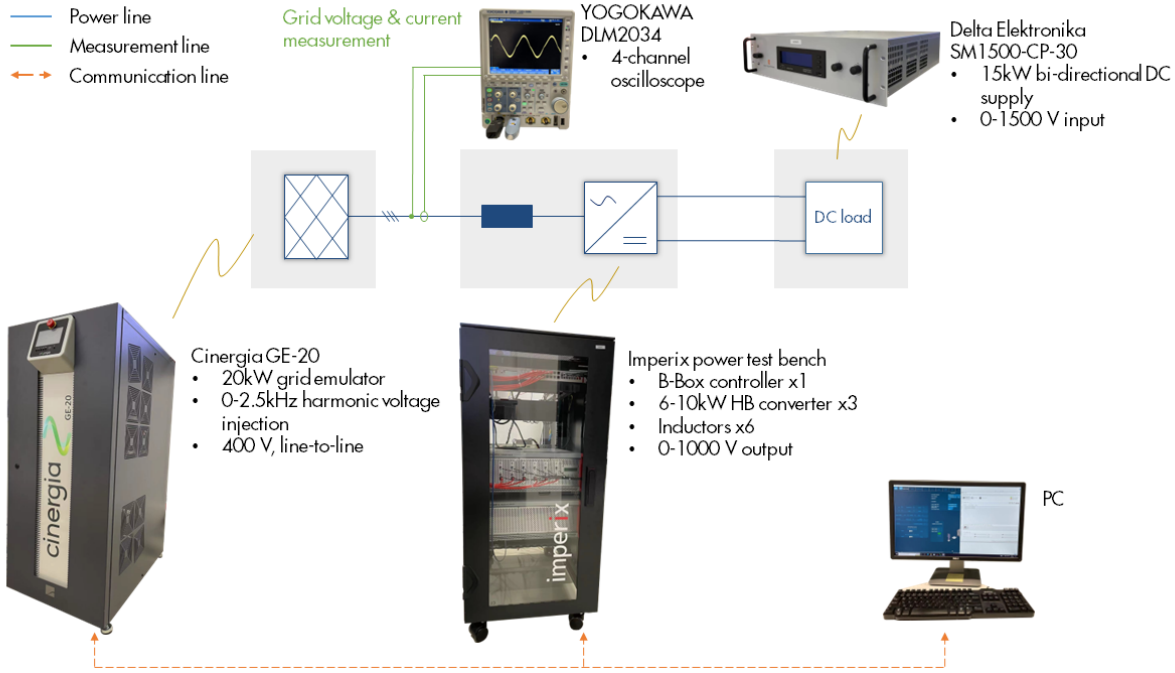

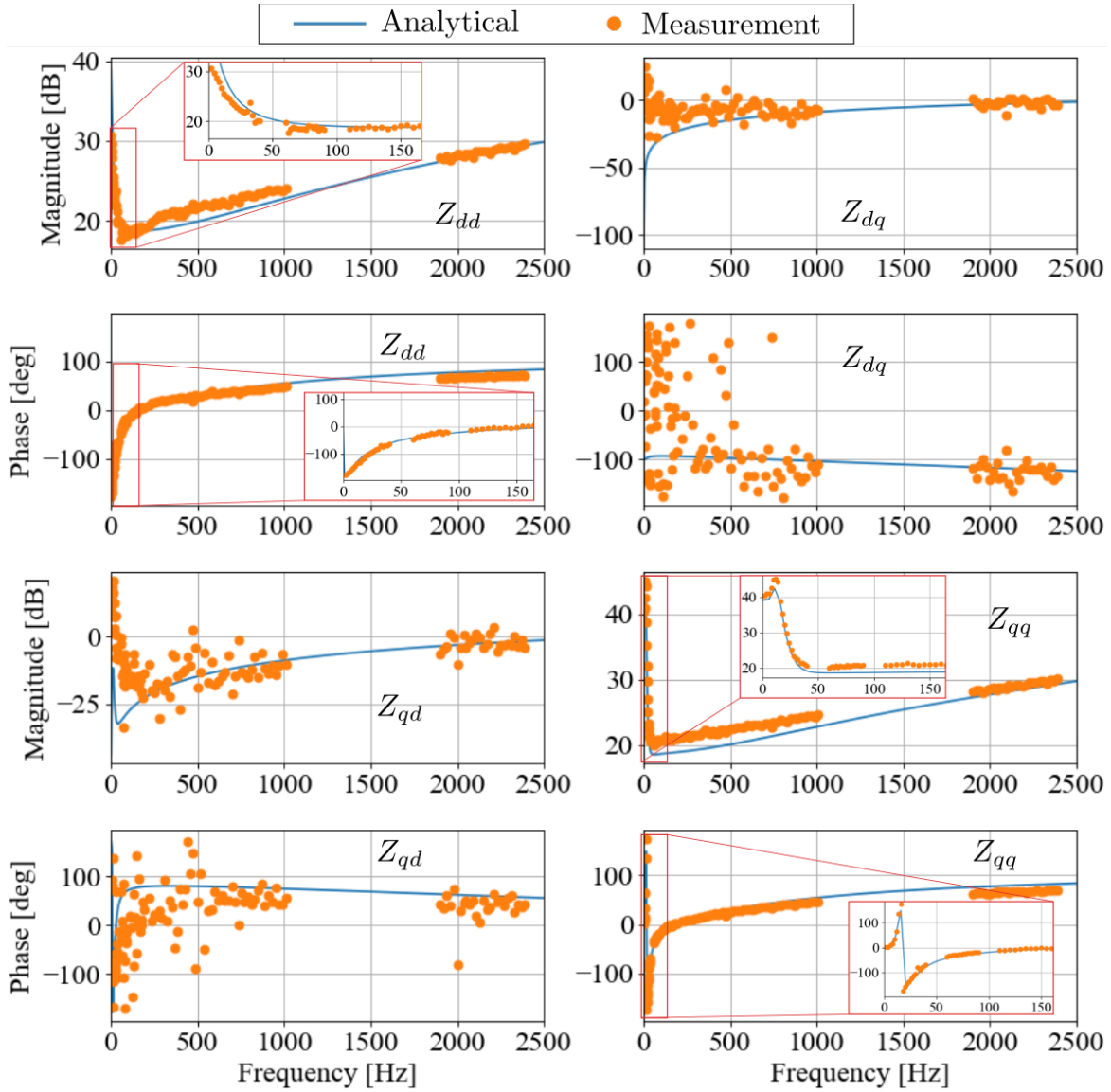

IMPLEMENTATION OF THE METHOD

Three designs used for the verification

Parameter	Design 1	Design 2	Design 3
L [mH]	2.5	2.5	1.25
K_{pi}	9	15.7	1.57
K_{ppll}	1.21	4	2.42
K_{ii}	1000	15297	306
K_{ipll}	228	634	914
C_{out} [mF]	1.67	1.67	3.21
K_{pu}	0.2	0.43	0.33
K_{iu}	2	10.47	4.66
U_{dc} [V]	385		
f_{sw} [kHz]	20		
E_g [V]	$110\sqrt{2}$		

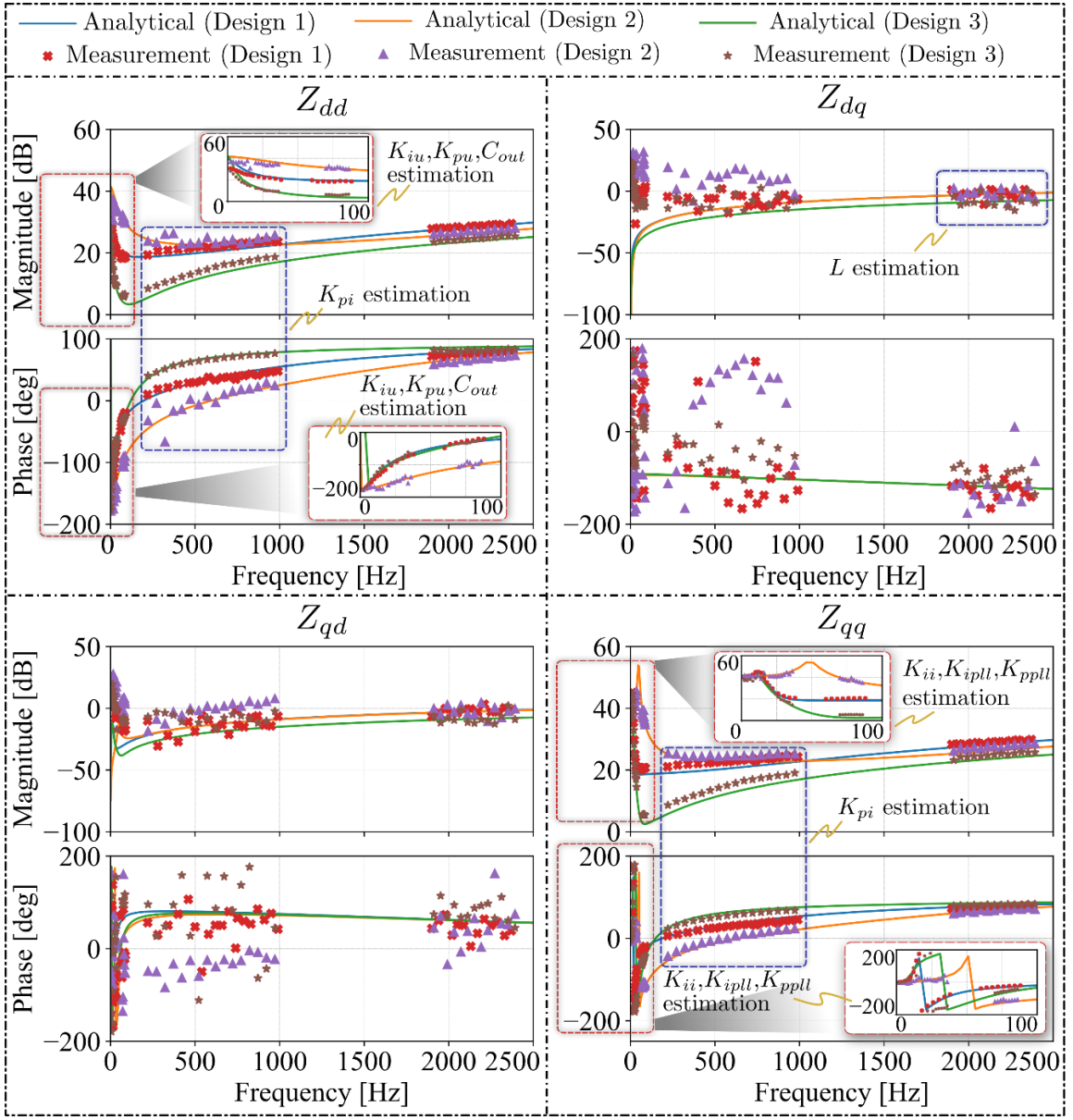

IMPLEMENTATION OF THE METHOD

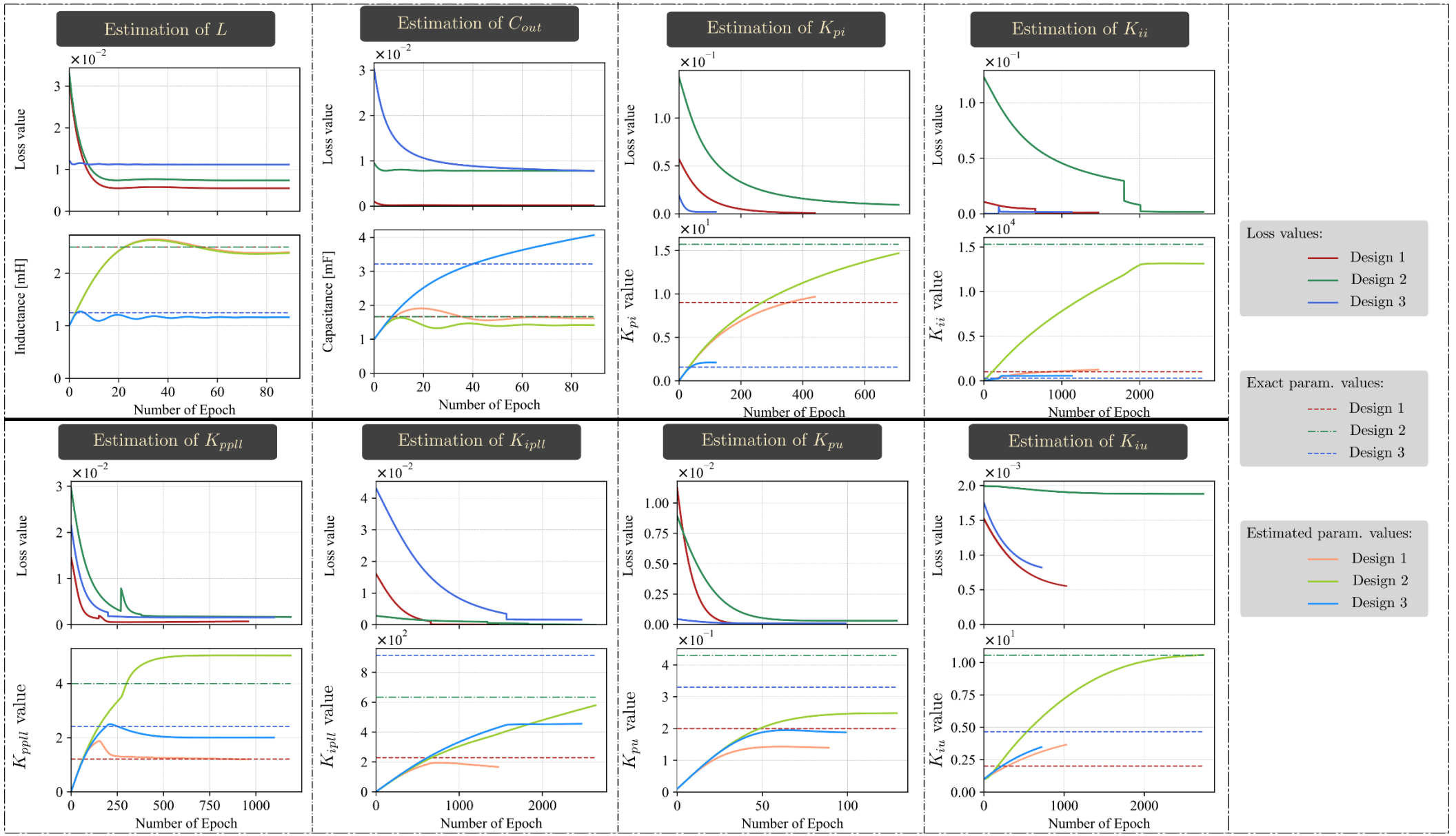

IMPLEMENTATION OF THE METHOD

Design 1			
	Exact	Proposed approach (error %)	Normal approach (error %)
L [mH]	2.5	2.4 (4%)	12.6 (404%)
K_{pi}	9	9.7 (8%)	0.39 (96%)
K_{ppll}	1.21	1.2 (1%)	0.43 (64%)
K_{ii}	1000	1264 (26%)	0.62 (100%)
K_{ipll}	228	166 (27%)	0.74 (100%)
C_{out} [mF]	1.67	1.62 (3%)	0.2 (88%)
K_{pu}	0.2	0.14 (30%)	0.37 (85%)
K_{iu}	2	3.63 (82%)	1.53 (24%)
Estimation time	N.A.	8 min.	24 min.

Design 2			
	Exact	Proposed approach (error %)	Normal approach (error %)
L [mH]	2.5	2.39 (4%)	12.9 (416%)
K_{pi}	15.7	14.69 (6%)	0.81 (95%)
K_{ppll}	4	5.04 (26%)	0.83 (79%)
K_{ii}	15297	13144 (14%)	1.86 (100%)
K_{ipll}	634	579 (9%)	1.7 (100%)
C_{out} [mF]	1.67	1.42 (15%)	0 (100%)
K_{pu}	0.43	0.25 (42%)	0.4 (7%)
K_{iu}	10.47	10.58 (1%)	2.34 (78%)
Estimation time	N.A.	17 min.	46 min.

Design 3			
	Exact	Proposed approach (error %)	Normal approach (error %)
L [mH]	1.25	1.16 (7%)	8.06 (545%)
K_{pi}	1.57	2.1 (34%)	0.47 (70%)
K_{ppll}	2.42	2.02 (17%)	0.44 (82%)
K_{ii}	306	558 (82%)	0.6 (100%)
K_{ipll}	914	453 (50%)	1.37 (100%)
C_{out} [mF]	3.21	4.08 (27%)	0.4 (88%)
K_{pu}	0.33	0.19 (42%)	0.61 (85%)
K_{iu}	4.66	3.45 (26%)	1.59 (66%)
Estimation time	N.A.	11 min.	30 min.

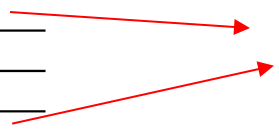

Get stuck at saddle points or local minima

IMPLEMENTATION OF THE METHOD

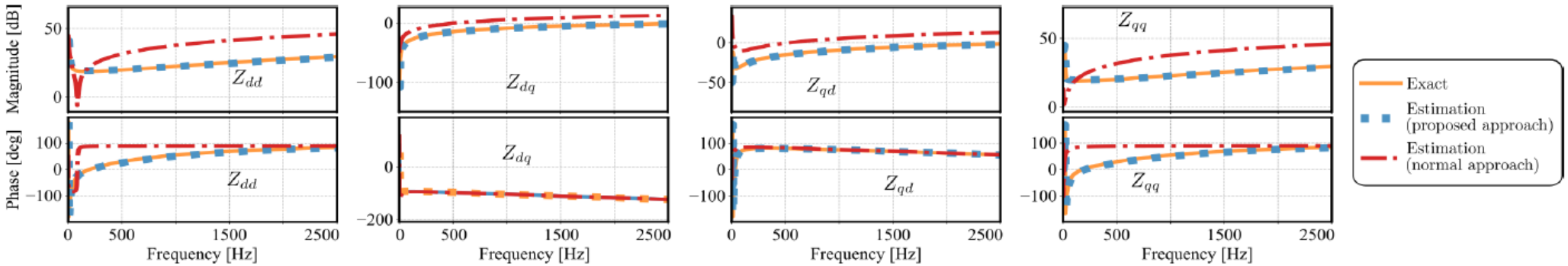

(a) Design 1

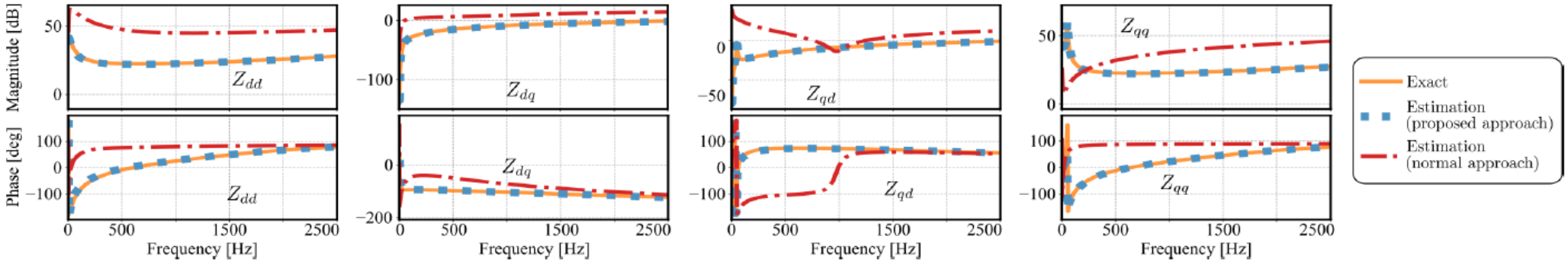

(b) Design 2

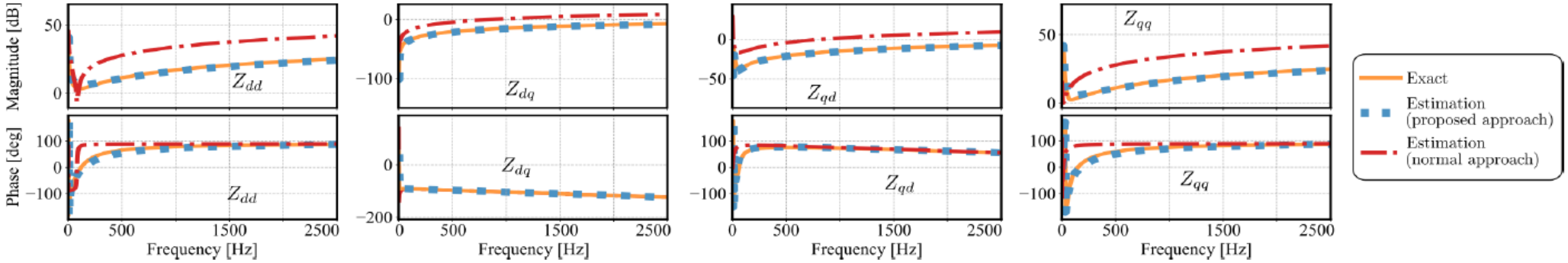

(c) Design 3

WRAP UP

- The unknown parameter values of a PFC can be **decrypted from the impedance curve**.
- The influential frequency range per parameters is related to the loop bandwidth of the loop that they are involved into, which helps to reduce the complexity of the task by **changing it from identifying all parameters together to identifying them in a sequence**.
- Selecting impedance data within a frequency range where the impedance is **sensitive to the changes** of the parameter to be estimated can **reduce saddle points** in the loss function, making it **more convex**.
- By applying the previous measure, the **accuracy** of the estimated parameters **can be improved**.

OUTLINES

I. Introduction
- Standards
- Power conversion
- Grid impact
- Technical trends

II. Dynamic modelling
- Impedance modelling
- Gray-box modelling
- Solutions and implementations

III. Analytic control design
- Motivations
- Small-signal stability criteria for charger's PFC
- Analytical derivation of design boundaries
- Analytic design procedure

IV. Q&A

GRID CONNECTION REQUIREMENTS

Impedance model of a charging system

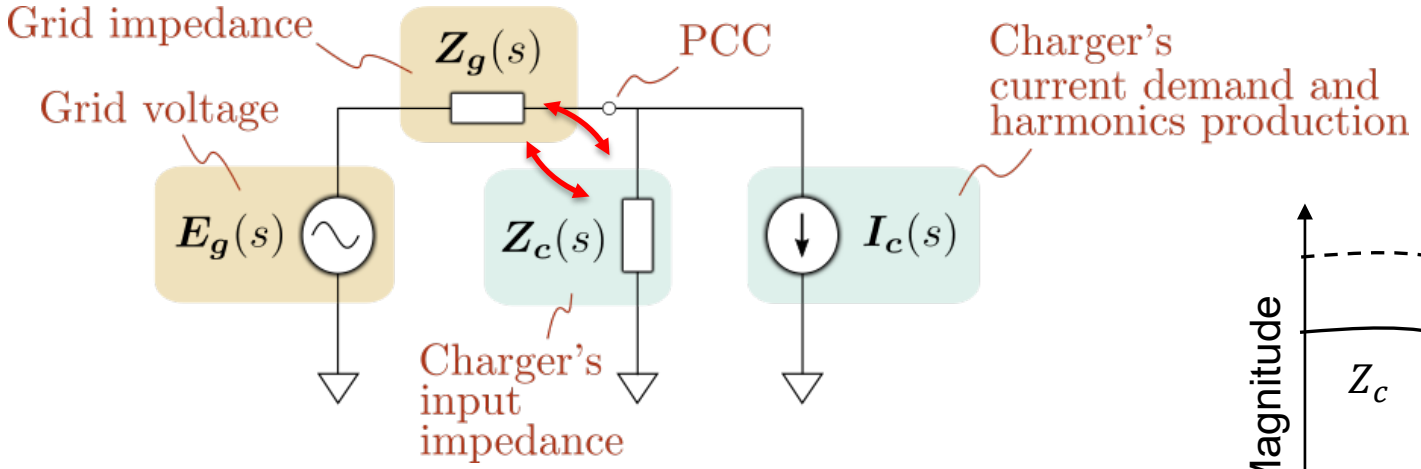

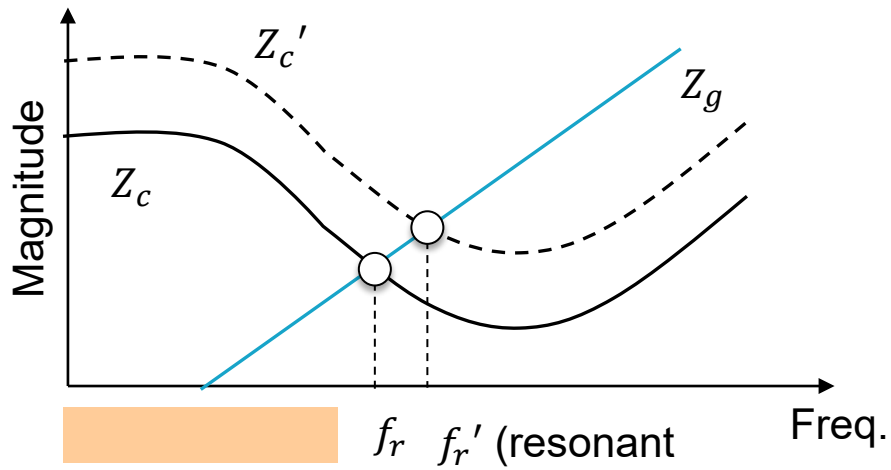

Non-passive region (negative resistance)

modify the controller parameters and the circuit parameters to:

- increase the magnitude of the input impedance
- reduce the non-passive region

How?

EXAMPLE OF IMPROVED PQ BY BETTER TUNING

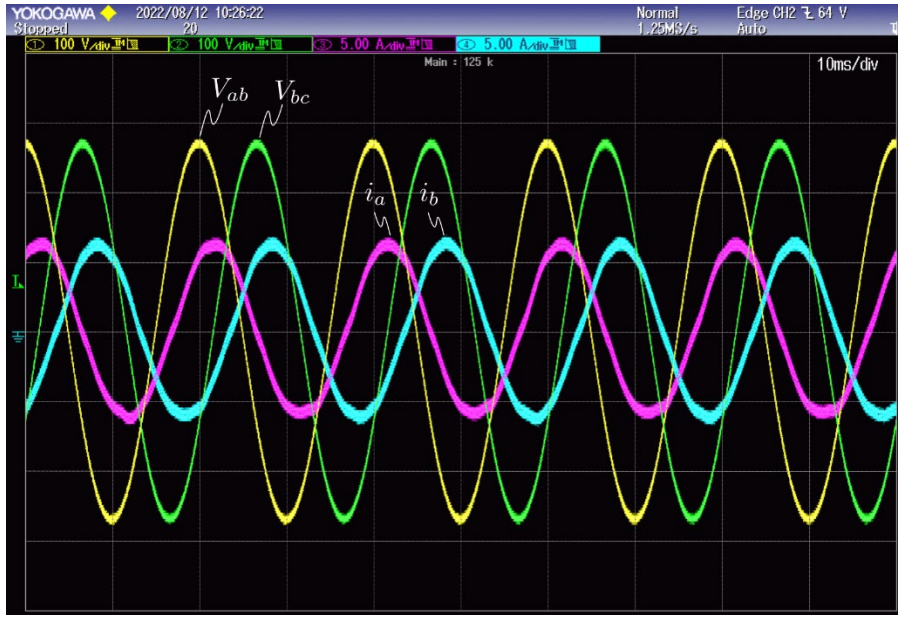

Clean grid
Clean current

5% THDv
Before
impedance
reshaping

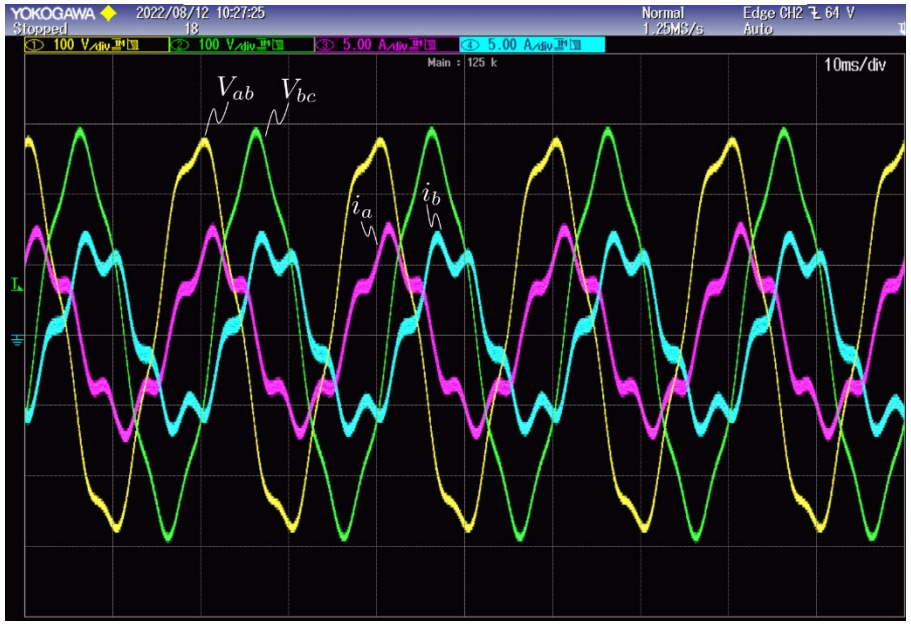

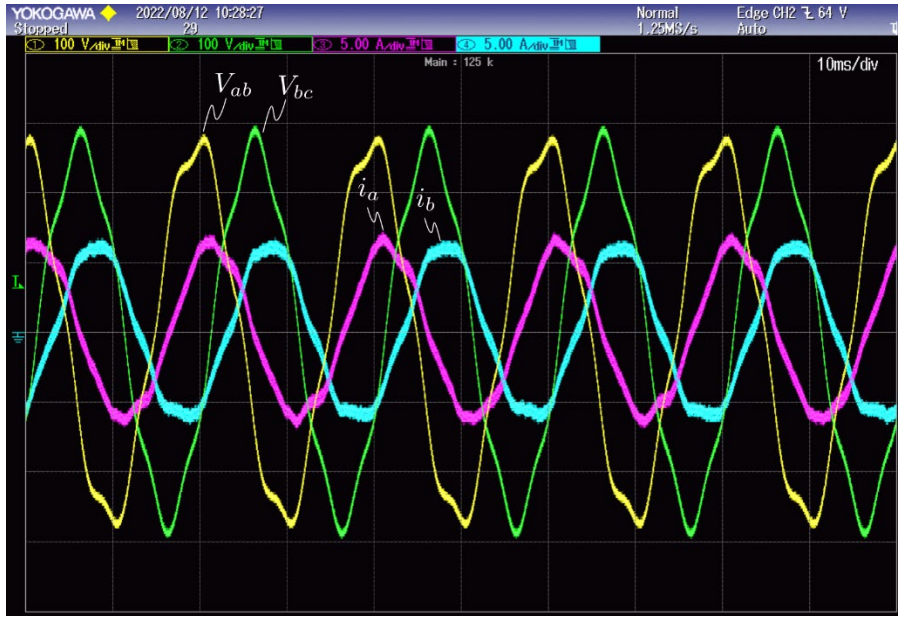

5% THDv
After
impedance
reshaping

EXAMPLE OF SMALL-SIGNAL INSTABILITY OF A PFC

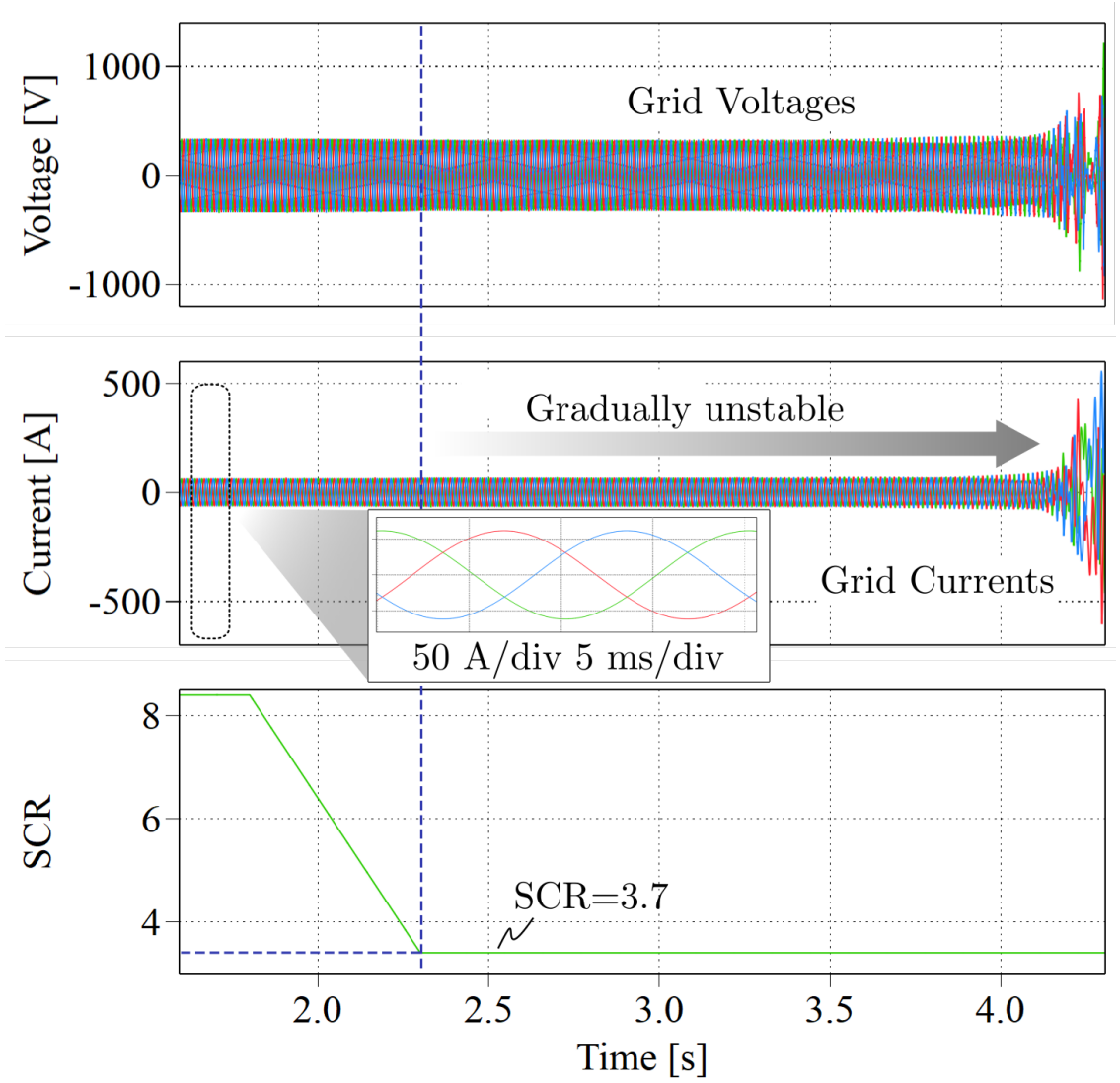

The PFC is stable when the grid is strong but becomes unstable when the grid becomes weak

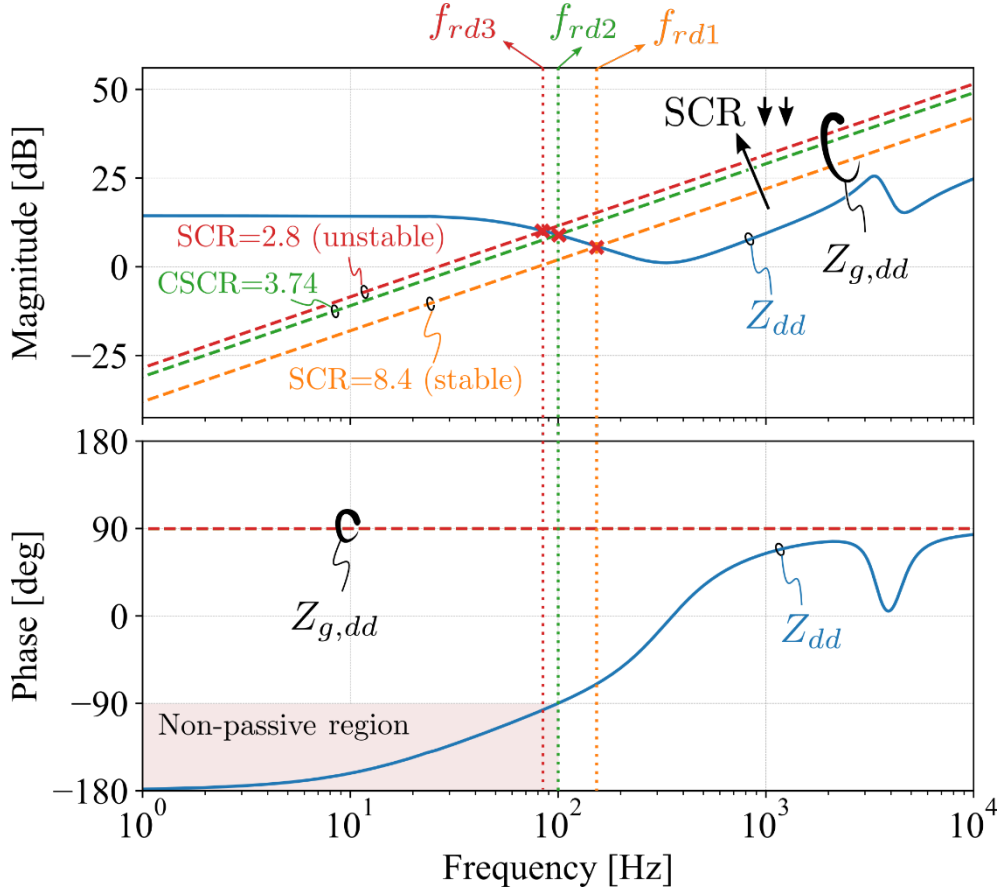

QUESTION: WHERE IS THE BOUNDARY?

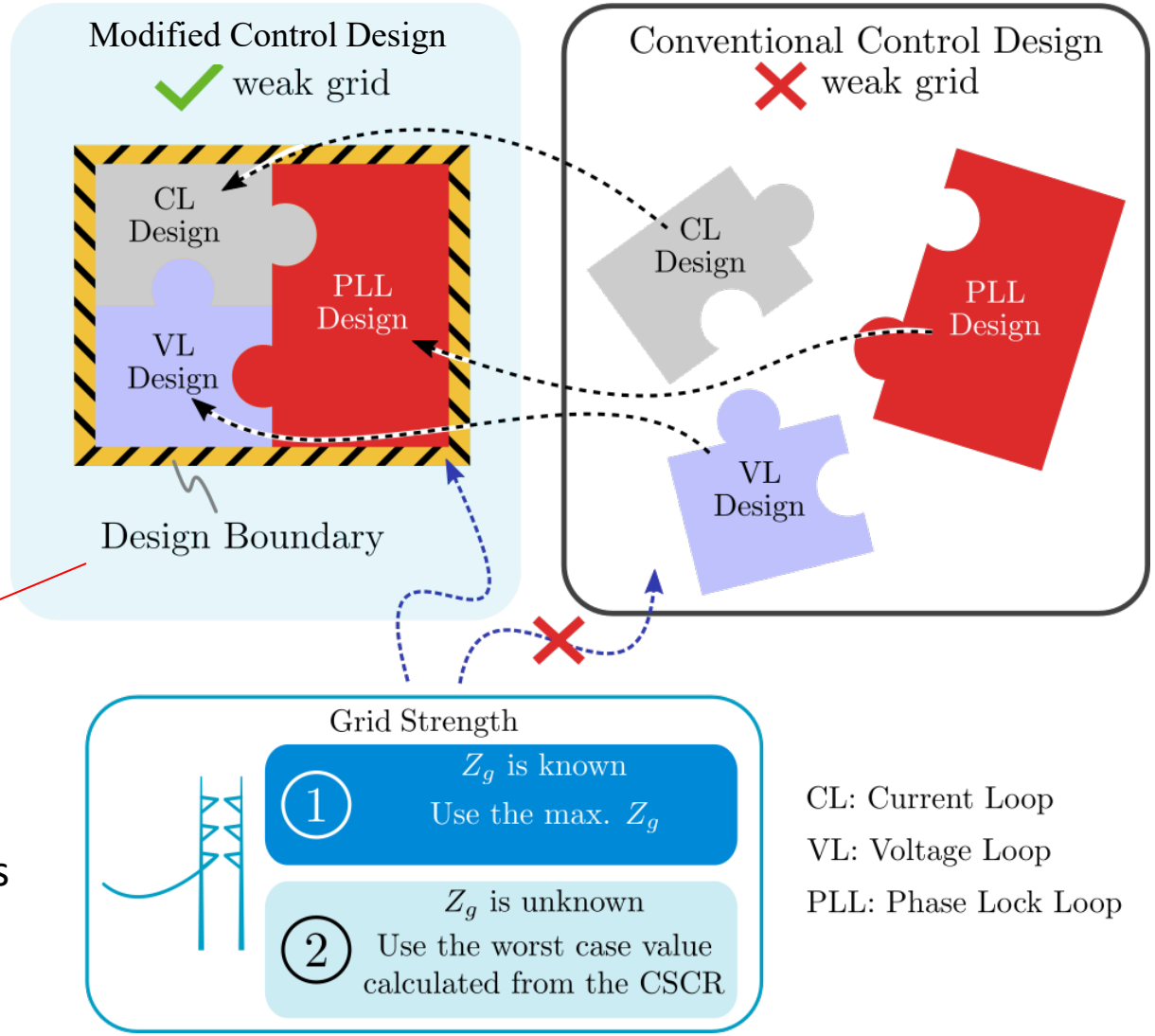

analytic expression of the design boundary?

Can be derived from impedance-based analysis

IMPEDANCE BASED STABILITY EVALUATION APPROACH

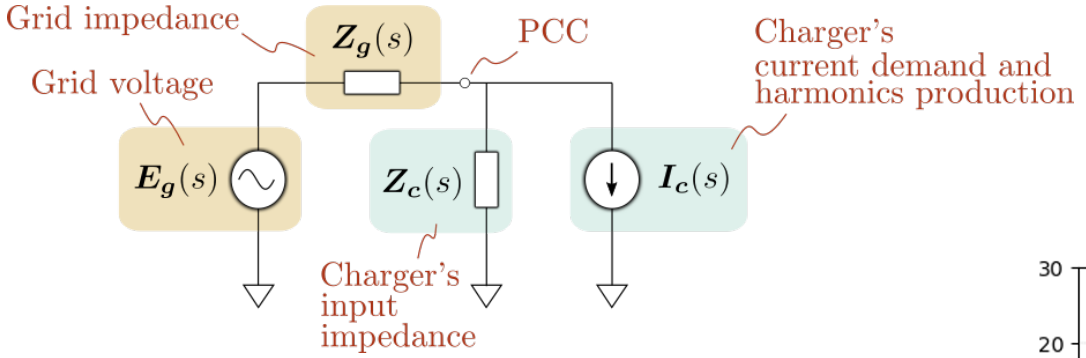

$$I_e = (I + Z_g Z_c^{-1})^{-1}(Z_c^{-1} E_g + I_c)$$

Complicated expression
Difficult to see how the control loops are related to the input impedance

Controller parameter tuning is finished via trial and error

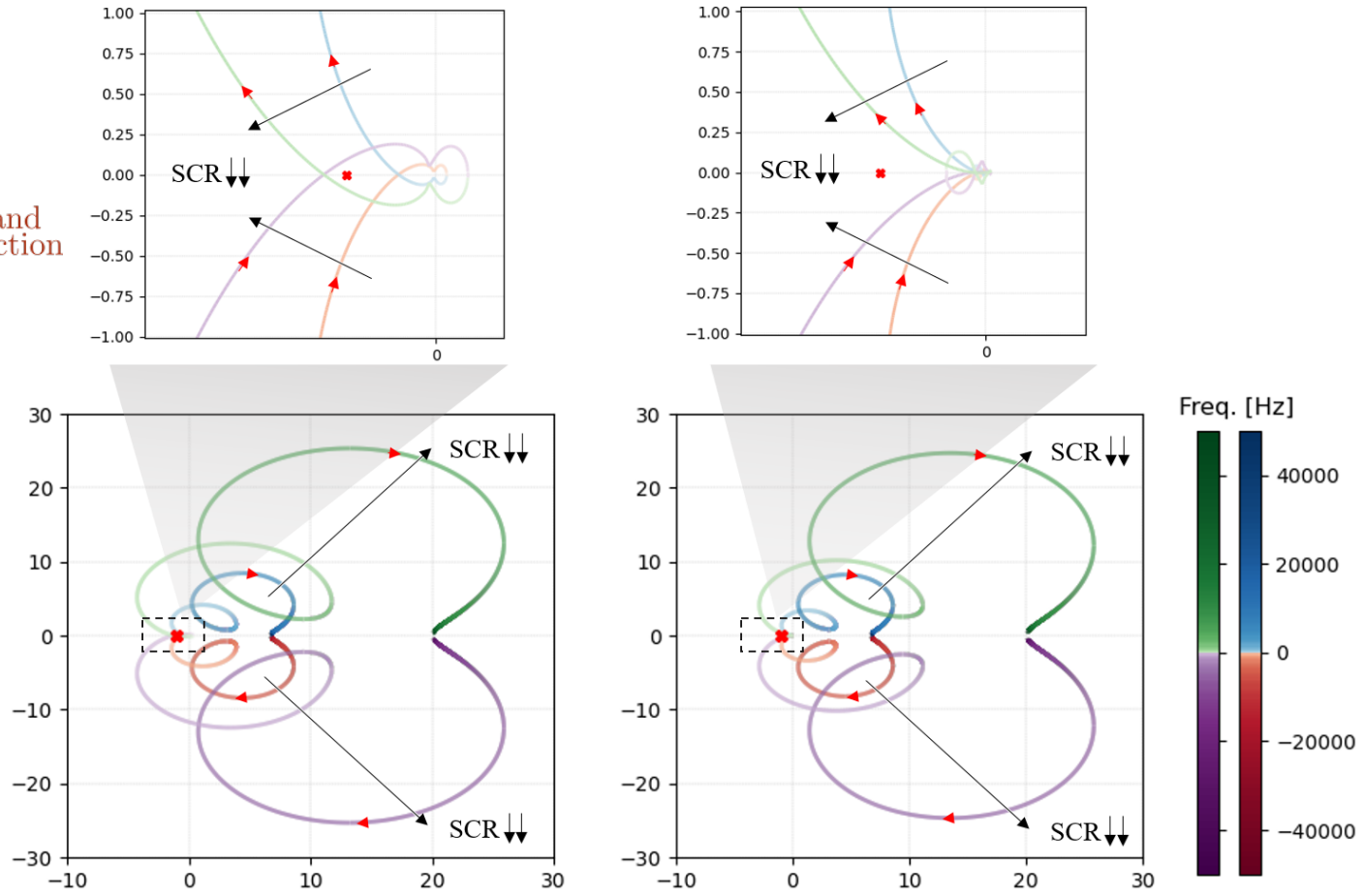

STABILITY CRITERIA SIMPLIFICATION FOR A PFC

$$\boldsymbol{I_e} = (I + \boldsymbol{Z_g Z_c}^{-1})^{-1}(\boldsymbol{Z_c}^{-1}\boldsymbol{E_g} + \boldsymbol{I_c})$$

$$\boldsymbol{Z_c}(s) = \begin{bmatrix} Z_{dd}(s) & Z_{dq}(s) \\ Z_{qd}(s) & Z_{qq}(s) \end{bmatrix}$$

For a PFC, the coupling impedance are small enough to be neglected

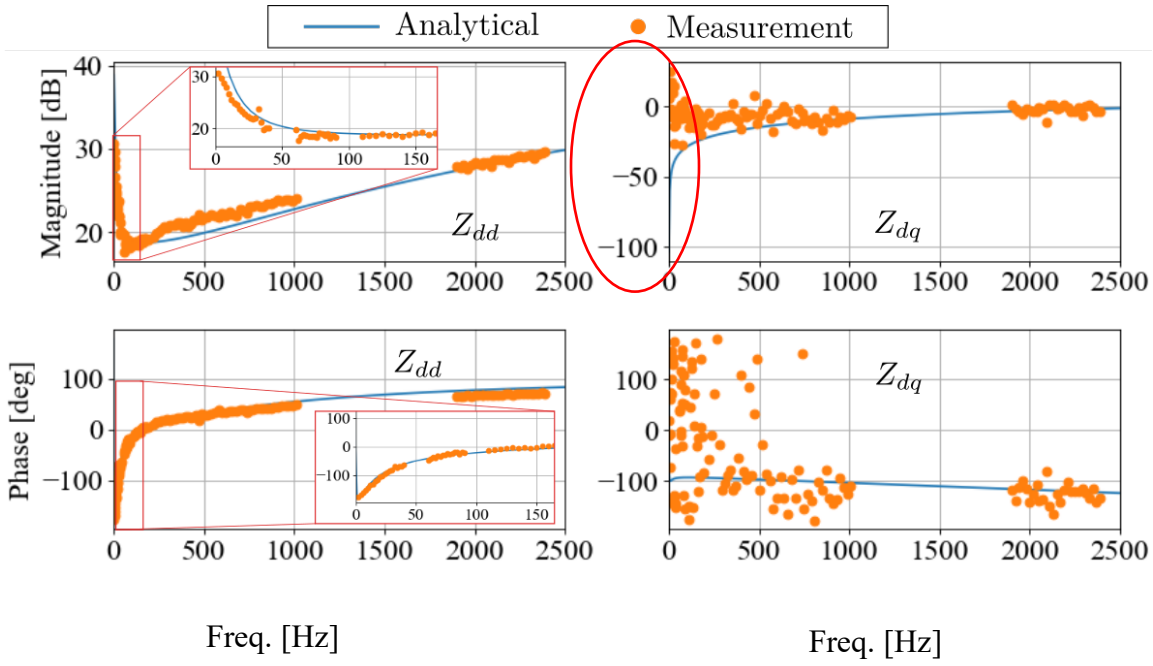

The MIMO system can be simplified as two SISO systems

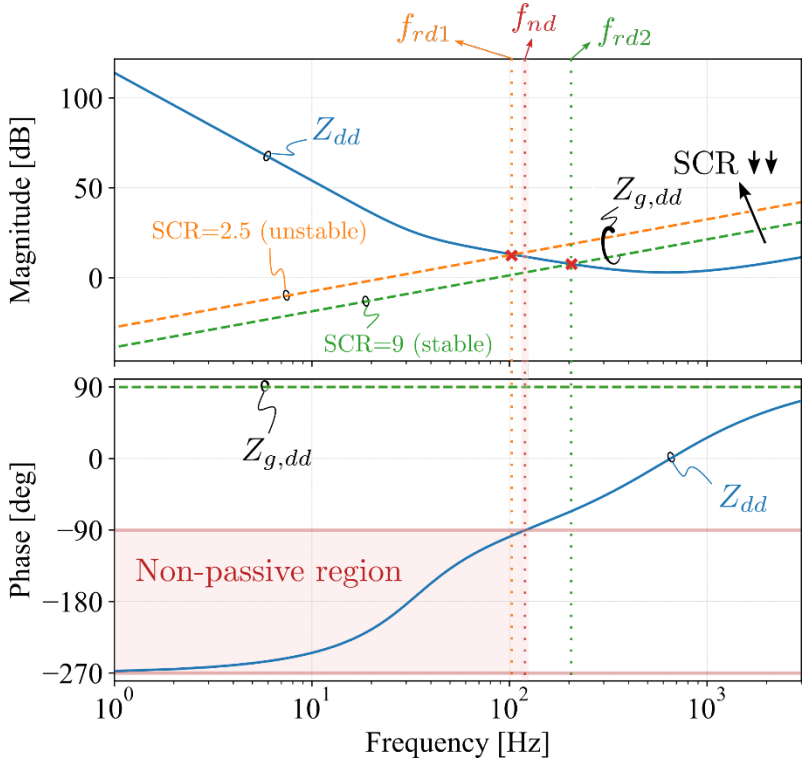

The stability criteria:

- $f_{nd} < f_{rd}$
- $f_{nq} < f_{rq}$

Boundaries for the selection of the controller parameters

Very complicate mathematic expression Simplification is needed

Small signal instability happens when the resonant frequency is located in the non-passive region (NPR)

WORST OPERATING POINT

Worst case for the d-axis system is when the charging power is the maximum

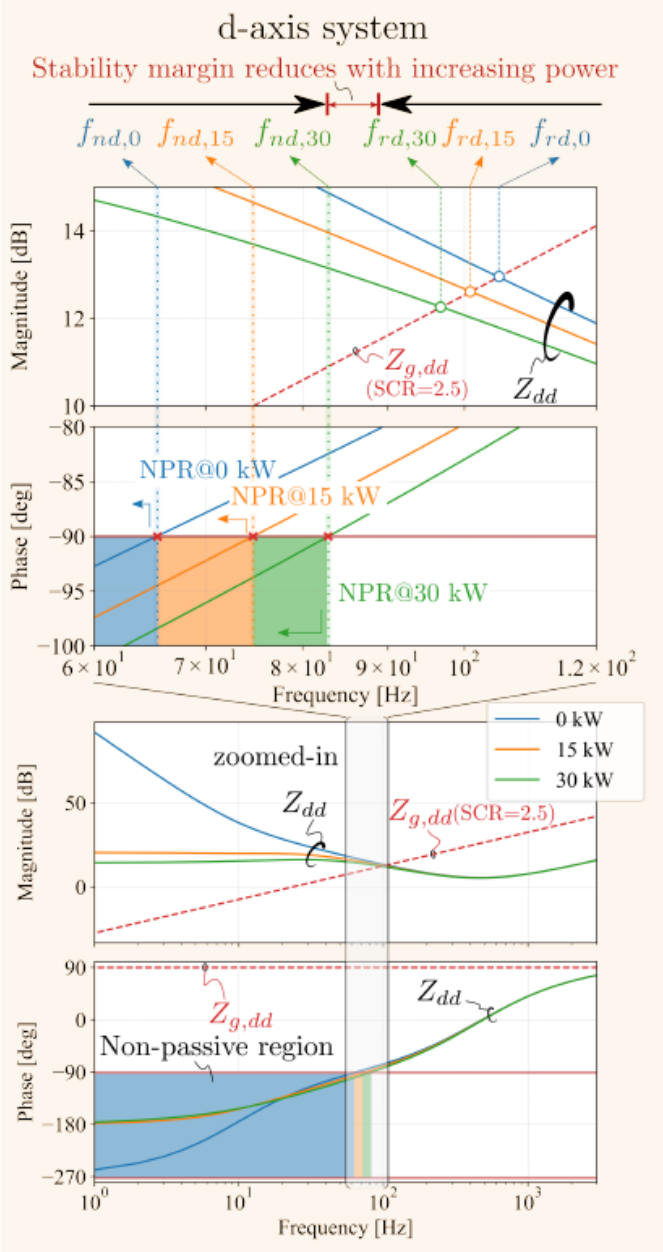

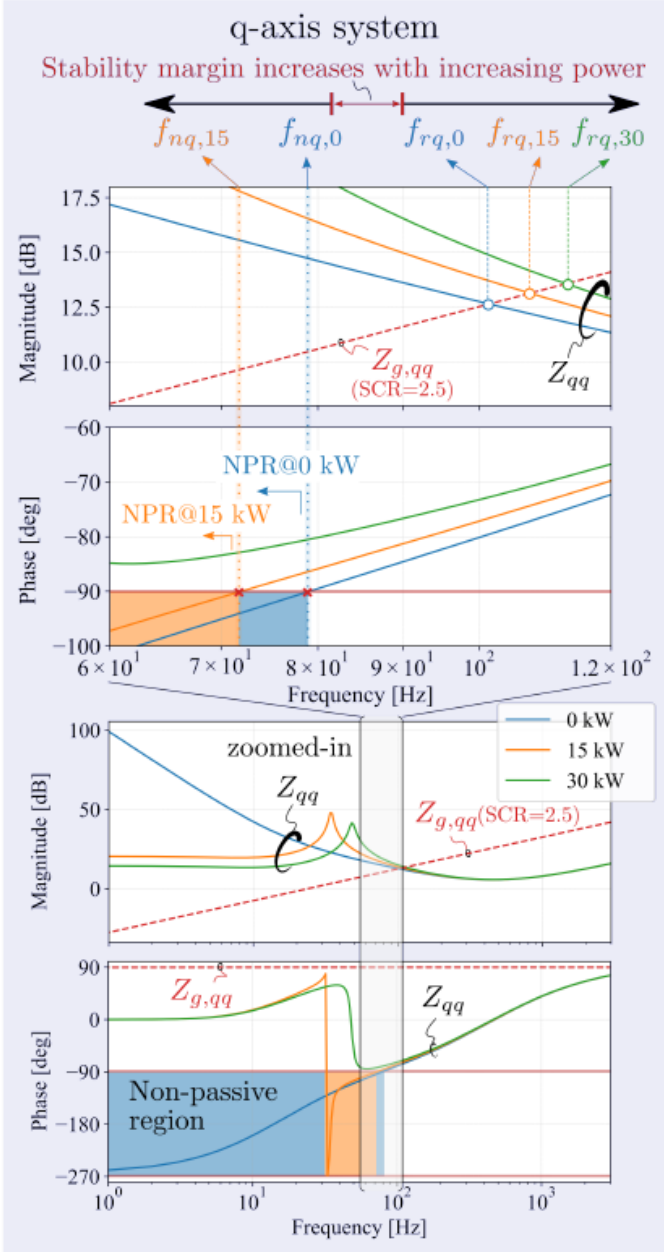

Worst case for the q-axis system is when the charging power is zero

INFLUENCE OF PARAMETERS ON IMPEDANCE

inductor

CL cut-off freq. (bandwidth)

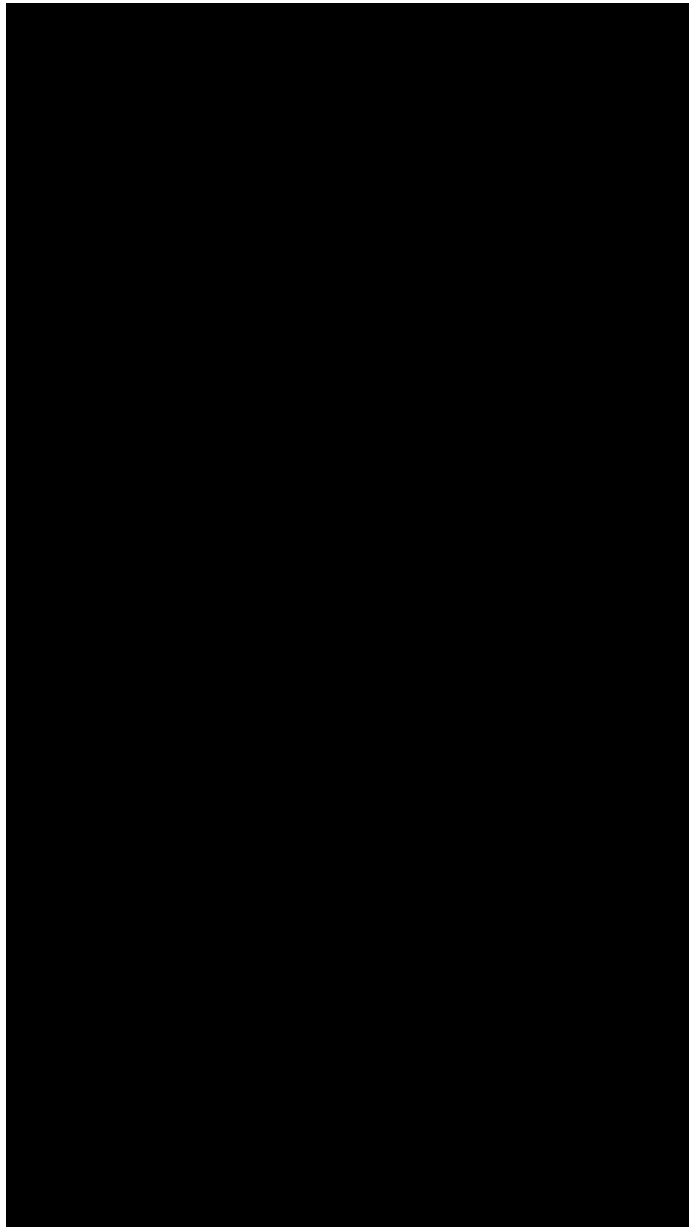

Observations from the numerical analysis

	Resonant freq.	Non-passive region range	Recommendations for stability
$L \uparrow$	$\uparrow$	–	Increase L
$\omega_{ci} \uparrow$	$\uparrow\uparrow$	$\uparrow$	Increase ω_{ci}
$\delta_i \uparrow$	$\downarrow$	$\downarrow\downarrow$	Increase δ_i
$\omega_{cv} \uparrow$	$\uparrow$	$\uparrow\uparrow$	Decrease ω_{cv}
$\delta_v \uparrow$	–	$\downarrow$	Increase δ_v
$\omega_{cpll} \uparrow$	–	$\uparrow$	Decrease ω_{cpll}
$\delta_{pll} \uparrow$	–	$\downarrow$	Increase δ_{pll}

Can we get an analytical expression?

NEED OF SIMPLIFICATION

Goal	$f_{nd} < f_{rd}$ $f_{nq} < f_{rq}$
Break down	$Re\{Z_{dd}(j \cdot 2\pi f_{nd})\} = 0$ $\quad |Z_{dd}(j \cdot 2\pi f_{rd})| = |Z_{g,dd}(j \cdot 2\pi f_{rd})|$ similar for f_{nq} and f_{rq}
Full order model	$\boldsymbol{Z_C}(s) = (\boldsymbol{G_{e2i}}(s) + \boldsymbol{G_v}(s)\boldsymbol{G_{d2dc}}(s)\boldsymbol{G_{d2v}^{-1}}(s))^{-1} \times (\boldsymbol{I} + \boldsymbol{G_{i_{ol}}^{-1}}(s) + \boldsymbol{G_v}(s)\boldsymbol{G_{i2dc\_tot}}(s))$
Element expressions	$Z_{dd}(s) = \left(Ls + R + \frac{3E_g^2}{2C_d U_{dc}^2 s}\right)\left(1 + G_{oi,dd}(s)\right)\left(1 + G_{ov}(s)\right)\frac{1}{1 - T(s)}$
	$Z_{qq}(s) = (Ls + R)\frac{1 + G_{oi,qq}(s)}{1 - G_{cpll}(s)(1 - (k_{pi} + k_{ii}/s)I_d/E_g)e^{-sT_{del}}}$
	$\|Z_{dd}(j\omega)\| = ?$ $\quad Re\{Z_{dd}(j\omega)\} = ?$ $\quad |Z_{qq}(j\omega)| = ?$ $\quad Re\{Z_{qq}(j\omega)\} = ?$

We are looking for a simple expression of the design constrain that can be easily applied in practice

ASSUMPTIONS FOR SIMPLIFICATIONS

Assumptions:

1. Control delay can be neglected
2. The damping ratio of the control loops are fixed at 0.707

The NPR is located in low frequency ranges

$$Z_{dd}(s) = L\frac{s^4 + \omega_{ci}s^3 + a_2\omega_{ci}s^2 + a_1\omega_{ci}s + a_0}{s^3 - I_d b_2[\omega_{ci}s^2 + b_1\omega_{ci}s + a_0/\omega_{cv}]}$$

$$Z_{qq}(s) = L\frac{s^4 + \omega_{ci}s^3 + c_2\omega_{ci}s^2 + c_1\omega_{ci}s + c_0}{s^3 + I_d d_2[\omega_{ci}s^2 + d_1\omega_{ci}s + c_0/\omega_{cpll}]}$$

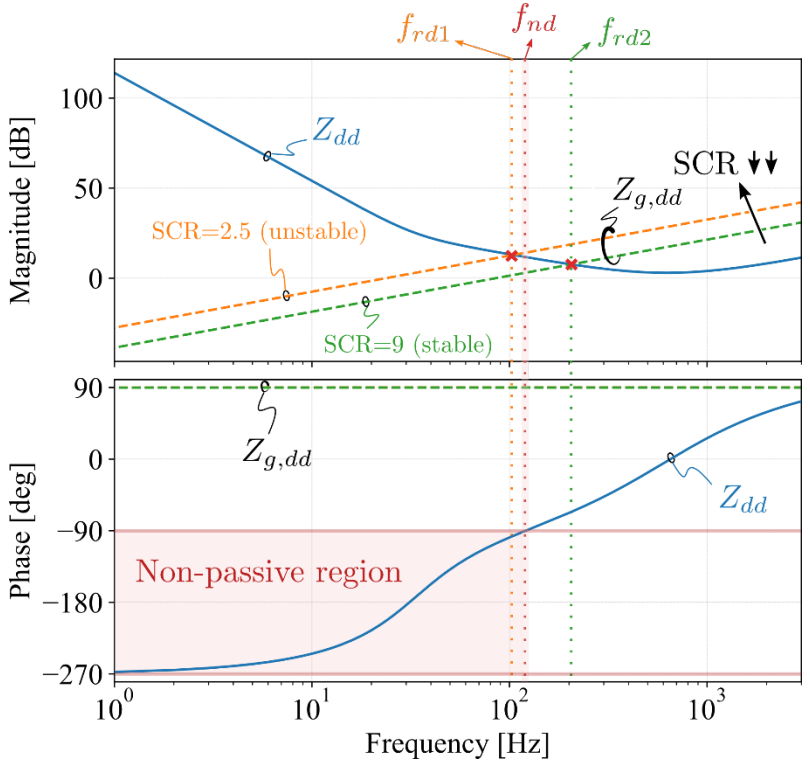

APPROXIMATION OF THE MAXIMUM NPR FREQUENCY

$$Re\left(Z_{dd}(s)|_{P=P_{max}}\right) = L\frac{s^4 + \omega_{ci}s^3 + a_2\omega_{ci}s^2 + a_1\omega_{ci}s + a_0}{s^3 - I_d b_2\left[\omega_{ci}s^2 + b_1\omega_{ci}s + \frac{a_0}{\omega_{cv}}\right]} = 0$$

Maximum NPR frequency when the charging power is the maximum is

$$\omega_{nd,P_{max}} = \sqrt{\frac{\omega_{ci}}{2}\cdot\frac{k_1 + \sqrt{k_1\cdot(k_1 + 4k_2\omega_{ci})}}{2}}$$

$$k_1 = \omega_{cv} + \frac{3E_g}{2C_d U_{dc}^2} I_m \qquad k_2 = \frac{L}{E_g} I_m \omega_{cv}$$

Observations:

- $I_m \uparrow \Rightarrow \omega_{nd,P_{max}} \uparrow$
- $\omega_{cv} \uparrow \Rightarrow \omega_{nd,P_{max}} \uparrow$
- $\omega_{ci} \uparrow \Rightarrow \omega_{nd,P_{max}} \uparrow$
- $L \uparrow \Rightarrow \omega_{nd,P_{max}} \uparrow$
- $k_1 < \omega_{nd,P_{max}} < \frac{\omega_{ci}}{2}$

$$Re\left(Z_{qq}(s)|_{P=0}\right) = L\frac{s^4 + \omega_{ci}s^3 + c_2\omega_{ci}s^2 + c_1\omega_{ci}s + c_0}{s^3 + I_d d_2\left[\omega_{ci}s^2 + d_1\omega_{ci}s + \frac{c_0}{\omega_{cpll}}\right]} = 0$$

Maximum NPR frequency when the charging power zero is

$$\omega_{nq,P_0} = \sqrt{\frac{\omega_{cpll}\omega_{ci}}{2}}$$

Observations:

- $\omega_{ci} \uparrow \Rightarrow \omega_{nq,P_0} \uparrow$
- $\omega_{cpll} \uparrow \Rightarrow \omega_{nq,P_0} \uparrow$
- $\omega_{cpll} < \omega_{nq,P_0} < \frac{\omega_{ci}}{2}$

APPROXIMATION OF THE RESONANT FREQUENCY

$$k_1 < \omega_{nd,P_{max}} < \frac{\omega_{ci}}{2} \qquad \omega_{cpll} < \omega_{nq,P_0} < \frac{\omega_{ci}}{2}$$

We are interested in the expressions of the $\omega_{rd,P_{max}}$ and the ω_{nq,P_0} only when they are located in the two ranges, respectively

Approximated resonant frequency

$$|Z_{dd}(j\omega)|_{P=P_{max}}| \approx \left|\frac{jL\omega_{ci}^2\omega}{-2\omega^2 - k_2\omega_{ci}^2 - j2k_2\omega_{ci}\omega}\right|$$

$$\omega_{rd,P_{max}} = \frac{\omega_{ci}}{\sqrt{2}}\sqrt{\frac{L}{L_g} - \frac{L}{E_g}I_m\omega_{cv}}$$

Observations:

- $I_m \uparrow \Rightarrow \omega_{rd,P_{max}} \downarrow$
- $\omega_{cv} \uparrow \Rightarrow \omega_{rd,P_{max}} \downarrow$
- $\omega_{ci} \uparrow \Rightarrow \omega_{rd,P_{max}} \uparrow$
- $L \uparrow \Rightarrow \omega_{rd,P_{max}} \uparrow$
- $L_g \uparrow \Rightarrow \omega_{rd,P_{max}} \downarrow$

$$|Z_{qq}(j\omega)|_{P=0}| \approx \left|\frac{L\omega_{ci}^2}{2\omega}\right|$$

$$\omega_{rq,P_0} = \frac{\omega_{ci}}{\sqrt{2}}\sqrt{\frac{L}{L_g}\frac{\omega_{ci}^2}{2}}$$

Observations:

- $\omega_{ci} \uparrow \Rightarrow \omega_{rq,P_0} \uparrow$
- $L \uparrow \Rightarrow \omega_{rq,P_0} \uparrow$
- $L_g \uparrow \Rightarrow \omega_{rq,P_0} \downarrow$

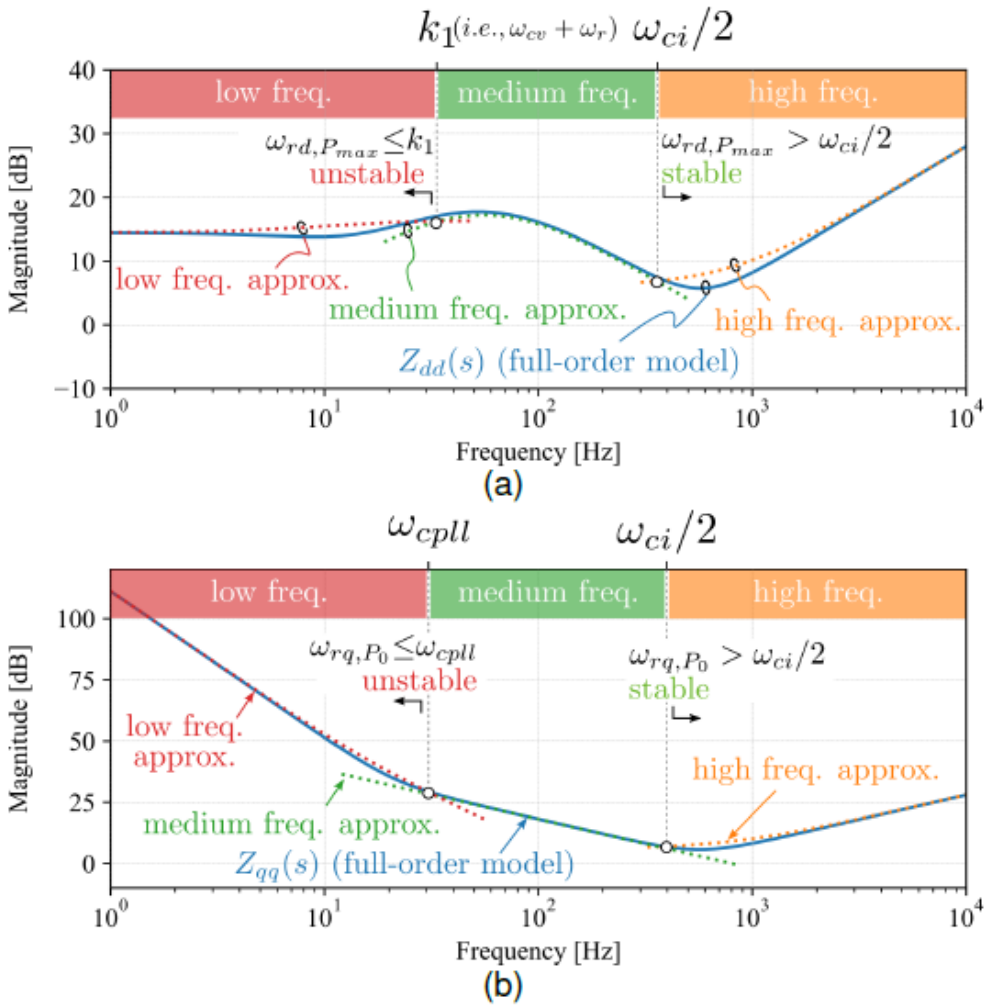

DERIVED DESIGN BOUNDARY

Stability criterion for the d-axis system

Constraint on VL & CL bandwidth

$$\underbrace{\sqrt{\frac{\omega_{ci}}{2}\cdot\frac{k_1+\sqrt{k_1\cdot(k_1+4\cdot k_2\cdot\omega_{ci})}}{2}}}_{\omega_{nd,P_{max}}} < \underbrace{\frac{\omega_{ci}}{\sqrt{2}}\cdot\sqrt{\frac{L}{L_g}-\frac{L}{E_g}\cdot I_m\cdot\omega_{cv}}}_{\omega_{rd,P_{max}}}$$

$$k_1 = \omega_{cv} + \omega_r, \quad k_2 = \frac{L}{E_g}\cdot I_m\cdot\omega_{cv}$$

Stability criterion for the q-axis system

Constraint on PLL & CL bandwidth

$$\underbrace{\sqrt{\frac{\omega_{cpll}\cdot\omega_{ci}}{2}}}_{\omega_{nq,P_0}} < \underbrace{\sqrt{\frac{L}{L_g}\cdot\frac{\omega_{ci}^2}{2}}}_{\omega_{rq,P_0}}$$

The influential parameters are highlighted in red.

Summary of the influences of the parameters

Action	Consequences				Stability impact
	$\omega_{nd,P_{max}}$	$\omega_{rd,P_{max}}$	ω_{nq,P_0}	ω_{rq,P_0}	
$\omega_{ci}\uparrow$	$\uparrow$	$\uparrow$	$\uparrow$	$\uparrow$	–
$\omega_{cv}\uparrow$	$\uparrow$	$\downarrow$	N.A.	N.A.	Negative
$\omega_{cpll}\uparrow$	N.A.	N.A.	$\uparrow$	N.A.	Negative
$L\uparrow$	$\uparrow$	$\uparrow$	N.A.	$\uparrow$	–
$L_g\uparrow$	N.A.	$\downarrow$	N.A.	$\downarrow$	Negative

Source: L Wang, et. al. “Analytic Design of an EV Charger Controller for Weak Grid Connection,” *TIE*, 2024

VISUALIZATION OF THE DESIGN BOUNDARY

The obtained upper limit of the bandwidth of the PLL and the voltage control loop

$$\omega_{cpll} < \frac{2 \cdot P_{max} \cdot \omega_1}{3 \cdot E_g^2} \cdot \mathrm{SCR} \cdot L \cdot \omega_{ci}$$

★ Observations: $\omega_{cpll,max}$ can be increased by ω_{ci} ↑, L ↑ and SCR↑

$$\omega_{cv} < \omega_1 \cdot \mathrm{SCR} \cdot \left(1 - \frac{\sqrt{1 + 4 \cdot h \cdot \omega_{ci} \cdot \left(1 + \frac{\omega_r}{\omega_1 \cdot \mathrm{SCR}}\right)} - 1}{2 \cdot h \cdot \omega_{ci}}\right)$$

$$\omega_r = \frac{3E_g}{2C_d U_{dc}^2} I_m \qquad h = \frac{L}{E_g} I_m$$

★ Observations: $\omega_{cv,max}$ can be increased by ω_{ci} ↑, L ↑ and SCR↑

Visualization of the design boundary

SCR = 9

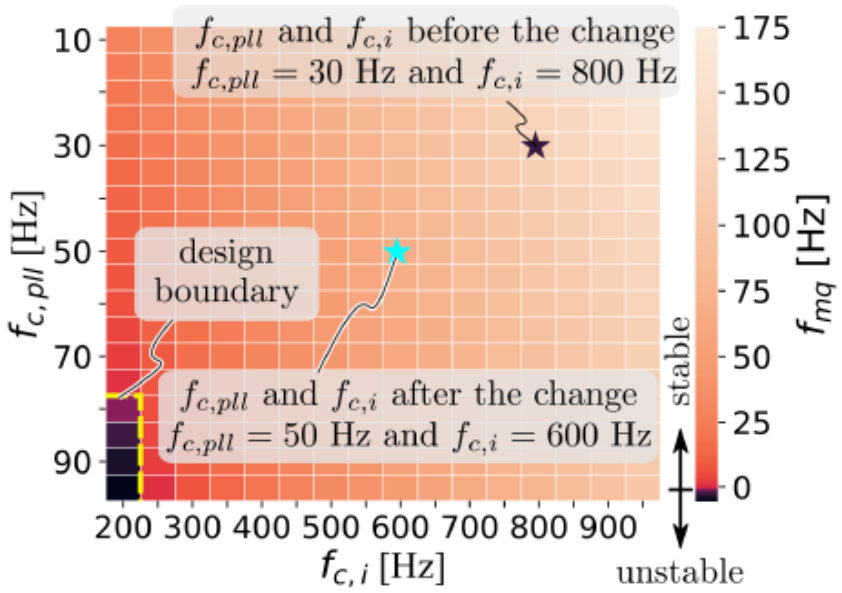

SCR = 2.5

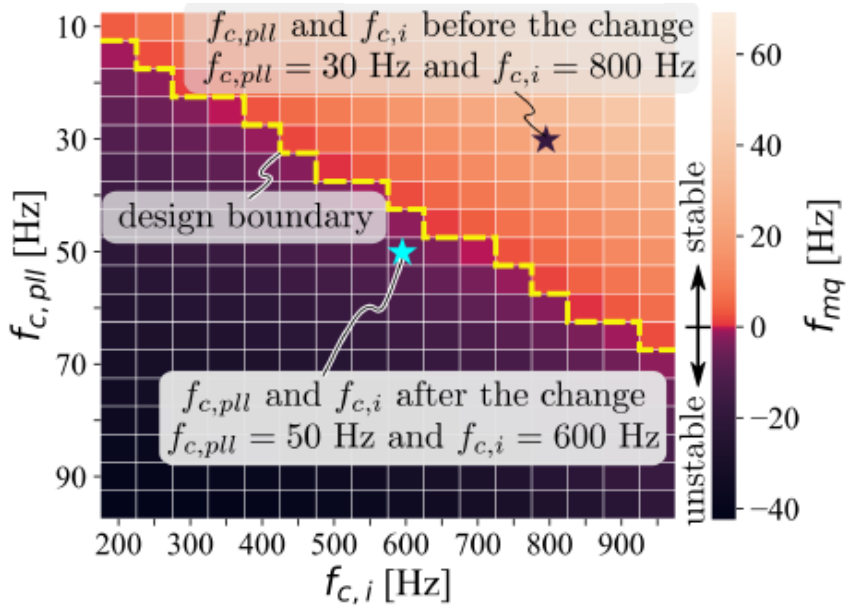

DESIGN PROCEDURE

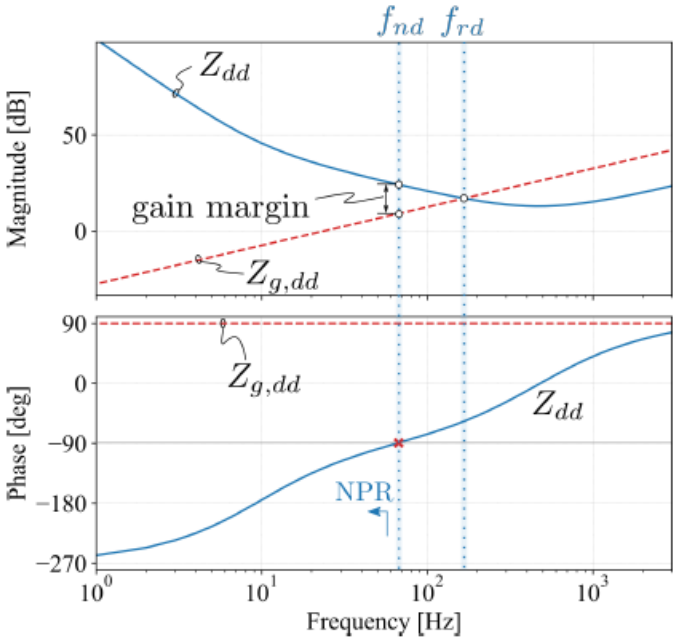

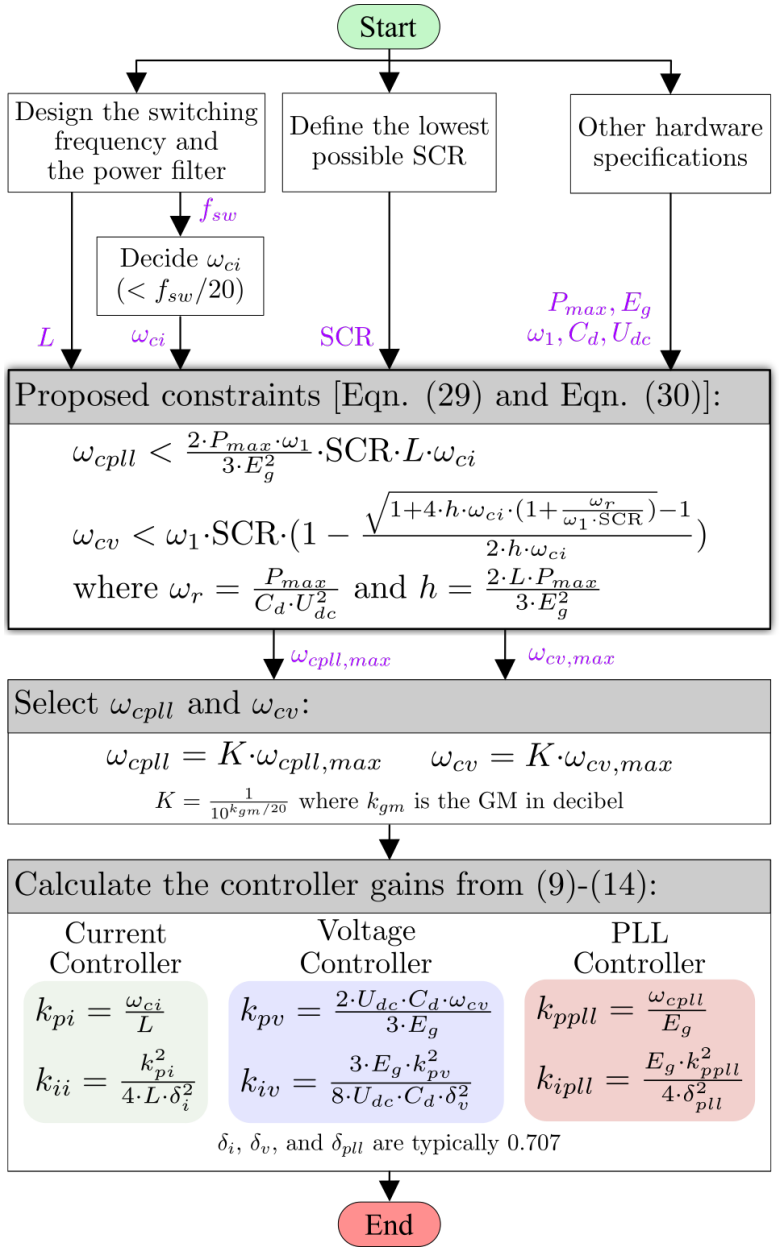

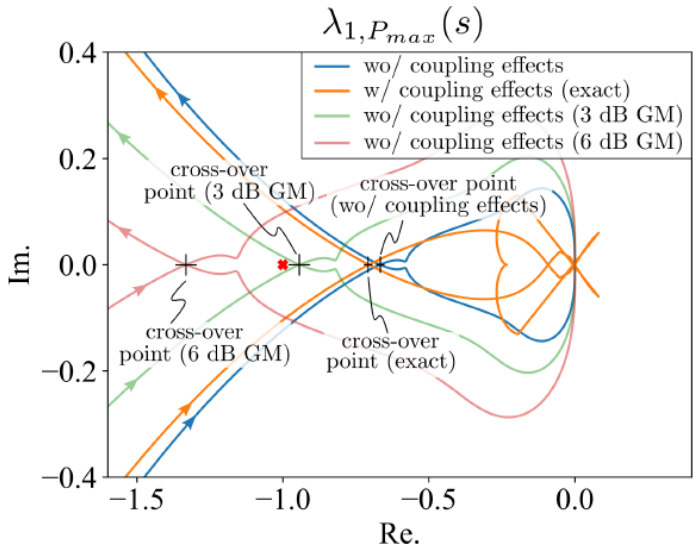

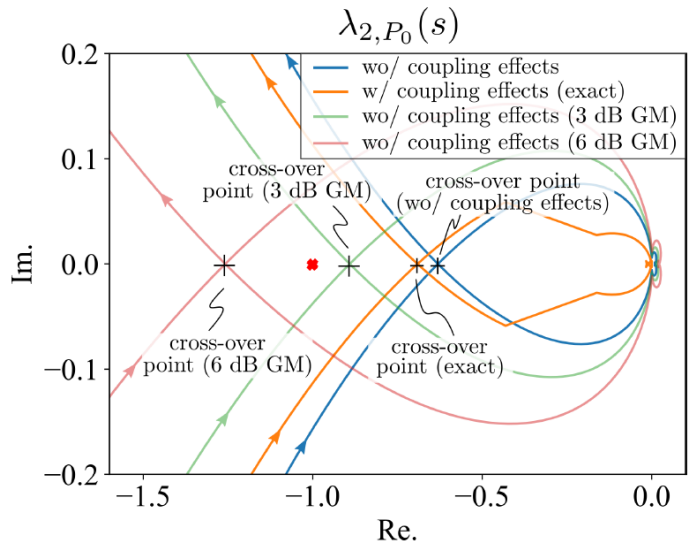

VERIFICATION OF THE DESIGN BOUNDARY

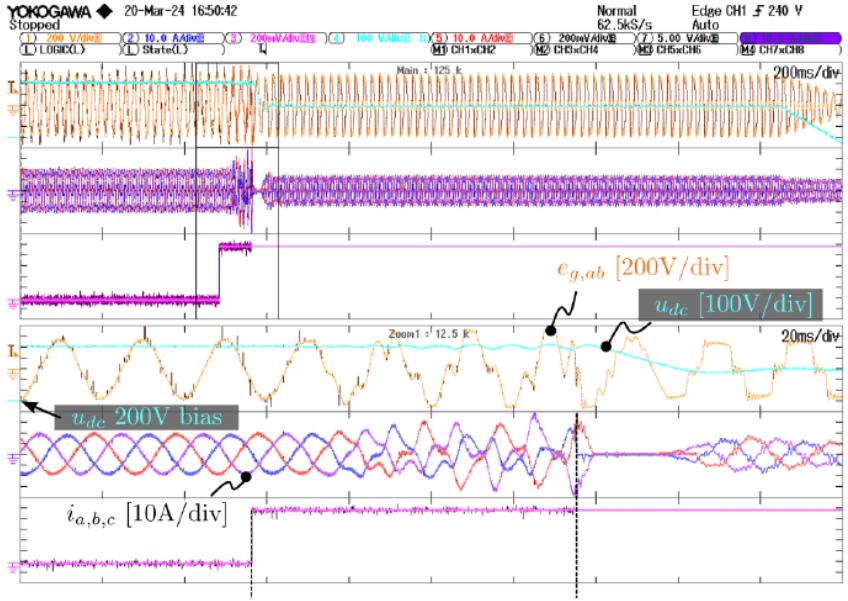

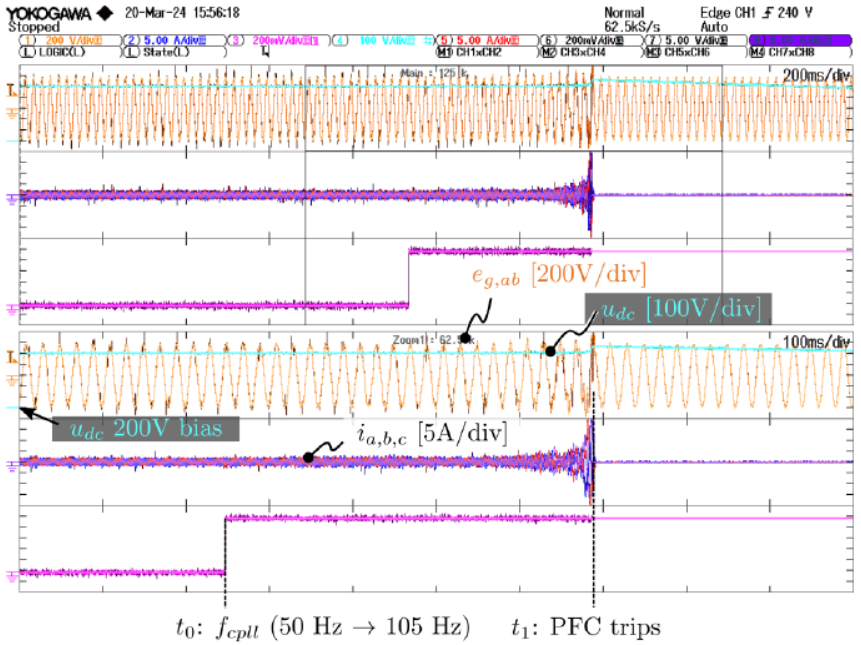

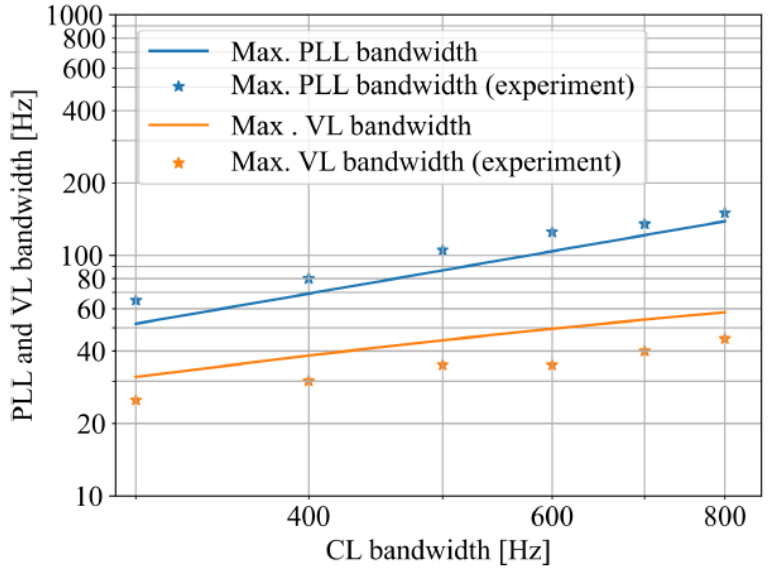

WRAP UP

- The impedance-based stability criteria for an EV charger's PFC can be simplified. The more **specific stability criteria for the PFC** guaranteeing small signal stability in the whole charging power range are **summarized**.
- For a PFC, the upper limit of the PLL cut-off frequency (≈ bandwidth) and the upper limit of the DC voltage loop cut-off frequency (≈ bandwidth) **are derived analytically**.
- The derived expressions of the upper limits indicate that the **upper limits** are **constraint** by the **current loop cut-off frequency** (≈ bandwidth), the **filter inductance**, and the **short-circuit ratio**.
- Based on the derived upper limits, a **design procedure** is given, which facilitates the controller parameter tuning and **does not need trail and error**.

Q&A

Zian Qin
z.qin-2@tudelft.nl

Lu Wang
lu.wang@hitachienergy.com